COMPUTATION OF NEUTRON FLUX DISTRIBUTION IN LARGE NUCLEAR REACTORS VIA REDUCED ORDER MODELING

by

RAJASEKHAR ANANTHOJU

ENGG01201104012

BHABHA ATOMIC RESEARCH CENTRE, MUMBAI

A thesis submitted to the

Board of Studies in Engineering Sciences

In partial fulfilment of the requirements

for the degree of

DOCTOR OF PHILOSOPHY

of

HOMI BHABHA NATIONAL INSTITUTE

March, 2017

STATEMENT BY AUTHOR

This dissertation has been submitted in partial fulfillment of requirements for an advanced degree at Homi Bhabha National Institute (HBNI) and is deposited in the Library to be made available to borrowers under rules of the HBNI.

Brief quotations from this dissertation are allowable without special permission, provided that accurate acknowledgement of source is made. Requests for permission for extended quotation from or reproduction of this manuscript in whole or in part may be granted by the Competent Authority of HBNI when in his or her judgment the proposed use of the material is in the interests of scholarship. In all other instances, however, permission must be obtained from the author.

RAJASEKHAR ANANTHOJU

DECLARATION

I, hereby declare that the investigation presented in the thesis has been carried out by me. The work is original and has not been submitted earlier as a whole or in part for a degree/diploma at this or any other Institution/University.

RAJASEKHAR ANANTHOJU

List of Publications based on this thesis

Journal Publications

1. Rajasekhar Ananthoju, A. P. Tiwari, and Madhu N. Belur, "A Two-Time-Scale Approach for Discrete-Time Kalman Filter Design and Application to AHWR Flux Mapping," *IEEE Transactions on Nuclear Science*, Vol. 63 (1), pages 359-370, 2016.

2. Rajasekhar Ananthoju, A. P. Tiwari, and Madhu N. Belur, "Model Reduction of AHWR space-time kinetics using balanced truncation," *Annals of Nuclear Energy*, Vol. 102, pages 454-464, 2017.

Conference Publications

1. Rajasekhar. A, A. P. Tiwari, and Madhu N. Belur, "Application of model order reduction techniques to Space–time kinetics model of AHWR," In 2015 *IEEE International Conference on Industrial Instrumentation and Control Applications (ICIC)*, Pune, India, pages 873-878, 2015.

DEDICATED TO MY FAMILY

ACKNOWLEDGEMENTS

I would like to express my sincere gratitude and respect to my guide Dr. A. P. Tiwari for giving me an opportunity to work in the area of Nuclear Reactor Dynamics and State Estimation Theory, and for his invaluable guidance, support and encouragement in all stages of this research work. Without his vast experience, substantial knowledge in Reactor Control Theory and insight into the research problem, I would not have been able to complete this research work.

I would also like to express my sincere gratitude to my co-guide Dr. Madhu N. Belur for his guidance, support and encouragement during the course work at IIT Bombay and research work.

I am indebted to my guide and co-guide, for their valuable suggestions and advices in refining my manuscripts during the initial submission and review process. It has been a great honour and privilege to me to work under their guidance and to be their student.

I would like to thank Dr. (Smt.) Archana Sharma, Chairman and other members of the Doctoral Committee, for their valuable comments and suggestions during the annual progress reviews, oral general comprehensive examination and pre-synopsis presentations. I would also like to thank Dr. Kallol Roy, former chairman of doctoral committee .

I wish to express my sincere thanks to Dr. S. R. Shimjith at Reactor Control Systems Design Section (RCSDS), BARC for valuable technical discussions and inputs. I would like to thank Shri. A. K. Mishra, Shri S. Subudhi and other members of RCSDS for their help and support during my research work.

I express my thanks to Shri Y. V. Sagar, my co-researcher and friend for sharing his material and experience in simulating the mathematical model of the reactor. Thanks are also due to Shri Jagadish Kota, my friend for his emotional support during my stay in Mumbai.

I am indebted to Homi Bhabha National Institute, Mumbai for giving me this opportunity and to carry out the research work in real time reactor problem at RCSDS, BARC, Mumbai.

And last but certainly not the least, I would like express my heartfelt thanks to my family members: Smt. Sandhya Rani, my mother; Shri A. Sesha Chary, my father; Smt. A. Hema Sireesha, my sister, and Dr. G. H. V. C. Chary, my brother-in-law, for all their unconditional love, care and support. My parents have always encouraged me towards higher studies and sacrificed a lot, I am grateful to them. My mother deserves special mention for her stay with me and having her beside me during this research is the great source of my motivation and dedication.

RAJASEKHAR ANANTHOJU

Contents

Synopsis

Because of potential for accidents or sabotage at nuclear power plants, the operation and control of these plants represents a complex problem. Several safety and control features are engineered at the design stage and operational policies are incorporated to avoid accidental release of radioactivity to the general population. The problems are further complicated in case of large nuclear reactors [113].

The current generation modern power reactors are increasing in size to get the benefit from the economies of generation of electricity. An useful parameter for assessing the effective size of a reactor is neutron migration length M, a measure of the average distance travelled by a neutron from its appearance as a fission neutron to its absorption as a thermal neutron. For a given reactor design, M is determined by the material composition of the reactor core, primarily the fuel-to-moderator ratio and is essentially independent of core size R. As the core size increases, the ratio R^2/M^2 increases, the migration length becomes a smaller fraction of the reactor core dimension. Thus, each neutron's zone of influence becomes a smaller fraction of the core volume, and the various regions of the core become loosely coupled. Any deliberate attempt to operate the reactor with flattened radial and axial flux distributions coupled with xenon poisoning effect leads to complex operational and control problems. The mechanism of ^{135}Xe production and its removal by neutron absorption and radioactive decay are such that oscillations of thermal flux are induced in large thermal reactors. Such oscillations induced by ^{135}Xe can broadly be classified into two categories - fundamental mode or global power oscillations and higher mode or spatial oscillations. Generally speaking, global power oscillations can be readily noticed and suppressed by control system while spatial oscillations are not. Here, the global reactor power can remain constant so that no change in the coolant outlet temperature is effected, the oscillations being in spatial distribution of power inside the core.

If these oscillations are left uncontrolled, the power density and time rate of change of power at some locations in the reactor core may exceed the respective design limits.

These xenon induced spatial oscillations and subsequent local overpowers pose a potential threat to the fuel integrity of the reactor. Therefore, the detailed knowledge of axial and radial flux distribution in the core during the course of their operation is crucial.

Modern reactors have provisions for online spatial control and monitoring of flux or power distribution during the course of their operation. The time varying neutron flux distribution is computed by an online Flux Mapping System (FMS), with the help of flux mapping algorithms. The measurement signals of several in-core flux detectors are processed to generate the detailed three dimensional flux map, which helps for spatial control purpose. In CANDU-6 reactors and in Indian 540 MWe Pressurized Heavy Water Reactors (PHWRs), 102 Vanadium detectors are used for flux mapping, while in PWRs it is carried out by Rhodium detectors installed in about 45 fuel assemblies. Over the years, research has been carried out to evolve an efficient flux mapping algorithm for the improvement of accuracy in flux mapping with less computational effort. Most of the algorithms existing in the literature are based on three principles, namely the Flux Synthesis, Internal boundary condition and simultaneous least squares solution of neutron diffusion and detector response equations.

The most popular and traditional method for flux mapping is known as Flux Synthesis Method (FSM) [46]. It uses the available detector measurements and performs least squares fit with pre-computed flux modes, determined based on reactivity devices configuration. Determination of flux modes requires the knowledge of core configuration and considerable insight into the reactor operation. There are other synthesis methods such as Harmonic Synthesis Method (HSM) [95] and Harmonic Expansion Method (HEM) [133] to improve the accuracy of flux mapping, however the accuracy of reconstruction depends on selection of the reference case. Selection of a suitable reference case which reflects the actual core condition results in improvement of the reconstruction accuracy. During the core configuration changes, the reference case has to be renewed, which can be a time consuming process.

A Method based on direct online solution of neutron diffusion equations with detector

readings as the internal boundary condition is reported in [52]. A method which obtains a least squares solution of the core neutronics design equations alongwith the in-core detector response equations is reported in [47]. Applicability of this least squares method requires to solve the overdetermined system of equations resulting in the framework of mapping algorithm. Another approach with the combination of FSM and least squares method, known as modified flux synthesis method has been proposed for Indian 700 MWe PHWR in [80]. This method takes longer computation time than FSM does [47] and detector signal uncertainty can also deteriorate the performance of flux mapping calculations. A common drawback of the aforesaid methods is that they fail to account for time variation of neutron flux distribution during the reactor operation and the accuracy might be degraded considerably in presence of uncertainty in the detector readings.

In contrast to this, model based estimation methods such as the Kalman filter [53], which infer the system dynamic state on the basis of a sequence of noisy measurements, offer interesting potential for successful online application. The Kalman filter has received a huge interest from the industrial community and has played a key role in many engineering fields since 70's, ranging, without being exhaustive, trajectory estimation, state and parameter estimation for control and diagnosis, data merging, signal processing, *etc.* It is a recursive computational algorithm that processes measurements to deduce a minimum error estimate of the state of a system by utilizing: knowledge of system and measurement dynamics, assumed statistics of system noises and measurement errors, and initial condition information.

Advanced Heavy Water Reactor (AHWR) [119] is a 920 MW (thermal), vertical, pressure tube type, heavy water moderated, boiling light water cooled natural circulation reactor being designed in India. The radial dimensions of the core are very large. Therefore, from neutronic view-point, the behavior tends to be loosely coupled, due to which a serious situation called 'flux tilt' may arise in AHWR followed by an operational perturbation. These operational perturbations might lead to slow xenon induced

oscillations, which might cause changes in axial and radial flux distribution from the nominal distribution. Knowledge of any such changes during the reactor operation is crucial. Therefore, it is necessary to provide online monitoring and control schemes during the reactor operation. To monitor the core flux distribution, 200 Self Powered Neutron Detectors (SPNDs) are proposed to be provided at different elevations of the assembly covering entire AHWR core from top to bottom [1]. An efficient flux mapping algorithm in AHWR can ensure better reactor regulation and core monitoring, as more accurate estimates of channel and zonal powers will be available to Reactor Regulating System (RRS) and Core Monitoring System.

This thesis presents a Discrete-time Kalman filter (DKF) formulation for flux mapping in AHWR which is quite different from the existing methods as it can take care of both time varying phenomena and random errors in the detector readings. For this, a reasonably accurate mathematical model which represents the time-dependent core neutronics behaviour of AHWR core is required. A space-time kinetics model with 17 nodes in the core and which exhibits all the essential control related properties and yields accurate transient response characteristics is utilized for the studies as it is more suitable for flux distribution studies owing to its simplicity and the structure, thus facilitating selection of state variables for the system in a straightforward manner. An important characteristic of the model based on nodal methods is that the order of mathematical model depends on the number of nodes into which the reactor spatial domain is divided. A rigorous model with more number of nodes will give good accuracy in designing of DKF algorithm for flux mapping. However, at the same time, nuclear reactor models often exhibit simultaneous presence of dynamics of different speeds. Such behavior leads the mathematical model exhibiting multiple time-scales, which may be susceptible to numerical ill-conditioning.

The work in this thesis begins with derivation of estimation model for flux mapping studies in the AHWR. The nonlinear mathematical model (core neutronics and control rod dynamics equations) is linearized around the steady-state full power operation by

considering a small perturbation in the system and then the equations are cast into standard state-space form. It is characterized by 80 states, 4 inputs and 200 outputs. A keen observation of the eigenvalues of the estimation model reveals that they fall into two distinct clusters. First cluster has 21 eigenvalues consisting of 5 eigenvalues at the origin and the other 16 eigenvalues ranging from -6.2977×10^{-2} to -5.1852×10^{-2} and the second one is of 59 eigenvalues ranging from -4.751×10^{2} to -8.4578. This indicates the presence of two-time-scales in the estimation model. The modern control design and analysis studies with this model are accompanied by serious numerical ill-conditioning problems. In this context approximation of high dimensional system by simplified models or model order reduction is a common procedure in engineering practice. Model order reduction is defined as the problem of finding a simpler mathematical model for a complex large-scale system.

The main intent of model order reduction is to preserve the important dynamic characteristics of the model while certain less important characteristics are ignored. In the past few decades, several analytical model reduction techniques have been proposed for the state-space models. Davison [14] proposed one of the first model reduction technique. The principle of this method is to neglect eigenvalues of the original system which are farthest from the origin and retain only dominant eigenvalues and hence the time constants of the original system in the reduced order model. This implies that the overall behaviour of the reduced-order model will be very similar to that of the original model, since the contribution of unretained eigenvalues are important only at the beginning of the response, whereas the eigenvalues retained are important throughout the whole response. Simultaneously, Marshall [77] developed a technique which preserves the steady-state of the original system by exciting the modes in the reduced model differently from those in the original system.

For the mathematical models involving the interaction of slow and fast dynamics, a method based on decomposition of higher order model into slow and fast systems by two-time-scale methods and singular perturbation analysis [65] has been proposed for

model order reduction. The approach makes use of the standard singularly perturbed form representation of dynamic systems in which the derivatives of some state variables are multiplied with a small positive scalar, ε. The model reduction is achieved by setting $\varepsilon = 0$ and substituting the solution of states whose derivatives were multiplied with ε, in terms of the other state variables. Essentially the singular perturbation approach to order reduction can be related to the "dominant mode" techniques which neglect the high frequency parts and retain low frequency parts of models.

Model order reduction based on the assessment of degree of controllability and observability has been suggested in [81, 94] which is popularly known as balanced truncation. In order to obtain the original system in balanced form, its basis should be transformed into another basis where the states which are difficult to reach are simultaneously difficult to observe. It can be achieved by simultaneously diagonalizing the reachability and the observability gramians [70], which are the solutions respectively to reachability and observability Lyapunov equations. The positive diagonal entries in the order of decreasing values in the diagonal reachability and observability gramians in the new basis are called Hankel singular values of the system. The reduced order model is obtained simply by truncation of the states corresponding to the smallest singular values. The number of states that can be truncated depends on how accurate the approximate model is needed. There are some other techniques to obtain the balanced truncation *viz.*, Schur method [98], balance square root method [132] similar to [81], however, they differ in the algorithms for obtaining the balancing transformation. The aforesaid methods can be efficiently applied when the system is asymptotically stable and minimal, however, for the systems where the stabilization is the major concern their straightforward application is not possible. Balanced truncation for unstable systems has also been attempted in [131]. Usually unstable poles cannot be neglected, therefore model reduction in this situation can be treated by first separating the stable and unstable parts of the model and then reducing the order of the stable part using balanced truncation methods.

For the estimation model of AHWR various model order reduction techniques, *viz.*, Davison's and Marshall's dominant mode retention techniques; balanced truncation technique and model decomposition into slow and fast subsystems based on singular perturbation analysis, have been applied to obtain a reduced order model from the original high order model, and results reported in this thesis.

Application of methods based on retention of dominant modes requires diagonalization. For the estimation model, it is quite difficult task to get the model into diagonal form as there are multiple eigenvalues at the origin of the complex s-plane. This is due to the fact that the model contains slow control rod dynamics. In this thesis, a systematic method has been suggested to handle the numerical ill-conditioning occurring in the computations due to the presence of the slow control rod dynamics by decoupling the higher order model into very slow and fast models. Model order reduction techniques based on Davison's and Marshall's dominant mode retention are then applied to retain the slow dynamics. Finally the reduced order model has been formulated by augmenting the control rod dynamics to the model corresponding to the slow dynamics. Also, it is essential for model order reduction based on Davison's and Marshall's techniques, to identify the modes to retain and those to truncate/reduce.

The distance between two eigenvalue clusters of the estimation model, computed by dividing the largest absolute value of the slow (first) group by the smallest absolute value of the fast (second) group, is $\varepsilon = 0.0074$. This value is small enough to motivate the use of singular perturbation analysis and two-time-scale based techniques [61, 63]. Therefore it would be possible to decompose the model into a slow subsystem of order 21 and a fast subsystem of order 59, by the application of singular perturbation. For carrying out this, a regrouping of states variable has been suggested in the thesis.

Finally, comparative study has also been presented in this thesis from the view point of transient performance between different reduced order models of AHWR, namely, Davison's technique, Marshall's technique, singular perturbation analysis and balanced truncation by comparing their performances relative to each other and with the original

model. All of these methods are found to be effective, however the overall accuracy in the approximation using the balanced truncation approach is found to be far superior.

Among these, Davison's and Marshall's techniques require diagonalization and balanced truncation technique requires a modal decomposition into unstable and stable subsystems. Also, it is essential for model order reduction based on Davison's and Marshall's techniques, to identify the modes to retain and those to truncate/reduce. In contrast, singular perturbation techniques require a decomposition of the state-space systems into fast/slow subsystems using block diagonalization methods. Davison's and Marshall's techniques result into a simplified model that retains the slowly varying dynamics while the application of singular perturbation analysis and two-time-scale methods decompose the model into two subsystems *viz.*, slow and fast, thus providing better approximation of dynamics of the system. Quite similar to this, application of balanced truncation yields a reduced model in which both the slow and fast dynamic characteristics are simultaneously retained yielding good accuracy in approximation of high order model by reduced order model.

The task of flux-mapping in AHWR has been formulated as linear stochastic estimation problem and the solution is obtained by Kalman filtering technique. It utilizes estimation model and available detector measurements corrupted with white Gaussian noise. However, direct implementation of the DKF algorithm to this high-order stiff estimation model is not feasible as the designing procedure is accompanied by serious numerical ill-condition caused by the simultaneous presence of slow and fast phenomena typically present in a nuclear reactor. In particular, the set of recursive equations for computation of DKF gains, as a solution to weighted least squares problem, is ill-conditioned. Consequently, serious numerical difficulties are expected if the DKF gain matrix is to be computed on the basis of the full order Riccati equation. Fortunately, this situation can easily be handled by singular perturbation analysis and two-time-scale methods. This thesis presents a novel technique to address the numerical ill-conditioning problems in full order design by decoupling the DKF equations according to the order

of the slow and fast subsystems. Finally this technique has been applied for estimation of detailed mesh, channel and zonal fluxes in the AHWR.

The effectiveness of the Kalman filtering technique for flux mapping has been examined in three cases. In the first case, decay of non-zero initial condition is observed. The states of the estimation model are non-zero while the reactor is assumed to be at steady–state. In the second, the movement of one or multiple Regulating Rods (RRs) is simulated. Finally in the third case, xenon-induced spatial oscillation is considered. SPND signals (measurements) were generated under the same transient situations from a separate set of off-line computations using a 128 node scheme, for the first two cases, and the 17 node scheme for the third case. Measurement noise of the order of 2 % has been assumed for each SPND. This noise is equivalent to 2 % random fluctuations around the full power steady–state value in each detector. DKF based flux mapping algorithm was processed for the estimation of detailed flux distribution in AHWR for the respective cases. To characterize the performance of DKF, error analysis has been carried out to determine the the Root Mean Square (RMS) error and relative error. The efficacy of the algorithm has been validated from simulations.

The contributions of this thesis are as follows:

1. The monitoring and control of time-varying axial and radial flux distribution in operational large reactors is a challenging problem. Although several researchers addressed the flux mapping problem of the other reactors with various advanced algorithms and methodologies, they have a common disadvantage of failing to take into account the time variation and loss of accuracy in presence of random errors. The algorithm suggested in this report is based on Kalman filtering technique which can take care of both the stated factors.

2. For validation of different techniques of flux mapping, computation results generated using a high fidelity model is a necessity. Hence, a model based on 128-nodes in the core of the AHWR resulting into 1168th order is developed.

3. Different approaches of obtaining reduced order models from the original higher order estimation model of AHWR *viz.*, Davison's, Marshall's, singular perturbation and balanced truncation techniques have been explored to solve the numerical ill-conditioning in control design and analysis.

4. The concept of application of Kalman filtering theory has been extended to the near optimal estimation of core flux distribution in AHWR.

5. A novel technique has been suggested based on two-time-scale formulation of Kalman filtering problem for the time-dependent neutron diffusion equation to near-optimum estimation of the core flux profile in AHWR.

The conclusions from the work are:

- The proposed DKF algorithm can accurately estimate the time dependent neutron flux distribution during the typical reactor operating conditions. The degradation of DKF algorithm accuracy is also very less against the detector random errors. Therefore, the proposed method can serve an effective alternate to the existing flux mapping techniques.

- Before deployment in the AHWR, the efficacy of the technique needs to be established further and it should be demonstrated using plant data, such as from PHWRs that it yields improvement in accuracy compared to that resulting from existing techniques.

- The algorithm should also be assessed from the viewpoint of implementation that the computations could be performed in real-time using hardware and other resources, suitable for control and instrumentation systems in nuclear reactors.

Possible future extension of the work would be:

- A reduced order Kalman filter can be designed based on the simplified model obtained from balanced truncation approach for the estimation of core flux distribution in AHWR.

- Optimality and availability of DKF based flux mapping algorithm can be verified under the faults in some of the SPND signals.

List of Figures

List of Tables

Acronyms

3-D	Three Dimensional
AHWR	Advanced Heavy Water Reactor
DKF	Discrete-time Kalman filter
FEM	Finite Element Method
FLOPS	Floating Point Operations
FMS	Flux Mapping System
FSM	Flux Synthesis Method
ICDH	In-core Detector Housing
MM	Moment Matching
PHWR	Pressurized Heavy Water Reactor
RMS	Root Mean Square
RRS	Reactor Regulating System
RR	Regulating Rod
SPND	Self Powered Neutron Detector
SVD	Singular Value Decomposition

Nomenclature

A_{hk}	Area of interface between nodes h and k
$\mathbf{A}$	System matrix of linear continuous-time
$\mathbf{A}_{11}, \mathbf{A}_{12}, ..etc.$	Submatrices of $\mathbf{A}$
$\mathbf{B}$	Input matrix of linear continuous-time
$\mathbf{B}_1, \mathbf{B}_2$	Submatrices of $\mathbf{B}$
C_h	Concentration of one group delayed neutron precursor in node-h
C_{ih}	Concentration of i^{th} group of delayed neutron precursor in node-h
D_g	Diffusion co-efficient for neutrons of g^{th} enery group
$\boldsymbol{e}$	Error vector
E	Orthogonal similarity transformation
$\mathbf{G}$	State space representation or Transfer function
H_l	%-in position of the l^{th} RR
I	Iodine concentration
$\mathbf{I}$	Identity matrix

J_u	Neutron current density in u
K_h	Multiplication factor in node-h
$\mathbf{K}$	Kalman gain
$\boldsymbol{L}_O, \boldsymbol{L}_R$	*Cholesky factors*
m	number of inputs
m_d	Total number of delayed neutron precrsor groups
n	Original system order
n_1	Order of slow subsystem
n_2	Order of fast subsystem
N_h	Number of all neighbouring nodes to node-h
p	number of outputs
$\mathbf{P}$	Covariance matrix of state estimate
$\mathbf{Q}$	Covariance matrix of process noise
r	Reduced system order
R_h	Ratio of fast neutron flux to the thermal neutron flux in the volume element of node-h
$\mathbf{R}$	Covariance matrix of measurement noise
t	Time variable
$\mathbf{T}$	Similarity transformation
$\mathbf{u}$	Input vector

$\mathbf{U}$	Orthogonal matrix
$\boldsymbol{v}$	Measurement noise vector
V_h	Volume of the node-h
$\boldsymbol{V}$	Modal matrix
$\mathbf{V}$	Orthogonal matrix
$\boldsymbol{w}$	Process noise vector
$\mathbf{W}_O$	*Reachability Gramian*
$\mathbf{W}_R$	*Observability Gramian*
$\mathbf{x}$	State vector of the system
$\hat{\mathbf{x}}$	Estimate of state vector
$\mathbf{x}_k$	State vector of the system in discrete domain at time instant k
X	Xenon concentration
$\mathbf{y}$	Measurement or output vector
$\mathbf{z}$	Modal state vector
Z_p	Total number of nodes present in core region
Z_r	Total number of nodes present in reflector region
β	Effective fraction of delayed neutrons
β_i	Fraction of delayed neutrons of i^{th} group precursor
$\mathbf{\Gamma}$	Input matrix in discrete domain
δ	Deviation from respective steady state value

ℓ	Prompt neutron life-time
ϵ	A small positive parameter
η	Similarity transformation
γ_I	Average fractional yield of Iodine
γ_{Xe}	Average fractional yield of Xenon
κ	Scalar Weighting factor
μ_i	Eigenvalue i
λ_i	Decay constant of ith group of delayed neutron precursors
λ_I	Decay constant of Iodine
λ_X	Decay constant of Xenon
ν	Mean number of fission neutrons
ω	Coupling coefficient between nodes
ω_{hk}	Coupling co-efficient charecterizing leakage of neutrons from node h to k
ϕ	One–group neutron flux
ϕ_g	Neutron flux in energy group-g
$\mathbf{\Phi}$	System matrix in discrete domain (State transition matrix)
ρ_h	Reactivity in node-h
σ	Microscopic cross-section
$\boldsymbol{\sigma}$	Hankel singular value
Σ	Macroscopic cross-section

Σ_{12}	Scattering cross-section from group-1 to group-2
Σ_{21}	Scattering cross-section from group-2 to group-1
Σ_{ag}	Absorption cross-section for energy group-g
Σ_{fg}	Fission cross-section for energy group-g
τ	Sampling period
$\triangle_{hk}$	Center to center distance between volume elements of nodes $h$and k
υ	Mean velocity of neutrons
υ_g	Mean velocity of neutrons in energy group-g
$\boldsymbol{\Psi}$	Output matrix of linear continuous-time
ϑ	Control signal

Operations

$\boldsymbol{\mu}(\mathbf{A})$	Eigenvalues of $\mathbf{A}$
$\mathbf{A}^T$	Transpose of $\mathbf{A}$
$\mathbf{A}^{-1}$	Inverse of $\mathbf{A}$

Superscripts

0	Staeady state value
bal	Balanced system

Subscripts

1	Fast group
2	Slow group

a	Absorption
bal	Balanced system
F	Fast subsystem
f	Fission
G	Core average flux
g	Energy group
I	Iodine
k	Sampling instant k in discrete domain
Q	Quadrant
S	Slow subsystem
s	Stable subsystem
us	Unstable subsystem
V	Volume element
X	Xenon
Z	Fuel channel

Other Notations

$\mathbb{C}$	Complex s plane
$\mathbb{R}$	Real space
$E[.]$	Expected value

Chapter 1

Introduction

Electricity is closely related to the economic development of a country. With the growth in the number of industries utilizing fossil fuels as raw materials for production of electricity, the reserves of fossil fuels *i.e.*, coal, oil and gas are also fast depleting. Diversified energy resource base is essential to meet electricity requirements and to ensure long term energy security with the limited resources of coal and oil available in any country. In the current scenario alternative sources of energy like nuclear power, wind power and solar power can meet the future energy demands of the nation. When compared to other sources of energy, nuclear power has the unique capacity to release huge amount of energy from a very small quantity of active material. The energy liberated during this process is greater than that liberated from the combustion of the same quantity of coal. Moreover, the possible energy reserves in the form of uranium and thorium are many times greater than those of fossil fuels [19].

The concept of nuclear reactors has its origin in the discovery of nuclear fission in 1939. In a nuclear fission, a neutron is bombarded on a heavy nucleus such as ^{235}U and two or more fragments are produced. This reaction has two interesting features. One is the significant amount of kinetic energy (about 200 MeV) of fission fragments which is then converted into heat, and another is: a few (on the average 2 to 3) neutrons are also produced. These facts immediately suggested the possibility of utilizing the emergent

neutrons to cause further fissions in other heavy nuclei and thus to have a self sustained steady fission chain reaction. Such a system, called nuclear reactor, could then act as a steady source of energy. Since the first reactor built by Enrico Fermi in 1942, the field has continuously evolved leading to many complex nuclear reactors of today.

Now the world wide trend is to construct nuclear reactors of large capacity which can be operated with relatively uniform flux distribution. The Indian Nuclear power program today comprises of existing reactors, reactors under construction, and design of future reactors which will provide long term energy security of the country. In 2005, a 540 Mwe Pressurized Heavy Water Reactor (PHWR) is commissioned for large-scale electricity generation. Even a large capacity of 700 MWe PHWR and Advanced Heavy Water Reactor (AHWR) are also under design [119]. They share several similarities in the concept of the pressure tubes and calandria tubes, but the tubes orientation in the AHWR is vertical and horizontal in PHWR [116]. The PHWR utilizes natural uranium as fuel, whereas the AHWR utilizes enriched uranium-thorium, plutonium-thorium mixed oxide fuels. Also, PHWR is non-boiling heavy water moderated reactor, whereas the AHWR is boiling light water cooled, heavy water moderated natural circulation reactor.

From the economic point of view large nuclear reactors reduce the per unit electricity generating cost. Hence, large sized nuclear reactors are preferred to achieve economy in power production. However, large sized reactors show neutronic decoupling [19], *i.e.*, these reactors show deviation in power distribution from the nominal. Commonly used methodology to understand the neutronic decoupling phenomena in nuclear reactors is based on comparison of characteristic size. The characteristic size of the reactor core is expressed in units of neutron migration length M. It is a measure of the average distance travelled by a neutron from its appearance as a fission neutron to its absorption as a thermal neutron. For a given reactor design, M is determined by the material composition of the reactor core, primarily the fuel-to-moderator ratio and is essentially independent of core size R. As the core size increases, the ratio R^2/M^2 increases, the

migration length becomes a smaller fraction of the reactor core dimension. Thus, each neutron's zone of influence becomes a smaller fraction of the core volume, and the various regions of the core turn out to be loosely coupled. Any deliberate attempt to operate the reactor with flattened radial and axial flux distributions coupled with xenon poisoning effect leads to complex operational and control problems [114, 128]. The mechanism of ^{135}Xe production and its removal by neutron absorption and radioactive decay are such that oscillations of thermal flux are induced in large thermal reactors. Such oscillations induced by ^{135}Xe can broadly be classified into two categories - fundamental mode or global power oscillations and higher mode or spatial oscillations. Generally speaking, global power oscillations can be readily noticed and suppressed by control system while spatial oscillations are not. Here, the global reactor power can remain constant so that no change in the coolant outlet temperature is effected, the oscillations being in spatial distribution of power inside the core.

If these oscillations are left uncontrolled, the power density and time rate of change of power at some locations in the reactor core may exceed the respective design limits, resulting into increased chance of fuel failure. Therefore, to maintain the total power and power distribution within the design limits, large reactors are provided with mechanisms for total power control and spatial power control. If due to some hypothetical reason, the spatial control scheme is ineffective, xenon-induced oscillations might occur. These xenon induced spatial oscillations and subsequent local overpower pose a potential threat to the fuel integrity of the reactor. Therefore, monitoring of the axial and the radial flux distribution in the core during the operational condition is crucial. Modern reactors have provisions for online spatial control and monitoring of flux or power distribution during the course of their operation. The three-dimensional (3-D) power distribution is one of the basic operation parameters which can determine many other important parameters such as power peaking factor, and quadrant tilt ratio *etc.*, used to evaluate the operating condition of the reactor and the margin of safety.

In general, the time varying neutron flux distribution in large nuclear reactors is

computed by an online Flux Mapping System (FMS). In-core Self Powered Neutron Detectors (SPNDs) are being increasingly used for continuous monitoring of neutron flux in power reactors. SPNDs, which are placed at strategic locations within the core, can help in successful implementation of both the online FMS and flux tilt control. The in-core SPNDs used for the monitoring purpose can sense the neutron flux only over a small volume. FMS processes the measurement signals of several in-core SPNDs with the help of software routine called flux mapping algorithm and generates detailed 3-D core flux profile. Apart from this, functions such as flow changes in coolant channels, reactivity device movements and ensuring that peaking factors are within analyzed safety limits, are also required in large reactors. These functions are performed from the information about axial, azimuthal and radial flux distributions obtained through in-core SPNDs based FMS. However, these functionalities of online FMS vary from reactor to reactor.

With India's five to six times larger reserves of thorium than that of natural uranium, thorium utilization for large scale energy production has been an important goal of the nuclear power program. The AHWR [119] can provide efficient commercial utilization of thorium and thereby it forms an important milestone in the nuclear power program. The physical dimensions of the core are several times large compared to the neutron migration length. Any operational reactivity disturbance such as online refueling, control rod movements *etc.*, might lead to slow xenon induced oscillations, which might cause changes in axial and radial flux distribution from the nominal distribution. Knowledge of any such changes during the reactor operation is crucial. To monitor the core flux distribution, 200 SPNDs are proposed [1] to be provided in AHWR. An efficient flux mapping algorithm in AHWR can ensure better reactor regulation and core monitoring, as more accurate estimates of channel and zonal powers will be available to Reactor Regulating System (RRS) and Core Monitoring System.

In nuclear reactor two basic sources of information are available for determination of spatial flux distribution. These sources are nominal core specifications alongwith mathematical model and measurements from in-core SPNDs, which combine through

flux mapping algorithms, ultimately to provide power/flux map. However, both these sources are subjected to statistical fluctuations and the mapping accuracy may be degraded. Flux mapping algorithm plays a major role in mapping the 3-D flux distributions from in-core SPNDs. And this knowledge ensures the safe operation of reactor. Therefore, considerable effort has been expanded over the years to evolve an efficient flux mapping algorithm.

Most of the algorithms available today employ the Flux Synthesis Method (FSM), Internal Boundary Condition method and the method based on simultaneous least squares solutions of neutron diffusion and detector response equations [80]. These methods assume that the neutron flux profile in the reactor is independent of time. They fail to account for time variation of neutron flux distribution during the reactor operation. Also, the accuracy of mapping might be degraded considerably in presence of uncertainty in the detector readings. Therefore, some algorithms which can take care of both time varying phenomena and detector random errors become necessary to improve the online computation of core power/flux distribution. In this context state estimation methods like Kalman filter are more promising approach with the availability of the space-time kinetics model which represents the time dependent behavior of the AHWR.

In this thesis, Discrete-time Kalman filter (DKF) formulation for flux mapping in AHWR has been presented. It utilizes the time dependent core neutronics equations and available detector measurements corrupted with white Gaussian noise. However, direct implementation of the DKF algorithm to the high-order stiff estimation model of AHWR is not feasible as the design procedure is accompanied by serious numerical ill-conditioning caused by the simultaneous presence of slow and fast phenomena typically present in a nuclear reactor. In particular, the set of recursive equations for computation of DKF gains, as a solution to weighted least squares problem, is ill-conditioned. Consequently, serious numerical difficulties are expected if the DKF gain matrix is to be computed on the basis of the full order Riccati equation. Therefore, for the AHWR system application of model order reduction techniques, *viz.,* Davison's and Marshall's

dominant mode retention techniques; balanced truncation technique and model decomposition into slow and fast subsystems based on singular perturbation analysis has been explored.

Finally, to address the numerical ill-conditioning, the task of flux mapping problem in AHWR has been formulated as a problem of optimally estimating the time dependent neutron flux at a large number of mesh points in the core. The solution is obtained using the well known Kalman filtering technique which works alongwith a space–time kinetics model of the reactor. However, as stated the attempt to solve the Kalman filtering problem in a straight forward manner is not successful due to severe numerical ill-conditioning caused by the simultaneous presence of slow and fast phenomena, typically present in a nuclear reactor. Hence, a grouping of state variables has been suggested whereby the original high order model of the AHWR is decoupled into a slow subsystem and a fast subsystem. Now according to the order of the slow and fast subsystems, the original time update and Kalman gain equations have also been decoupled into separate sets of equations for the slow and fast subsystems. The decoupled sets of equations could be solved easily. The proposed method has been validated in a number of typical transient situations. Overall accuracy in the estimation using the proposed methodology has been found very good for mesh fluxes, channel fluxes, quadrant fluxes and the core average flux.

Objectives of the Thesis

In large nuclear reactors such as the AHWR, the physical dimensions of the core are very large compared to the neutron migration length. Therefore, operational perturbations might lead to slow xenon induced oscillations, which might cause changes in axial and radial flux distributions from the nominal distribution. Knowledge of any such changes during the reactor operation is crucial and needs to be continuously monitored and displayed to the operator.

This task is accomplished by an online Flux Mapping System, which employs a suitable algorithm to estimate the core flux distribution from the readings of a large number of in-core detectors. Most of the algorithms available today employ the Flux Synthesis method, Internal Boundary Condition method, and the method based on simultaneous least squares solutions of neutron diffusion and detector response equations. A common feature of these methods is the assumption that the neutron flux profile in the reactor is independent of time. An efficient flux-mapping algorithm in AHWR can ensure better reactor regulation and core monitoring, as more accurate estimates of channel and zonal powers will be available to the Reactor Regulating System (RRS) and Core Monitoring System. This thesis proposes a new method of flux mapping. Its main objectives are:

- Development of suitable mathematical model which describes the time-dependent core neutronics behavior of the AHWR core.

- Development of a stringent nonlinear mathematical model for validation of proposed flux mapping algorithm.

- To design an efficient flux mapping algorithm which accounts the time variation of neutron flux distribution as well as random noise in detector readings.

- To investigate the applicability of different types of state observers like Kalman filter for the estimation of 3-D neutron flux distribution.

- Evaluation and application of various model order reduction methods to handle the numerical ill-conditioning that could arise out of existence of multiple time–scales.

- To examine the effectiveness of the proposed algorithm under different operating transients of the reactor.

- To evaluate the efficacy of the proposed technique through simulation data.

Contributions of the Thesis

The contributions of the thesis are as follows:

- The monitoring and control of time-varying axial and radial flux distribution in operational large reactors is a challenging problem. Although, several researchers addressed the flux mapping problem of the other reactors with various advanced algorithms and methodologies, they have a common disadvantage of failing to account the time variation and loss of accuracy in presence of random errors. The algorithm suggested in this report is based on Kalman filtering technique which can take care of both the stated factors.

- For validation of different techniques of flux mapping, computation results generated using a high fidelity model is a necessity. Hence, a model based on 128-nodes in the core of the AHWR resulting into 1168th order is developed.

- Different approaches of obtaining reduced order model from the original higher order estimation model of AHWR *viz.*, Davison's, Marshall's, singular perturbation and balanced truncation techniques have been explored to solve the numerical ill-conditioning in control analysis and design.

- The concept of application of Kalman filtering theory has been extended to the near optimal estimation of core flux distribution in AHWR.

- A novel technique has been suggested based on two-time-scale formulation of Kalman filtering problem for the time-dependent neutron diffusion equation to near-optimum estimation of the core flux profile in the AHWR.

Organization of the Thesis

The objective of this thesis is to design a flux mapping algorithm for computation of neutron flux distribution in large nuclear reactors. For this the proposed DKF based

algorithm has been applied to the AHWR for different test cases and validated. The rest of the thesis is organized as follows. Chapter 2 presents the literature survey on existing flux mapping algorithms, model order reduction, singular perturbation methods in control analysis and design, modeling of nuclear reactors and Kalman filtering theory. In chapter 3, brief review of AHWR core configuration; detailed mathematical modeling; methods for generating steady–state neutron flux distribution and reconstruction techniques are given. In chapter 4, theory of model order reduction and algorithmic approach for some of the model order reduction techniques are presented. In chapter 5, comparative study of different reduced order models of the AHWR has been presented. In chapter 6, a two-time-scale approach for discrete-time Kalman filter has been presented to solve the numerical ill-conditioning occurred in design for computation of 3-D flux neutron distribution. Its validation has also been illustrated with numerical and graphical results for the AHWR. Chapter-7 draws the important conclusions from the work and presents the future scope.

Chapter 2

Literature Survey

This chapter presents the literature survey of various techniques on flux mapping algorithms, model order reduction techniques, singular perturbations and two-time-scale methods for design and analysis, modeling of nuclear reactors and theory of Kalman filter. However, this survey is not intended to be exhaustive.

2.1 Flux Mapping Algorithms

Flux mapping algorithms play fundamental role in generating the 3-D neutron flux distribution from readings of in-core SPNDs. The knowledge of 3-D flux distribution ensures the safe operation of reactor. In CANDU-6 reactors and in Indian 540 MWe Pressurized Heavy Water Reactors (PHWR), 102 Vanadium detectors are used for flux mapping, while in PWRs it is carried out by Rhodium detectors installed in about 45 fuel assemblies. Over the years, research has been carried out to evolve an efficient flux mapping algorithm for the improvement of accuracy in flux mapping with less computational effort. Most of the algorithms existing in the literature are based on three principles, namely the Flux Synthesis, Internal boundary condition and simultaneous least squares solution of neutron diffusion and detector response equations.

The most popular and traditional method for flux mapping is known as FSM [46].

It uses the available detector measurements and performs least squares fit with pre-computed flux modes, determined based on reactivity devices configuration. Determination of flux modes requires the knowledge of core configuration and considerable insight into the reactor operation. There are other synthesis methods such as Harmonic Synthesis Method (HSM) [27, 95] and Harmonic Expansion Method (HEM) [133] to improve the accuracy of flux mapping, however the accuracy of reconstruction depends on selection of the reference case. Selection of a suitable reference case which reflects the actual core condition results in improvement of the reconstruction accuracy. During the core configuration changes, the reference case has to be renewed, which can be a time consuming process.

A method based on direct online solution of neutron diffusion equations with detector readings as the internal boundary condition is reported in [52, 59]. A method which obtains a least squares solution of the core neutronics design equations alongwith the in-core detector response equations is reported in [23, 47, 71]. Applicability of this least squares method requires to solve the overdetermined system of equations resulting in the framework of mapping algorithm. Another approach with the combination of FSM and least squares method, known as modified flux synthesis method has been proposed for Indian 700 MWe PHWR in [80]. This method takes longer computation time than FSM does [47] and detector signal uncertainty can also deteriorate the performance of flux mapping calculations. Several other approaches for flux mapping have also been proposed. Among them a few are: Rational mapping [7], Statistical framework based on Kalman filter and maximum likelihood estimation techniques [8], combination of harmonic synthesis and least squares approach [136], ordinary krigging method [92], *etc.*

As already stated, the traditional FSM method and other synthesis methods such as HEM, HSM, etc., have some inherent deficiencies such as pre-computation of flux modes requiring detailed knowledge about the core configuration, considerable insight into the reactor operation, and selection of the reference case, which needs to be renewed. Therefore, they may not be feasible for on-line monitoring. They cannot calculate the

time dependent neutron flux distribution during the reactor operation and the accuracy might be degraded considerably in presence of uncertainty in the detector readings. Hence, a new algorithm which does not require pre-computation of flux modes, and which accounts for the time variation as well as random noise in detector measurements would be an attractive alternative.

With this motivation we have attempted Discrete-time Kalman filter (DKF) formulation for flux mapping which is quite different from the existing methods as it can take care of both time varying phenomena and random errors in the detector readings.

2.2 Model Order Reduction

Description of large-scale systems by mathematical models involves a set of differential or difference equations. These models can be used to simulate the system response and predict the behavior. Sometimes, these mathematical models are also used to modify or control the system behavior to conform with certain desired performance. In practical control engineering applications with the increase in need for improved accuracy these mathematical models lead to high order and complexity [2]. In many situations, high-order, complex mathematical models accurately represent the problem at hand, but are unsuitable for the desired application; for instance, for analysis, optimization or for control design. Ideally, control engineer would like to develop a model with low number of states but it should capture the system dynamics accurately over a range of frequencies and forcing inputs.

On the other hand, well established modern control concepts which are valid for any system order may not give fruitful control algorithms in control design. Moreover, working with very high order, high-fidelity model involves computational complexity and need for high storage capability. Sometimes, the presence of small time constants, masses, *etc.* may give rise to an interaction among slow and fast dynamic phenomena with attendant ill-conditioning or stiff numerical problems [65]. When analyzing and

controlling these large–scale dynamic systems, it is extremely important to look for and to rely upon efficient simplified reduced order models which capture the main features of the full order complex model.

In control engineering, model order reduction techniques are fundamental both to facilitate the design of controller/observer where particular numerically heavy procedures are involved (optimal control, adaptive control, H-infinity based methodologies, filtering techniques), and to obtain low-order controllers with which to reduce hardware requirements. In fact, from a high-order model, a low-order model must be obtained so as to be able to design a low-order controller/observer.

An overview of model order reduction methods across the broad spectrum of approaches indicates the following scenarios. There are different approaches for model order reduction of large-scale systems, the major difference being the representation/domain of the model: either frequency or time. All the model order reduction techniques provide high fidelity, low-order models, which are used for the modern control design applications. The model reduction techniques differ from one another by the type of model used for approximation, whether it belongs to frequency domain or time domain. However, this may not be crucial since it is easy to change the model representation domain.

The main reasons for obtaining low-order models are as follows [25]:

1. To have low-order models so as to simplify the understanding of a system.

2. To reduce computational efforts in simulation problems.

3. To decrease computational efforts and so make the design of the controller/observer numerically more efficient.

4. To obtain simpler control laws and simple control structure.

The model order reduction philosophy is a common procedure in engineering practice. The concept originated way back in 1892 with the introduction of Padé approxi-

mation but the interest of researchers was spurred only after the work of Rosenbrock on distillation columns [97].

In the last five decades considerable attention was devoted to the problem of deriving reduced-order models for complex large-scale systems, without any reference to particular system structure (MIMO-SISO). Davison [14] proposed one of the first model reduction techniques. The principle of this method is to neglect eigenvalues of the original system which are farthest from the origin and retains only dominant eigenvalues. Hence, the time constants of the original system will be in the reduced order model. This implies that the overall behavior of the reduced-order model will be very much similar to the original model. Because, the contribution of unretained eigenvalues are important only at the beginning of the response, whereas the eigenvalues retained are important throughout the whole response. As pointed out subsequently by Chidambara [17], the method does not provide for steady-state agreement between the dominant state variables of the original and reduced models. Further arguments of Chidambara and Davison [15, 16] led to several variations of Davison's original approach: Chidambara's first method, Chidambara's second method and Davison's 'first-modified' method. Later, Davison [18] proposed 'second-modified' method. Simultaneously, Marshall [77] developed a technique which preserves the steady-state of the original system by exciting the modes in the reduced model differently from those in the original system.

Aoki [3] proposed another systematic method to approximate the large-scale dynamic systems by generalizing the concept of aggregation. Further, Siret *et al.* [120] proposed an algorithm for obtaining the best possible approximate model by minimizing the error criterion which results in optimal aggregation matrix as the solution of linear matrix equation. Later, Fossard [26] proposed a modification to Davison's original method which ensures both initial and final (steady-state) agreement between the original and reduced models. Several additional techniques have been developed later and the review paper of Genesio and Milanese [35] indicates all the techniques. However, they represent

minor extensions to one or another of the procedures mentioned above.

It is of central concern to determine the number and choice of modes to be retained in the reduced order model. However, aforesaid methods did not provide any information on selection of eigenvalues to be retained. Therefore, attempts in this direction have been made to select the size of the reduced order model using reduction techniques: Davison, Marshall, and Chidambara where satisfactory dynamic and steady-state responses are desired. Mahapatra [74, 75], Iwai and Kubo [51], Elrazaz and Sinha [20], Enright and Kamel [22], Litz [73], Gopal *et al.* [39] proposed various modal techniques. These methods are optimal in the sense that the integral of the square of the errors between the dominant state variables in the original and approximate models is minimized.

For the state-space models, another model reduction scheme based on the assessment of degree of reachability and observability, which is well grounded in theory and most commonly used is the so-called balanced truncation first introduced by Mullis and Roberts [82] and later extended to systems and control literature by Moore [81]. In order to obtain the original system in balanced form [94], its basis should be transformed into another basis where the states which are difficult to reach are difficult to observe. It can be achieved by simultaneously diagonalizing the reachability and the observability Gramians [70], which are the solution to reachability and observability Lyapunov equations. The positive decreasing diagonal entries in the diagonal reachability and observability Gramians in the new basis are called Hankel singular values of the system. The reduced order model is obtained simply by truncation of the states corresponding to the smallest singular values. The number of states that can be truncated depends on how accurate the approximate model is needed. There are some other techniques to obtain the balanced truncation *viz.*, optimal Hankel norm approximation [38], Schur method [98], balanced square root method [132] similar to [81], however, they differ in the algorithms to obtain the balancing transformation.

The aforesaid methods can be efficiently applied when the system is asymptotically stable and minimal, however, for the systems where the stabilization is the major concern their straightforward application is not possible. Balanced truncation for stable nonminimal systems has been attempted in [131]. Balanced truncation for unstable systems has also been attempted in [5, 57, 99]. Usually unstable poles cannot be neglected, therefore model reduction in this situation can be treated by first separating the stable and unstable parts of the model and then reducing the order of the stable part using balanced truncation methods. Pertinent literature survey on balanced truncation methods and obtaining balanced transformation procedure can be found in [2, 5, 42, 93]. Balanced truncation is probably the most popular projection and Singular Value Decomposition (SVD) based method. Moment Matching (MM), known as Krylov Methods, such as Lanczos method, Arnoldi method, *etc.*, combination of SVD and MM, known as SVD-Krylov Methods are also available for model order reduction. A good review of these methods has been presented in [2]. Enns [21] has extended the balanced truncation scheme to the frequency weighted case by modifying the controllability/observability Gramians to reflect the presence of the input/output weights. A review of frequency weighted balanced model reduction techniques has been presented in [36].

In frequency domain approach also, several methods have been reported for model order reduction. Among them, the important methods are Padé approximations [106], Routh approximations [49], moment matching techniques, Padé and modal analysis [107], continued fraction [10], and combination of Routh stability criterion and Padé approximation [108]. Other contributions for model order reduction of discrete time models can be found such as continued fraction/Padé approach [45, 105], LMI based approaches [40], multi-point continued fraction and Padé approximations [72], stability preserving methods [11, 109], optimal approaches [45]. A good review on the available techniques can also be found in [2, 25, 89, 121, 128].

2.3 Singular Perturbation Theory and Time–Scale Methods

Singular perturbation theory/techniques have been a traditional tool of fluid dynamics the modeling, analysis and design of control systems [60]. Their use has spread to other areas of mathematical physics and engineering, where the same terminology of "boundary layers" and "inner" and "outer" matched asymptotic expansions continued to be used. In control systems, boundary layers are a characteristic of system's two-time scale behavior. They appear as initial and terminal "fast transients" of state trajectories and represent the "high-frequency" parts of the system response. High-frequency and low-frequency models of dynamical systems such as electrical circuits *etc.*, which have had a long history of their own, are naturally incorporated in the time-scale methodology. Singular perturbation theory also includes diverse problem-specific applications. For robotic manipulators, the slow manifold approach has been employed to separately design the slow (rigid system) dynamics and the fast (flexible) transients. Electric machines, power systems and nuclear reactor systems have been the areas of major applications of multi-time scale methods for aggregate (reduced order) modeling and transient stability studies. Singular perturbations are continue to be among the frequently used tools in nuclear reactor kinetics and also in flight dynamics *etc.*

The versatility of singular perturbation methods is due to their use of time–scale properties, common to both linear and nonlinear systems. However, this survey reviews the most special class of linear dynamical systems which are known as singularly perturbed systems. These are characterized by the presence of slow and fast variables, in the dynamics of many real–time systems such as power systems, nuclear reactor *etc.* Mathematically, the slow and fast phenomena are characterized by small and large time constants, or by system eigenvalues that are clustered into two disjoint sets. The slow system variables corresponds to the set of eigenvalues closer to the imaginary axis, and the fast system variables are represented by the set of eigenvalues that are far from the

imaginary axis.

Singular perturbations and time–scale techniques were introduced to control engineering in the late 1960s and have since become common tools for modeling, analysis and design of control systems for a variety of applications including state feedback, output feedback, Kalman filter and observer design. These techniques were first applied to optimal control and regulator design by Kokotovic *et.al.* [66]. Modeling of singularly perturbed continuous and discrete–time systems is presented in [125]. Singularly perturbed systems and time-scale methods have been studied extensively in last five decades [60, 62, 64]. Survey of singular perturbations and time scale methods in control theory and applications prior to 2001 has been presented in [65, 87, 102]. A more recent review of singular perturbations and time-scale methods in control theory and applications such as optimal control, robust control, fuzzy control, network control, H_2/H_∞ control, stability analysis, numerical algorithms and other control problems during the period 2002-2014 has been presented in [135].

Singular perturbation methods are also useful for model order reduction. The order reduction procedure and its validation for both linear and nonlinear systems can be found in [65]. The approach makes use of the standard singularly perturbed form representation of dynamic systems in which the derivatives of some state variables are multiplied with a small positive scalar, ε. The model reduction is achieved by setting $\varepsilon = 0$ and substituting the solution of states whose derivatives were multiplied with ε, in terms of the other state variables. Essentially the singular perturbation approach to order reduction can be related to the "dominant mode" technique [14, 15, 16, 17, 18, 77] which neglect the "high frequency" parts and retain "low frequency" parts of models. In application, models of physical systems are put in the standard singularly perturbed form by expressing small time constants, small masses, large gains, *etc.*, in terms of ε. In power system models, ε can represent machine reactances or transients in voltage regulators; in industrial control systems it may represent time constants of drives and actuators; and in nuclear reactor models it is due to prompt neutrons [128]. Singular

perturbations are extensively used in aircraft and rocket flight models and in chemical reaction diffusion theory. Many order reduction techniques can be interpreted as singular perturbations [48, 104]. An alternate approach for the study of singularly perturbed linear systems with multi parameters and multi–time scales is given by Ladde *et.al.* [68, 69]. Detailed exposition of applications of singular perturbation analysis and time–scale methods in various fields has been given in [87].

Explicit decoupling transformations play very important role in the singularly perturbed systems containing small parameters. Under certain, usually very mild conditions, these transformations allow the linear system decomposition into independent two reduced-order subsystems *viz.* slow and fast. The decoupling transformation for linear singularly perturbed continuous–time varying systems is introduced in [9]. Recursive methods for linear singularly perturbed continuous–time invariant systems are presented in [12, 32, 63] and for discrete–time systems in [76] , in the spirit of parallel and distributed computations and parallel processing of information in terms of reduced order, independent, approximate slow and fast filters. These recursive techniques are also applicable to almost all areas of optimal control theory, in context of continuous and discrete–time, deterministic and stochastic singularly perturbed systems.

The procedure used for the time–scale decomposition of the algebraic Riccati equation into pure-slow and pure-fast algebraic Riccati equations facilitates a new insight into optimal filtering and control problems of linear systems [29]. The filtering problem for linear singularly perturbed continuous-time systems has been well documented in control theory literature [28, 32, 43, 44, 58, 62]. In [43, 44], a sub optimal slow and fast Kalman filters were constructed for the estimates of the state trajectories. In [32, 58], both the slow and fast Kalman filters are obtained using Taylor series [58] or fixed-point iterations [28] to calculate the corresponding filter parameters. The singularly perturbed discrete–time Kalman filter has been studied in [31, 55, 96]. The approaches presented in [55, 96] are based on the power series expansion. The recursive approach presented in [31], based on fixed-point iterations to the discrete-time filtering of singularly perturbed

systems achieves high accuracy for estimation. However, slow and fast filters are driven by the innovation process so that the additional communication channels have to be used in order to construct the innovation process. The results presented in [31] have been improved in [30] by deriving the pure-slow and pure-fast, reduced order, independent Kalman filter driven by system measurements. The method presented in [30] is based on exact decomposition of the global singularly perturbed algebraic filter Riccati equation into the pure-slow and pure-fast local algebraic filter Riccati equations.

It is well known that physical systems like nuclear reactor exhibit simultaneous dynamics of different speeds. Model decomposition based on singular perturbation and time–scale methods for controller design for reactors have also been applied for PHWR in [129, 130] and for AHWR in [83, 84, 85, 111, 112]. Singular perturbation methods in Kalman filter design are reported in [55, 67, 90, 96, 110].

2.4 Modeling of Nuclear Reactors

Large sized nuclear reactors are preferred to achieve economic power production. However, large sized reactors may show spatial instability [114, 128], *i.e.*, these reactors experience deviation in power distribution under certain transients. Their characteristics also change with fuel burn-up and operating power level. Therefore, analysis and control of neutron flux variation with respect to time within the reactor core is required. Usually, the variations are associated with long or short term changes induced by natural perturbations or imposed transients. For the analysis and control of the reactor under these transients and for ensuring safety and economy of operation, mathematical models need to be developed.

Nuclear reactors of small and medium size are generally described by the point-kinetics model, which characterizes every point in the reactor by an amplitude factor and a time dependent spatial shape function [37]. A major limitation of this model is that it cannot provide any information about the spatial flux/power distribution inside the

reactor core, and it is not valid in case of large reactors because the flux shape undergoes appreciable variation with time. Therefore, explicit consideration of the variation of the flux shape becomes necessary.

The central problem in analysis of large nuclear reactors is the determination of the spatial flux and power distribution in the reactor core under steady-state as well as transient operating conditions. There is, however, a considerable variation in the degree of accuracy and spatial details of the power distribution required in different facets of reactor analysis and design. Basically, the behavior of neutrons in a nuclear reactor is adequately described by the time-dependent Boltzmann transport equation [19]. However, numerical solutions of the coupled time-dependent transport and delayed neutron precursor's equations for reactor kinetics problems of practical interest are prohibitively difficult. So, approximate methods using the time-dependent group diffusion equations are employed. These methods can broadly be classified as space-time factorization methods, modal methods and direct methods [124].

Space–time factorization methods involve a factorization of the space and time dependent flux into a product of two parts. One part, called amplitude function, depends only on the time variable whereas the second part, called shape function, includes all of the space and energy dependence and is only weakly dependent on time [50, 91].

Modal methods, on the other hand, utilize an expansion of the flux in terms of precomputed time-independent spatial distributions through a set of time-dependent group expansion coefficients [123]. Another class of spatial methods called synthesis methods, which are almost equivalent to modal methods, are also prevalent. These methods use expansion functions that are static solutions of the diffusion equation for some specified set of initial conditions. Synthesis methods can often yield acceptable accuracy with a smaller number of expansion functions. However, selection of expansion functions for synthesis methods requires considerable experience.

Direct space–time methods solve the time-dependent group diffusion equations by partitioning the reactor spatial domain into a finite number of elemental volumes,

thereby obtaining spatially discretized forms of the coupled diffusion and delayed neutron precursors equations. Direct methods are further classified as finite difference methods, coarse-mesh methods and nodal methods [124]. In each of these methods, the reactor spatial domain is discretized by superimposing a computational mesh and the material properties are treated as uniform within each mesh box. Another method is the Finite Element Method (FEM) in which the group flux is approximated as the sum of multi-dimensional polynomials that are identically zero everywhere outside some elemental volume, or as higher order polynomials thereof [41].

Application of FEM and finite difference methods requires a relatively fine mesh to ensure accuracy, which makes them computationally intensive. On the contrary, coarse-mesh methods assume that the reactor may be adequately described by a model consisting of homogeneous regions that are relatively large. Determination of the multi-dimensional flux distribution within a mesh box is an integral part of the solution process.

Like coarse-mesh methods, nodal methods also consider the division of the reactor core into relatively large, non-overlapping nodes. However, direct results of the solution process are often the node averaged fluxes. These methods generally demand additional relationships between the face averaged currents and the node averaged fluxes, often denoted as coupling parameters. The coupling parameters can be obtained from accurate reference calculations to relate the node interface averaged currents to the node averaged fluxes [56]. A nodal model with finite difference approximation of multi-group diffusion equation has been developed for PHWR [128].

AHWR is a large nuclear reactor which requires a space–time kinetics model for accurate representation of the time dependent neutron flux behavior. In [116], a nodal model for AHWR, which exhibits all the essential control related properties and yields accurate response characteristics is developed. The same model is reformulated in terms of neutron flux equations in [101]. This model is more suitable for flux distribution studies in AHWR owing to its simplicity and structure, thus facilitating selection of state variables for the system in a straightforward manner. Nodal methods have been

used extensively for the analysis and simulation of Light Water Reactors and control system design of PHWR [126, 128]. Nodal methods have also been used for designing advanced controllers for AHWR [85, 111, 112, 115].

2.5 State Estimation and Theory of Kalman Filtering

Many real–time processes require to measure a large number of system state variables so as to own a sufficient quantity and quality of information on the system state and to ensure the required level of performance. However, the measurement of such a large number of physical states may not desirable as it indirectly decreases the reliability of the system and measurement of some physical states may not be possible directly. Sometimes, number of measurements are also limited to keep the failure rate minimum and to increase the reliability of the system. In this context, state estimation theory has played a major role in many applications, including without being exhaustive, trajectory estimation, state prediction for control or diagnosis, data merging and so on.

The state of a dynamical system is a set of variables that provide a complete representation of the internal condition or status of the system at a given instant of time [117]. When the state is known, the evolution of the system can be predicted if the excitations are known. Another way to say the same is that the state consists of system variables that prescribe the initial condition. When a model of the physical system is available, its dynamic behavior can be estimated for a given input by solving the dynamical equations. However, if the physical system is subjected to unknown disturbances and is partially instrumented, the response at the unmeasured degrees of freedom is obtained using state estimation. It is applicable to virtually all areas of engineering and science. Any discipline that is concerned with the mathematical modeling of its systems is a likely (perhaps inevitable) candidate for state estimation. This includes electri-

cal engineering, mechanical engineering, chemical engineering, aerospace engineering, robotics, economics, ecology, biology, and many others. The possible applications of state estimation theory are limited only by the engineer's imagination, which is why state estimation has become such a widely researched and applied discipline in the past few decades.

Estimation is the process of extracting information from all the data: data which can be used to infer the desired information and may contain errors. Modern estimation methods use known relationships to compute desired information from the measurements, taking account of measurement errors, the effects of disturbances and control actions on the system, and prior knowledge of the information. Diverse measurements can be blended to form "best" estimates, and information which is unavailable for measurement can be approximated in an optimal fashion [34].

The theory of state estimation originated with least squares method essentially established by the early 1800s with the work of Gauss [33]. The mathematical framework of modern theory of state estimation originated with the work of Wiener in the late 1940s, [134]. The field began to mature in the 1960's and 1970's after a milestone contribution was offered by R. E. Kalman in 1960 [53], which is very well-known as the Kalman filter. The Kalman filter is a recursive data processing algorithm, which gives the optimal state estimates of the systems that are subjected to stationary stochastic disturbances with known covariances.

Kalman filtering is an optimal state estimation process applied to a dynamical system that involves random perturbations. More precisely, the Kalman filter gives a linear, unbiased, and minimum error variance recursive algorithm to optimally estimate the unknown state of a dynamic system from noisy data taken at discrete-time intervals. It has been widely used in many industrial applications such as tracking systems, satellite navigation, and ballistic missile trajectory estimation *etc.* With the recent advances in high speed computing technology, DKF has become more useful for real-time complex applications. Some applications of Kalman filter to nuclear reactor systems can be found

in [6, 79].

The derivations for the Kalman filter and required mathematical background have been presented many times in the literature [34, 78, 117, 122]. Instead of reiterating these derivations, the basic algorithm has been presented in a later chapter.

2.5.1 Numerical ill-conditioning in Kalman Filters

Kalman filter design for high dimensional systems having interaction phenomena of slow and fast dynamics tends to suffer from numerical ill-conditioning [127]. Least squares problem generally gives rise to particularly ill-conditioned matrix inversion problems. Considering that Kalman filter is simply a recursive solution to a certain weighted least squares problem, it is not surprising that Kalman filter tends to be ill-conditioned. An awareness of ill-conditioning of Kalman filter was achieved after the nontrivial applications of [24] and [103]. Fine exposition of this computational difficulty has been given in [54] and detailed discussion has been given in [13].

Chapter 3

Mathematical modeling of Advanced Heavy Water Reactor

3.1 Brief description of the AHWR

In India, the AHWR is being designed to utilize the large amounts of thorium reserves with the objective of commercial power generation to provide the long term energy security of the nation [119]. Thorium in its natural state does not contain any fissile isotope as uranium does, therefore the AHWR utilizes enriched mixed oxide fuels such as uranium-thorium and plutonium-thorium. The current design of the AHWR is of 920 MW (thermal), vertical, pressure tube type, heavy water moderated and boiling light water cooled thermal reactor. Its core is surrounded by a low pressure reactor–vessel called calandria containing heavy water which acts as moderator and reflector. It relies on removal of the heat generated in the fuel by natural circulation of the coolant.

The AHWR is much like the PHWR, in that they share similarities in the concept of the pressure tubes and calandria tubes, but the tube's orientation in the AHWR is vertical, unlike that of the PHWR. The reactor design incorporates advanced technologies, together with several proven positive features of Indian PHWRs. These features include pressure tube type design, low pressure moderator, on-power refueling, diverse

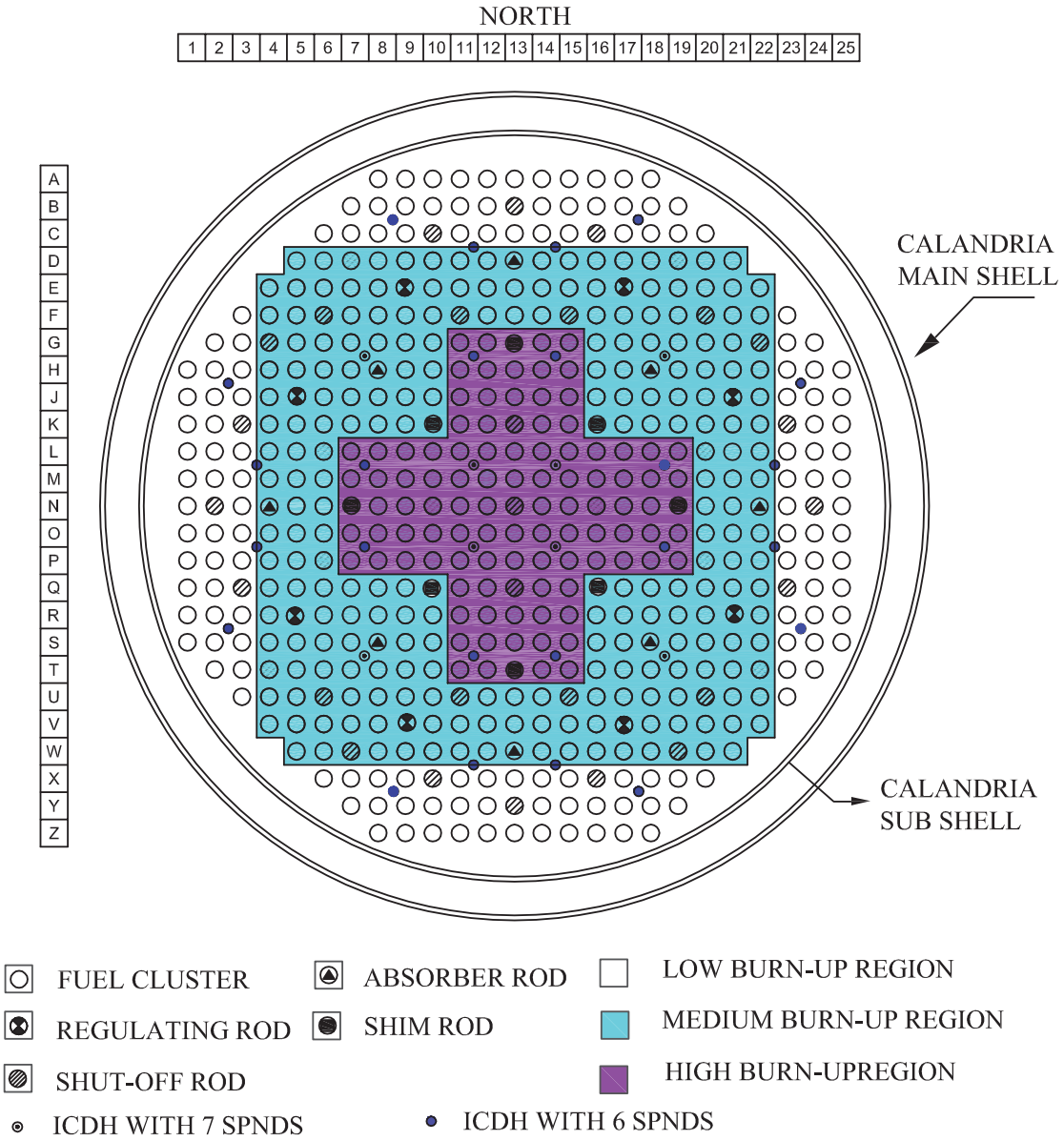

Figure 3.1: AHWR Core with reactivity devices and ICDH Locations

fast acting shut-down systems, and availability of a large low temperature heat sink around the reactor core. The AHWR incorporates several passive safety features. These include: Core heat removal through natural circulation; direct injection of emergency core coolant system (ECCS) water in fuel; and the availability of a large inventory of borated water in overhead gravity-driven water pool (GDWP) to facilitate sustenance of core decay heat removal.

The active core region of the AHWR is radially divided into three regions, with

Table 3.1: Dimensional details of the AHWR core

S.No	Aspect	Dimension (mm)
1	Lattice pitch in the core region	225
2	Active core height	3500
3	Reflector thickness (D_2O)–axial	750
4	Reflector thickness (D_2O)–radial	600
5	Inner diameter of the main shell of Calandria	6900
6	Inner diameter of the sub-shell of Calandria	6300
7	Inner diameter of Pressure tube	120
8	Outer diameter of Calandria tube	168

burn–up decreasing towards the periphery of the core and has 513 lattice locations. Out of these, 452 are occupied by fuel assemblies and the remaining 61 by control rods. These control rods include: 8 Regulating Rods (RRs), 8 Absorber Rods (ARs) and 8 Shim rods (SRs); and 37 shut-off rods. RRs are used to regulate the rate of nuclear fission, ARs and SRs, fully inside and outside the core respectively are used to meet the reactivity demands beyond the worth of RRs. Dimensional details of AHWR core are given in the Table 3.1. Fig. 3.1 shows the lattice layout of AHWR in which various control rods, burn-up regions, fuel elements and neutron detector locations are shown.

The large radial dimensions turn the neutronic behavior of the AHWR core to be loosely coupled due to which a serious situation called 'flux-tilt' may arise followed by operational perturbations. These operational perturbations might lead to slow xenon-induced oscillations, which might cause changes in axial and radial flux distribution from the nominal distribution. An online FMS is provided in AHWR for the purpose of monitoring spatial transients due to on-power refueling operations and reactivity device movements. To monitor the time varying flux distribution in the reactor core 200 SPNDs are proposed to be provided [1]. In–Core Detector housings (ICDHs) located at 32 inter–lattice locations, accommodate these SPNDs which are used for thermal neutron flux measurements. These locations are selected so as to obtain the maximum sensitivity of the flux mapping, *i.e.*, peaks of significant harmonics. Each ICDH oriented vertically and surrounded by four fuel channels inside the calandria houses the 200 SPNDs. These

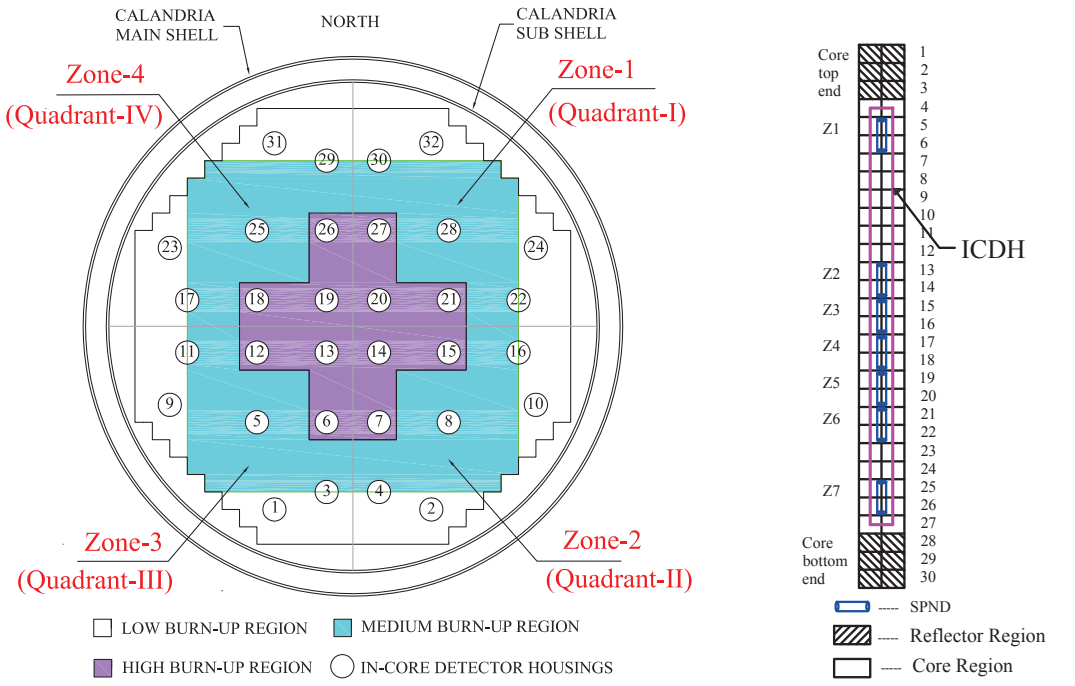

(a) AHWR Core layout with ICDH Locations

(b) Placement of SPNDs in ICDH

Figure 3.2: AHWR core layout (schematic).

SPNDs are placed at different elevations of the assembly covering entire AHWR core from top to bottom. Fig. 3.2 (a) shows the layout of AHWR core. Fig. 3.2 (b) shows the housing of 7 detectors in one of those intra-lattice locations, in which $Z_1, Z_2, \ldots, Z_7$ indicate the locations where SPNDs have been proposed to be placed. Placement of 200 SPNDs is given in Table 3.2.

The measurement signals of these SPNDs are processed by online FMS with the help of flux mapping algorithm to generate the detailed 3-D flux map, which helps for spatial control purpose. An efficient flux mapping algorithm in the AHWR can ensure better reactor regulation and core monitoring, as more accurate estimates of channel and zonal powers will be available to RRS and Core Monitoring System. In this thesis, model based estimation method has been proposed using Kalman filtering algorithm for the design of flux mapping algorithm. For this, suitable mathematical model which represents the time-dependent core neutronics behavior of AHWR core is derived in the following section.

Table 3.2: Placement of 200 SPNDs in 32 ICDHs [100]

ICDH No.	**Layer No.**							**No. of SPNDs**
	Z1	**Z2**	**Z3**	**Z4**	**Z5**	**Z6**	**Z7**	
1	D_1	-	D_{41}	D_{73}	D_{105}	D_{137}	D_{169}	6
2	D_2	-	D_{42}	D_{74}	D_{106}	D_{138}	D_{170}	6
3	D_3	-	D_{43}	D_{75}	D_{107}	D_{139}	D_{171}	6
4	D_4	-	D_{44}	D_{76}	D_{108}	D_{140}	D_{172}	6
5	D_5	D_{33}	D_{45}	D_{77}	D_{109}	D_{141}	D_{173}	7
6	D_6	-	D_{46}	D_{78}	D_{110}	D_{142}	D_{174}	6
7	D_7	-	D_{47}	D_{79}	D_{111}	D_{143}	D_{175}	6
8	D_8	D_{34}	D_{48}	D_{80}	D_{112}	D_{144}	D_{176}	7
9	D_9	-	D_{49}	D_{81}	D_{113}	D_{145}	D_{177}	6
10	D_{10}	-	D_{50}	D_{82}	D_{114}	D_{146}	D_{178}	6
11	D_{11}	-	D_{51}	D_{83}	D_{115}	D_{147}	D_{179}	6
12	D_{12}	-	D_{52}	D_{84}	D_{116}	D_{148}	D_{180}	6
13	D_{13}	D_{35}	D_{53}	D_{85}	D_{117}	D_{149}	D_{181}	7
14	D_{14}	D_{36}	D_{54}	D_{86}	D_{118}	D_{150}	D_{182}	7
15	D_{15}	-	D_{55}	D_{87}	D_{119}	D_{151}	D_{183}	6
16	D_{16}	-	D_{56}	D_{88}	D_{120}	D_{152}	D_{184}	6
17	D_{17}	-	D_{57}	D_{89}	D_{121}	D_{153}	D_{185}	6
18	D_{18}	-	D_{58}	D_{90}	D_{122}	D_{154}	D_{186}	6
19	D_{19}	D_{37}	D_{59}	D_{91}	D_{123}	D_{155}	D_{187}	7
20	D_{20}	D_{38}	D_{60}	D_{92}	D_{124}	D_{156}	D_{188}	7
21	D_{21}	-	D_{61}	D_{93}	D_{125}	D_{157}	D_{189}	6
22	D_{22}	-	D_{62}	D_{94}	D_{126}	D_{158}	D_{190}	6
23	D_{23}	-	D_{63}	D_{95}	D_{127}	D_{159}	D_{191}	6
24	D_{24}	-	D_{64}	D_{96}	D_{128}	D_{160}	D_{192}	6
25	D_{25}	D_{39}	D_{64}	D_{97}	D_{129}	D_{161}	D_{193}	7
26	D_{26}	-	D_{66}	D_{98}	D_{130}	D_{162}	D_{194}	6
27	D_{27}	-	D_{67}	D_{99}	D_{131}	D_{163}	D_{195}	6
28	D_{28}	D_{40}	D_{68}	D_{100}	D_{132}	D_{164}	D_{196}	7
29	D_{29}	-	D_{69}	D_{101}	D_{133}	D_{165}	D_{197}	6
30	D_{30}	-	D_{70}	D_{102}	D_{134}	D_{166}	D_{198}	6
31	D_{31}	-	D_{71}	D_{103}	D_{135}	D_{167}	D_{199}	6
32	D_{32}	-	D_{72}	D_{104}	D_{136}	D_{168}	D_{200}	6

3.2 Space–time kinetics modeling of AHWR

The central problem in the reactor analysis is the determination of the spatial flux and power distribution in the reactor core under steady–state as well as transient operating conditions as these minute details have significant importance in reactor control. The first and foremost difficulty in operation and control of large thermal nuclear reactors such as the AHWR is the development of suitable mathematical model for analysis. As already stated, reactors with small core size are adequately represented by the well-known point kinetics model. In large reactor core, the flux shape undergoes nonuniform variations which the point kinetics model fails to capture.

The behavior of neutrons in the reactor is adequately described by the time–dependent Boltzman transport equation. However, the numerical solution of the coupled time–dependent transport and delayed neutron precursor's equations for reactor kinetics studies may not be feasible. In recent times, multi-point kinetics or nodal models have been extensively used for the analysis and simulation of Light Water Reactors and control design of large thermal reactors such as the PHWR and AHWR. In the following subsections, a reasonably accurate space–time kinetics model which describes the time–dependent neutronics behavior of the AHWR core has been derived. It can be used for the purpose of estimation of neutron flux using DKF based flux mapping algorithm. This mathematical model is more suitable for flux distribution studies owing to its simplicity and the structure, thus facilitating selection of state variables for the system in a straightforward manner. It assumes that the reactor spatial domain is divided into relatively large number of rectangular parallelopiped shaped regions called nodes which are coupled through neutron diffusion. Neutron flux and other parameters in each node are represented by homogenized values integrated over its volume and the degree of coupling among these nodes is given by coupling coefficients.

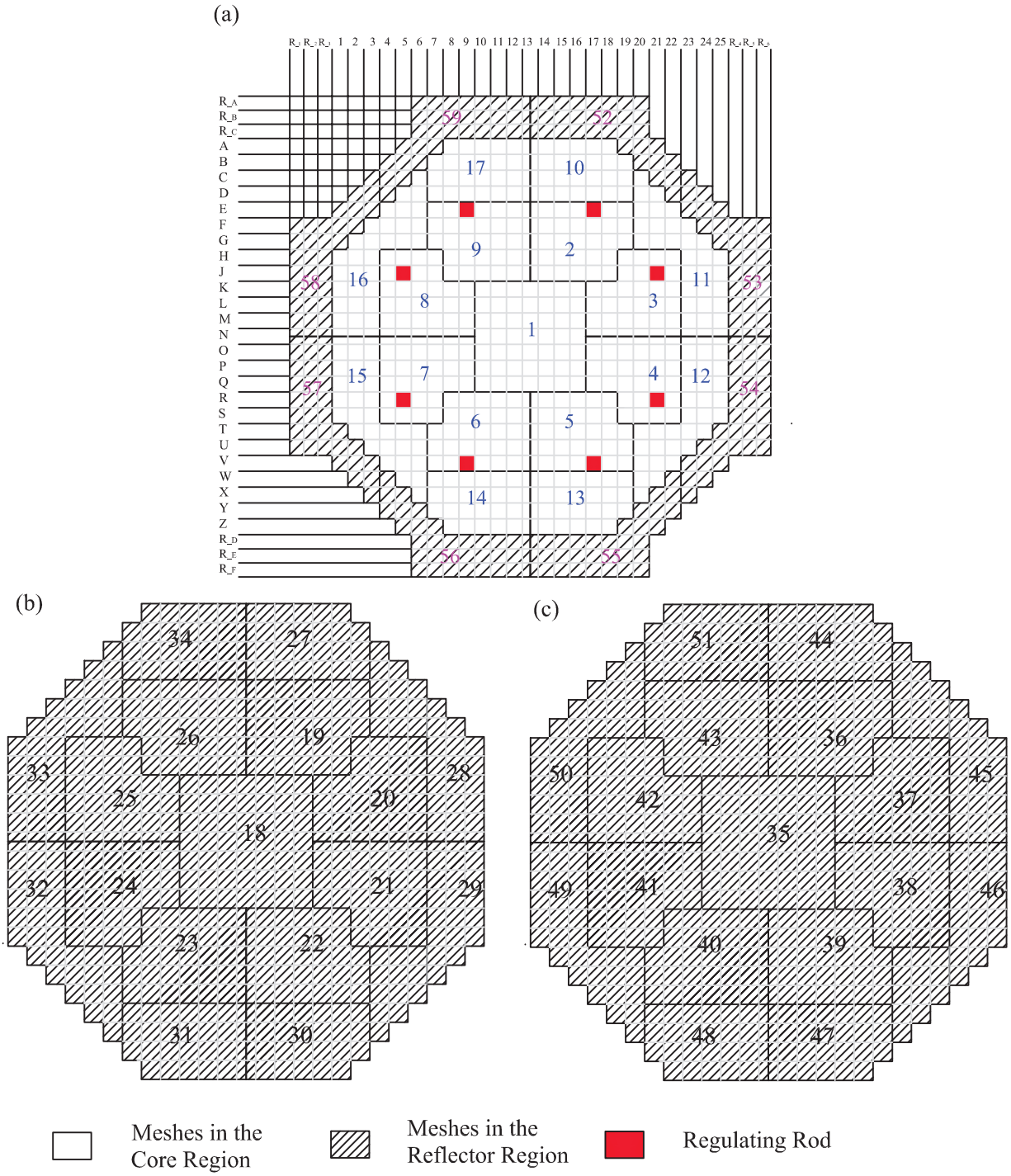

Figure 3.3: 17 Node scheme of AHWR for (a) the active core region (17 nodes in core and 8 nodes in side reflector) (b) top reflector region and (c) bottom reflector region.

3.2.1 Time–dependent core neutronics equations

The neutrons released in fission process have energies spanning the range from 10 MeV down to less than 0.01 eV. High energy neutrons are slowed down by various interactions *viz.,* absorption, scattering and fission with the atomic nuclei until they are thermalized. These interactions are characterized by the probability of occurrence of a particular neutron-nuclear reaction called cross section and depends significantly on neutron energy. It is impractical in reactor analysis to treat the neutron energy as a continuous variable, therefore the energy range of interest is divided into a finite number of discrete groups. In actual practice, one usually works with 2 to 20 groups in reactor calculations [19, 123]. However, for thermal reactor analysis it is adequate to work with two group neutron fluxes.

In order to derive the time–dependent core neutronics equations, the AHWR core is considered to be divided into 17 nodes as shown in Fig. 3.3(a). The top and bottom reflector regions are divided into 17 nodes each, in identical manner as the core as shown in Fig. 3.3(b) and Fig. 3.3(c) respectively, whereas the side reflector is divided into 8 nodes, giving 59 nodes in all.

AHWR operates with a slightly harder spectrum in the epithermal region and the contribution of up-scattering, though small, needs to be accounted. It is assumed that all the fission neutrons are generated as the fast neutrons. The nodal model of AHWR can be derived from the multigroup neutron diffusion equations with the help of two group equation and the associated equations for delayed neutron precursors' equations. It is illustrated in the following:

$$\frac{1}{v_1}\frac{\partial \phi_1}{\partial t} = \nabla D_1 \nabla \phi_1 - \Sigma_{a1}\phi_1 - \Sigma_{12}\phi_1 + \Sigma_{21}\phi_2 + (1-\beta)(\nu\Sigma_{f1}\phi_1 + \nu\Sigma_{f2}\phi_2) + \sum_{i=1}^{m_d}\lambda_i C_i, \quad (3.1)$$

$$\frac{1}{v_2}\frac{\partial \phi_2}{\partial t} = \nabla D_2 \nabla \phi_1 - \Sigma_{a2}\phi_2 + \Sigma_{12}\phi_1 - \Sigma_{21}\phi_2, \quad (3.2)$$

$$\frac{\partial C_i}{\partial t} = \beta_i(\nu\Sigma_{f1}\phi_1 + \nu\Sigma_{f2}\phi_2) - \lambda_i C_i, \quad i = 1, 2, ..., m_d, \quad (3.3)$$

where the subscripts 1 and 2 represents the parameters of fast and slow (thermal) group neutron fluxes. υ_g, ϕ_g, D_g, Σ_{ag} and Σ_{fg} respectively denote mean velocity of neutrons, neutron flux, diffusion coefficient, absorption cross section, fission cross section for energy group-g, g =1,2. Σ_{12} and Σ_{21} are the scattering cross sections from group-1 to group-2 and from group-2 to group-1 respectively. ν is the average number of fission neutrons and $m_d = 6$ is the total number of delayed neutron precursor groups. C_i, β_i and λ_i are the concentration, fraction and decay constant of delayed neutrons of ith group precursors. β is the effective fraction of delayed neutrons, $\beta = \sum_{i=1}^{m_d} \beta_i$.

The neutron fluxes ϕ_1 and ϕ_2 are functions of both space co–ordinates and time and parameters D_1, D_2, Σ_{a1}, Σ_{a2}, Σ_{f1} and Σ_{f2} are different for different locations and are given in Table 3.3. Now consider dividing the reactor into a number of small coarse mesh boxes (nodes). Within each mesh box, the neutron fluxes and other parameters are represented by the respective average values integrated over its volume. Then the neutron leakage from terms in (3.1) and (3.2) can be approximately given as

$$\nabla D_1 \nabla \phi_1 \simeq D_1 \nabla^2 \phi_1|_h, \tag{3.4}$$

$$\nabla D_2 \nabla \phi_2 \simeq D_2 \nabla^2 \phi_2|_h, \tag{3.5}$$

where h indicates a representative mesh box.

The net rate of fast neutron flow from a node h to its neighbour node k can be written as

$$D_1 \frac{d^2\phi_1}{du^2} V_h = J_u A_{hk}, \tag{3.6}$$

where V_h denotes the volume of box h and A_{hk} is the area of interface between the boxes h and k, perpendicular to the flow of neutron current. J_u denotes the neutron current density in the direction u. Using Fick's law, the above equation can be manipulated to obtain

$$D_1 \frac{d^2\phi_1}{du^2} = \frac{A_{hk}}{V_h} D_1 \frac{d\phi_1}{du} = \frac{D_1 A_{hk}}{V_h \triangle_{hk}} [-\phi_{1_h} + \phi_{2_k}], \tag{3.7}$$

Table 3.3: Two group cross-section data (Nominal values).

Material	Σ_{a1} (cm^{-1})	Σ_{a2} (cm^{-1})	Σ_{f1} (cm^{-1})	Σ_{f2} (cm^{-1})	$\nu\Sigma_{f1}$ (cm^{-1})	$\nu\Sigma_{f2}$ (cm^{-1})	Σ_{12} (cm^{-1})	Σ_{21} (cm^{-1})	D_1 (cm)	D_2 (cm)
Fuel										
High burn-up region-top	0.00333	0.0118	0.000 815	0.00481	0.00215	0.0216	0.00732	1.55	0.896	0.000221
High burn-up region-bottom	0.00357	0.0126	0.000863	0.00522	0.00221	0.0137	0.00785	1.55	0.897	0.000218
Medium burn-up region-top	0.00332	0.0118	0.000814	0.00480	0.00213	0.0125	0.00729	1.55	0.896	0.000220
Medium burn-up region-bottom	0.00356	0.0124	0.000846	0.00508	0.00221	0.0133	0.00787	1.55	0.897	0.000224
Low burn-up region-top	0.00330	0.0116	0.000802	0.00474	0.00202	0.0121	0.00728	1.55	0.896	0.000219
Low burn-up region-bottom	0.00357	0.0126	0.000863	0.00522	0.00221	0.0137	0.00785	1.55	0.897	0.000227
AR, RR	0.002922	0.007255	0	0	0	0	0.009011	9.92×10^{-5}	1.29940	0.85140
SR, SOR	0.006072	0.019909	0	0	0	0	0.006621	0.000258	1.27414	0.85382
Reflector	9.05×10^{-6}	6.45×10^{-5}	0	0	0	0	0.011427	9.26×10^{-7}	1.32590	0.83470

where $\triangle_{hk}$ denotes the centre to the centre distance between the two nodes. Based on the above, an approximation for the leakage terms in (3.4) and (3.5) could be

$$D_1\nabla^2\phi_1|_h = -\omega_{1hh}\phi_{1h} + \sum_{k=1}^{N_h}\omega_{1hk}\phi_{1k}, \tag{3.8}$$

$$D_2\nabla^2\phi_2|_h = -\omega_{2hh}\phi_{2h} + \sum_{k=1}^{N_h}\omega_{2hk}\phi_{2k}, \tag{3.9}$$

where

$$\omega_{ghk} = \frac{D_g A_{hk}}{V_h \triangle_{hk}} \quad \text{and} \quad \omega_{ghh} = \sum_{k=1}^{N_h}\omega_{ghk}, \quad g = 1, 2, \tag{3.10}$$

and N_h is the total number of neighboring nodes to Node h. Substituting (3.7) to (3.9) in (3.1) and (3.2), we have

$$\begin{aligned}\frac{1}{\upsilon_{1h}}\frac{\partial\phi_{1h}}{\partial t} = &-\omega_{1hh}\phi_{1h} + \sum_{k=1}^{N_h}\omega_{1hk}\phi_{1k} - (\Sigma_{a1h}\phi_{1h} + \Sigma_{12h}\phi_{1h}) \\ &+\Sigma_{21}\phi_2 + (1-\beta)(\nu\Sigma_{f1h}\phi_{1h} + \nu\Sigma_{f2h}\phi_{2h}) + \sum_{i=1}^{m_d}\lambda_i C_i,\end{aligned} \tag{3.11}$$

$$\frac{1}{\upsilon_{2h}}\frac{\partial\phi_{2h}}{\partial t} = -\omega_{2hh}\phi_{2h} + \sum_{k=1}^{N_h}\omega_{2hk}\phi_{2k} - \Sigma_{a2h}\phi_{2h} + \Sigma_{12h}\phi_{1h} - \Sigma_{21}\phi_2. \tag{3.12}$$

Adding (3.11) and (3.12), and defining one group flux $\phi_h = \phi_{1h} + \phi_{2h}$,

$$\omega_{hh} = \frac{\omega_{1hh} + \omega_{2hh}R_h}{(1+R_h)}; \quad \omega_{hk} = \frac{\omega_{1hk} + \omega_{2hk}R_h}{(1+R_h)}; \quad \Sigma_{ah} = \frac{\Sigma_{a1h} + \Sigma_{a2h}R_h}{(1+R_h)}; \tag{3.13}$$

$$\Sigma_{fh} = \frac{\Sigma_{f1h} + \Sigma_{f2h}R_h}{(1+R_h)}; \quad \upsilon_h = \frac{(1+R_h)}{\frac{1}{\upsilon_1} + \frac{R_h}{\upsilon_2}}; \quad R_h = \frac{\phi_{2h}}{\phi_{1h}} \tag{3.14}$$

we get

$$\frac{1}{\upsilon_h}\frac{\partial\phi_h}{\partial t} = -\omega_{hh}\phi_h + \sum_{k=1}^{N_h}\omega_{hk}\phi_k - \Sigma_{ah}\phi_h + (1-\beta)\nu\phi_h\Sigma_{fh} + \sum_{i=1}^{m_d}\lambda_i C_i, \tag{3.15}$$

Equation for variation in delayed neutron precursor density with time can be written as

$$\frac{dC_{ih}}{dt} = \beta_i \nu \phi_h \Sigma_{fh} - \lambda_i C_{ih}. \tag{3.16}$$

Further by defining prompt neutron life time ℓ_h, multiplication factor K_h and reactivity ρ_h as

$$\ell_h = \frac{1}{\Sigma_{ah} \upsilon_h}; \quad K_h = \frac{\nu \Sigma_{fh}}{\Sigma_{ah}} \quad \text{and} \quad \rho_h = \frac{K_h - 1}{K_h}, \tag{3.17}$$

we get

$$\begin{aligned} \frac{d\phi_h}{dt} &= -\omega_{hh} \upsilon_h \phi_h + \sum_{k=1}^{N_h} \omega_{hk} \upsilon_h \phi_k + (\rho_h - \beta) \frac{\phi_h}{\ell} \\ &\quad + \sum_{i=1}^{m_d} \upsilon_h \lambda_i C_{ih}, h = 1, 2, ...Z_p, \end{aligned} \tag{3.18}$$

$$\frac{dC_{ih}}{dt} = \frac{\beta_i \phi_h}{\upsilon_h \ell_h} - \lambda_i C_{ih}, i = 1, 2, ...m_d, \tag{3.19}$$

where ω_{hk} and ω_{hh} respectively denote the coupling co-efficients between kth and hth nodes and self coupling coefficient of hth node. The set of nonlinear equations (3.18) and (3.19) represents the core neutronics model of the AHWR without internal feedbacks, where Z_p=17 is the number of nodes in the core region. Fission reactions do not take place in reflector region, however the neutron leakage to reflector needs to be taken into account. Thus, for the nodes in the reflector region, the flux variation taking place can be described as

$$\frac{d\phi_h}{dt} = -\omega_{hh} \upsilon_h \phi_h + \sum_{k=1}^{N_h} \omega_{hk} \upsilon_h \phi_k, \quad h = Z_p + 1, .., Z_p + Z_r. \tag{3.20}$$

where Z_r=42 is the number of nodes in reflector region. It may be noticed that the total number of model equations would be $Z_p(m_d + 1) + Z_r$.

In order to account for the reactivity variations due to internal feedbacks and control devices, the reactivity term ρ_h in (3.18) is expressed as the sum of reactivity feedback

due to xenon and reactivity due to control rods, *i.e.*, $\rho_h = \rho_{hx} + \rho_{hu}$. Other factors for reactivity contribution such as fuel, coolant and moderator temperature are ignored due to their less significance.

Benchmark problems and their reference solutions are available for Light Water Reactors and PHWRs. These are useful for validation of simplified models. For the AHWR, however, such benchmarks are not available. Therefore, for validation of simplified space–time kinetics model and for validation of flux mapping algorithm a high fidelity model is required. It is generally expected that a scheme with a very large number of nodes will reproduce the flux distribution of the reactor core with good accuracy, and at the same time it will also capture all the essential properties of the reactor, but the model order will be correspondingly very large. Using (3.18)–(3.22) alongwith the 128-node scheme as shown in Fig 3.4, a nonlinear stringent model has been developed for validation purpose. In the 128-node scheme, the core region, top reflector region, and bottom reflector region each are divided into 128 nodes. The side reflector region is divided into eight nodes, giving 392 nodes in all. It may be noticed that the total mumber of model equations would be 1168 resulting into 1168^{th} order model, since $Z_p = 128$ and $Z_r = 264$.

The physical parameters such as volume of the nodes, area of interface, distance between the nodes, and the homogenized neutron cross-sections for the nodes under consideration are essential for computation of coupling coefficients and determination of the estimation model. The average coolant densities in the bottom half (for a length of 1.75 m from the core bottom) and top half (remaining 1.75 m length of the lattices) of the reactor core under full power operating conditions are calculated as 0.74 g/cc and 0.45 g/cc respectively, and corresponding cross sections given in Table 3.3 are used in the analysis. The delayed neutron data of the AHWR are given in Table 3.4.

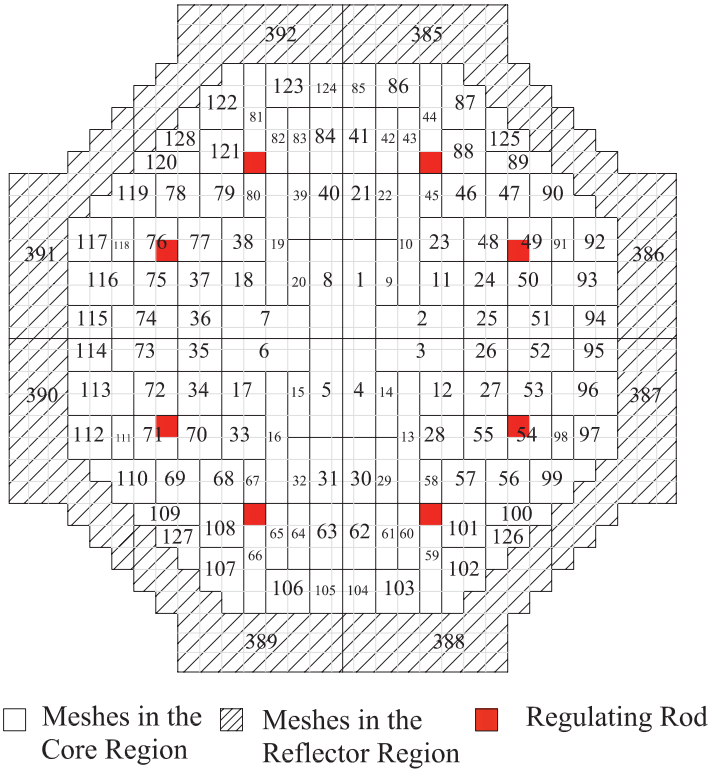

Figure 3.4: 128 Node scheme.

Table 3.4: Neutronic data of AHWR

Parameter	Value
β_1	0.000136
β_2	0.000745
β_3	0.000575
β_4	0.000855
β_5	0.000234
β_6	0.000098
λ_1	0.0127 s^{-1}
λ_2	0.0323 s^{-1}
λ_3	0.133 s^{-1}
λ_4	0.328 s^{-1}
λ_5	1.21 s^{-1}
λ_6	2.68 s^{-1}
λ_I	2.83 $\times 10^{-5}$ s^{-1}
λ_X	2.09 $\times 10^{-5}$ s^{-1}
γ_I	0.061
γ_X	0.003
σ_{aX}	2.65×10^{-18} cm^2
υ_1	1×10^7 cm/s
υ_2	3×10^5 cm/s

Table 3.5: RR banks

BANK	**RR**
I	RR_1, RR_3, RR_5, RR_7
II	RR_2, RR_4, RR_6, RR_8

Table 3.6: RRs and their locations

RR	RR_1	RR_2	RR_3	RR_4	RR_5	RR_6	RR_7	RR_8
Lattice Location	$E17$	$J21$	$R21$	$V17$	$V9$	$R5$	$J5$	$E9$
17-node scheme	2	3	4	5	6	7	8	9
128-node scheme	44	49	54	59	66	71	76	81

3.2.2 Formulation of regulating rod reactivity change

In small-scale transients involving normal operational and control situations in which flux mapping task is of significance, reactivity control requirements are fulfilled only by RRs, *i.e.*, ρ_h is essentially on account of RR movements. The AHWR has 8 RRs, each is situated in a distinct physical location of the reactor core as shown in Fig. 3.1. Reactivity contributed by the movement of a RR is a nonlinear function of its position. However, around the equilibrium position, the nonlinearity is very insignificant. Thus, the reactivity in node h due to the movement of RR-l in it is given by,

$$\rho_h = (-10.234H_l + 676.203) \times 10^{-6}, \tag{3.21}$$

where H_l is the %- in position of the lth control rod.

The 8 RRs are grouped into two banks as shown in Table 3.5, with one bank containing 4 RRs in the lattice locations E17, R21, V9 and J5, while the other containing the remaining 4 RRs in the lattice locations J21, V17, R5 and E9. The physical location of 8 RRs in 17-node scheme and 128-node scheme is given in Table 3.6. Bank-I of RRs is used for the automatic control of the AHWR. Each RR is attached through a rope–pulley mechanism to the respective reversible variable speed type RR drive having individual three phase induction motors and static frequency converters. Neglecting the friction, damping and rotational to linear motion transmission dynamics, the speed of

the regulating rod is directly proportional to the applied voltage ϑ_l to the drive motor, *i.e.*,

$$\frac{dH_l}{dt} = K_{RR}\vartheta_l, \quad l = 1, ..., 8, \tag{3.22}$$

where ϑ_l is the control signal. It is in the range of $\pm$1V and $K_{RR} = 0.56$, a constant.

3.2.3 Formulation of Xenon reactivity feedback

Iodine and xenon dynamics in each node h in the core region can be described as

$$\frac{dI_h}{dt} = \gamma_I \Sigma_{fh}\phi_h - \lambda_I I_h, \tag{3.23}$$

$$\frac{dX_h}{dt} = \gamma_X \Sigma_{fh}\phi_h + \lambda_I I_h - (\lambda_X + \sigma_{aX}\phi_h)X_h, \tag{3.24}$$

where I_h and X_h denote iodine and xenon concentrations respectively in node h, γ_I and γ_X are their respective fractional yields, and λ_I and λ_X are respective decay constants. The xenon reactivity feedback in a node h is given by

$$\rho_{hX} = \frac{\sigma_{aX}X_h}{\Sigma_{ah}}. \tag{3.25}$$

3.3 Steady–state Neutron Flux Distribution

For the study presented in this thesis, steady–state reference flux distributions are generated using finite-difference method (FDM) as described in [88]. Active core region of the AHWR alongwith reflector region is considered to be divided in fine meshes. Each channel in the core region is vertically divided into 24 mesh boxes making the reactor core into $12,312$ meshes, with 24 meshes along the reactor axis. The side, top and bottom reflector regions are assumed to be divided into 6048, 2295 and 2295 non-power generating meshes respectively. Therefore, core including reflector is assumed to be divided into 765 vertical sections and 30 horizontal planes, such that 30 meshes are along

Table 3.7: Dimensional details of mesh boxes

S.No	Region	Total number of meshes	Dimension of the mesh box (mm)		
			Length	Breadth	Height
1	Core	12312	225	225	145.83
2	Side Reflector	6048	200	225	145.83
3	Top Reflector	2295	200	225	250
4	Bottom Reflector	2295	200	225	250

the reactor axis. Among the 30 horizontal planes, first three and last three horizontal planes corresponds to top reflector and bottom reflector regions respectively, the rest 24 horizontal planes corresponds to the core region surrounded by reflector. With the division of core and reflector in this way, the total number of mesh boxes into which the core and reflector are divided, is 22950 meshes. The dimensional details of the finite difference mesh boxes are given in Table 3.7. Reactor exhibits quadrant core symmetry in flux and power distribution under full power operation.

3.3.1 Homogenization of Interaction Cross-sections

For the application of nodal core method all the neutron interaction cross–sections, diffusion coefficients and flux values should be represented by a single group homogenized constants which are constant throughout the volume of each node. By using fast, thermal group flux data generated from FDM method, two group cross-sections for each vertical section j are approximated using the volume-flux weighted homogenization [19] as described in the hereafter:

For vertical section j present in active core region:

$$\Sigma_{\zeta gj} = \frac{\sum_{k\in j,k=4}^{27} \Sigma_{\zeta gk}\phi_{gk}V_k}{\sum_{k\in j,k=4}^{27} \phi_{gk}V_k}, \quad g = 1, 2. \tag{3.26}$$

For vertical section j present in side reflector region:

$$\Sigma_{\zeta gj} = \frac{\sum_{k\in j,k=1}^{30} \Sigma_{\zeta gk}\phi_{gk}V_k}{\sum_{k\in j,k=1}^{30} \phi_{gk}V_k}, \quad g = 1, 2. \tag{3.27}$$

For vertical section j present in top reflector region:

$$\Sigma_{\zeta gj} = \frac{\sum_{k\in j,k=1}^{3} \Sigma_{\zeta gk}\phi_{gk}V_k}{\sum_{k\in j,k=1}^{3} \phi_{gk}V_k}, \quad g = 1, 2. \tag{3.28}$$

For vertical section j present in bottom reflector region:

$$\Sigma_{\zeta gj} = \frac{\sum_{k\in j,k=28}^{30} \Sigma_{\zeta gk}\phi_{gk}V_k}{\sum_{k\in j,k=28}^{30} \phi_{gk}V_k}, \quad g = 1, 2. \tag{3.29}$$

The group-wise homogenized constants of each node h were computed using

$$\Sigma_{\zeta gh} = \frac{\sum_{\forall j\in h} \Sigma_{\zeta gj}\phi_{gj}V_j}{\sum_{\forall j\in h} \phi_{gj}V_j}, \quad g = 1, 2; \quad h = 1, 2, ..., Z_r. \tag{3.30}$$

where Σ denotes the cross section, ζ denotes a neutron interaction and j denotes the vertical section indices in the reactor core. k denotes the index of the mesh box and it runs from 1 to 3, 4 to 27, 28 to 30 and 1 to 30 for vertical sections of top reflector, active core, bottom reflector and side reflector regions respectively. The steady-state equivalent mesh box fluxes were calculated by adding the two group flux data generated from FDM computations and is given by

$$\phi_{m_0} = \phi^0_{1m} + \phi^0_{2m}, \tag{3.31}$$

where ϕ^0_{1m} and ϕ^0_{2m} are the volume weighted homogenized fluxes in mesh box m, for the fast and thermal groups respectively. The steady–state equivalent flux in the vertical section j obtained from the fast and thermal energy groups is given by

$$\phi_{j_0} = \phi^0_{1j} + \phi^0_{2j}, \tag{3.32}$$

where ϕ^0_{1j} and ϕ^0_{2j} are the volume weighted homogenized fluxes in vertical section j, for the fast and thermal groups respectively. The steady–state equivalent flux in node h

obtained from both the fast and thermal energy groups is given by

$$\phi_{h_0} = \phi^0_{1h} + \phi^0_{2h}, \tag{3.33}$$

where ϕ^0_{1h} and ϕ^0_{2h} are the volume weighted homogenized fluxes in node h, for the fast and thermal groups respectively.

3.4 Reconstruction of 3-D Neutron Flux Distribution

Nodal methods have a fundamental limitation as they fail to predict the detailed flux shapes throughout the reactor core. Of course, such detailed information can be of vital importance in the course of designing and operation of the reactor. The methods for developing homogenized parameters for large nodes from detailed heterogeneous solutions and the problem of deriving local pin powers from the nodal solutions are generally applied to time–independent problems. The pin-by-pin flux distribution within each node is calculated using a de-homogenization method or Flux Reconstruction Method (FRM) [101] from nodal solutions. This method is superior than FDM in view of computational time and it is based on the assumption that the fine-mesh point flux can be expressed as the product of flux of the assembly to which it belongs, which is obtained through a vertical grid level weighting factor applied on the global flux, and a mesh box level weighting factor corresponding to it.

From (3.32) and (3.33), the weighting factor for each vertical section j in a node h is given by $\kappa_j = \phi_{j0}/\phi_{h0}$. The weighting factor for each mesh box m in any vertical grid j can be found from the axial flux distribution obtained from the steady–state FDM computation. The weighting factor for each mesh box m in a vertical grid j is defined as $\kappa_{jm} = \phi_{jm0}/\phi_{j0}$. During the transient, the fluxes in vertical grids and mesh boxes vary according to the transient value of the nodal flux and weighting factors κ_j and κ_{jm}

corresponding to vertical grid j and mesh box m. Transient value of flux in any vertical grid j is given by $\phi_j = \kappa_j \phi_h$, where ϕ_h is the transient value of flux of node h, in which vertical grid j is a member. On the other hand, transient value of flux in any mesh box m in vertical grid j is given by $\phi_{jm} = \kappa_{jm}\phi_j$. From the expression of ϕ_j,

$$\phi_{jm} = \kappa_{jm}\kappa_j\phi_h. \tag{3.34}$$

Substituting the values of κ_{jm} and κ_j, (3.34) can be written as

$$\phi_{jm} = \left(\frac{\phi_h}{\phi_{h0}}\right)\phi_{jm0} \tag{3.35}$$

Hence, the transient value of flux in any mesh box m is expressed as the ratio of transient to steady state–flux value of the node h it belongs to, multiplied by its own steady–state value. This way the neutron flux distribution can be reconstructed in all 22950 mesh boxes.

3.4.1 Reconstruction of SPND flux

Each ICDH is surrounded by 4 fuel channels and accommodates an assembly containing SPND detectors for thermal neutron flux measurement. In ICDH, each SPND is surrounded by 8 mesh boxes as shown in Fig. 3.5 (a). 2-D view and its cross-sectional view are shown in Fig. 3.5 (b). Flux reaching a SPND D, is computed by weighted average of fluxes in the surrounding 8 meshes [23] as follows:

$$\phi_{\mathrm{D}} = \frac{\sum_{m=1}^{8} \phi_m^{\mathrm{D}} D_m^{\mathrm{D}}}{\sum_{m=1}^{8} D_m^{\mathrm{D}}}, \tag{3.36}$$

where ϕ_m^{D} and D_m^{D} are the one–group flux and the diffusion coefficients of the surrounding mesh box m. In Section 3.4, a reconstruction method was presented to obtain the detailed flux distribution from the solution of (3.18)–(3.20). According to this method

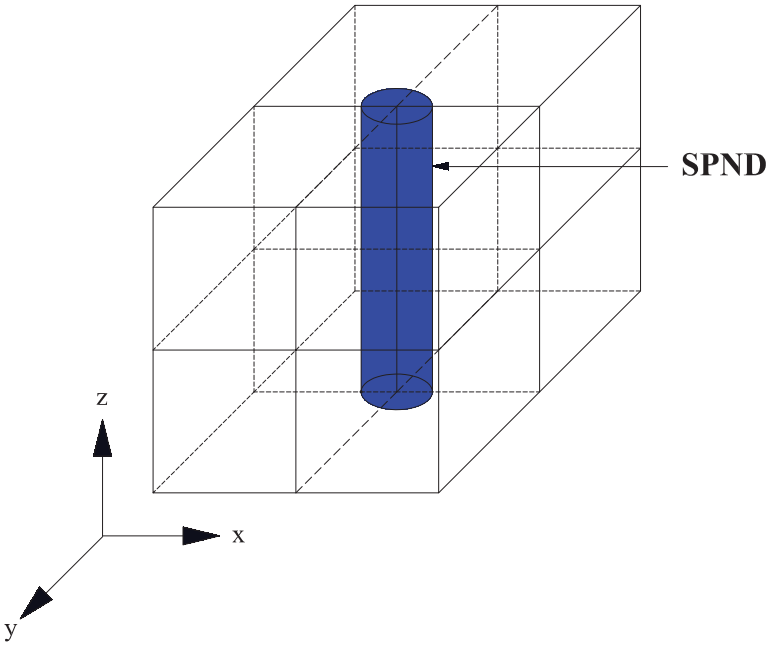

(a) 3-D view

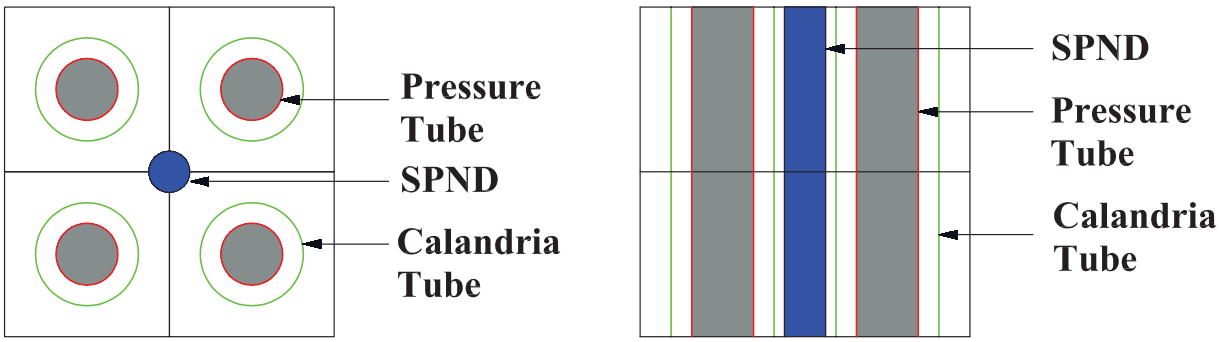

(b) 2-D view form XY plane and cross-sectional view

Figure 3.5: SPND in an ICDH surrounded by 8 mesh boxes.

the values of neutron fluxes in 22950 small volume elements can be determined as

$$\boldsymbol{\phi}_V = \boldsymbol{\kappa}_V \boldsymbol{\phi}_C \tag{3.37}$$

where $\boldsymbol{\phi}_V$ denotes a vector of 22950 flux values, $\boldsymbol{\phi}_C$ denotes the vector of flux values obtained form (3.18)–(3.20) and $\boldsymbol{\kappa}_V$ is a weighting matrix determined based on the detailed 3-D flux distribution computations. Subsequently the fluxes at SPND locations can be obtained from

$$\boldsymbol{\phi}_{\mathrm{D}} = \boldsymbol{\kappa}_{\mathrm{D}} \boldsymbol{\phi}_V \tag{3.38}$$

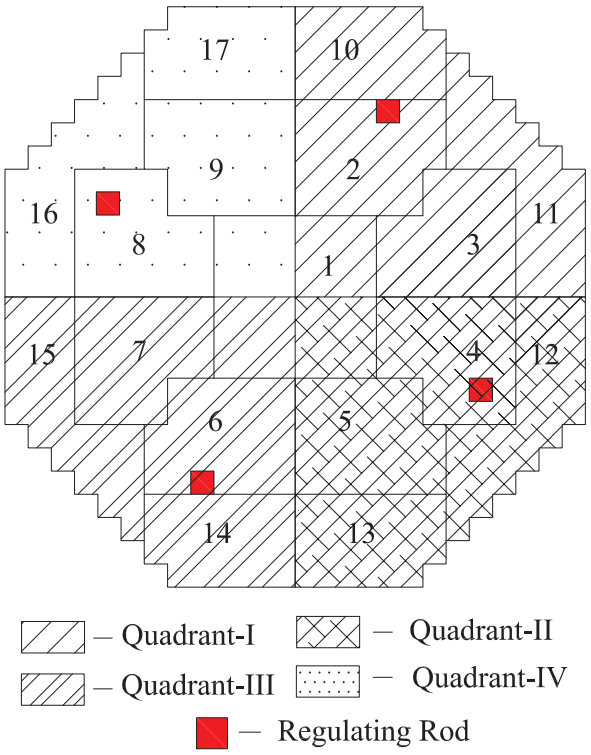

Figure 3.6: Four quadrants in the AHWR core.

where $\boldsymbol{\phi}_{\mathrm{D}}$ denotes the vector of fluxes at SPND locations and $\boldsymbol{\kappa}_D$ is a detector weighting matrix. Combining (3.37) and (3.38),

$$\boldsymbol{\phi}_{\mathrm{D}} = \boldsymbol{\kappa}_{\mathrm{D}}\boldsymbol{\kappa}_V\boldsymbol{\phi}_C = \boldsymbol{\kappa}_{\mathrm{D}V}\boldsymbol{\phi}_C \tag{3.39}$$

Thus, the fluxes at SPND locations are obtained from nodal fluxes. The SPNDs are assumed to give output signals proportional to local fluxes, *i.e.*, dynamic effects are ignored.

3.5 Model validation

To illustrate the dynamic behavior of the space–time kinetics model (3.18)–(3.22) derived in Section 3.2, open loop response under a few control relevant transients is presented in this section. During the simulation, core average flux and 4 quadrant fluxes were reconstructed under the same transient and compared with the reference solutions ob-

tained from a separate set of computations using a 128 node scheme as shown in Fig. 3.4. The four quadrant scheme of AHWR is shown in Fig 3.6. The quadrant and core average fluxes, from the nodal solutions, were computed using reconstruction technique as described in Section 3.4. It is as follows: quadrant fluxes are obtained as an average of all the mesh box fluxes in each quadrant; and the core average flux is computed as the average of all the quadrant fluxes. To characterize the accuracy of the model, the error in core-average and quadrant fluxes is computed using,

$$e_{\phi_i} = (\phi_{i_{ref}} - \phi_i) \times 100, \quad i = I, II, III, IV, \tag{3.40}$$

where $\phi_{i_{ref}}$ denotes the reference value of neutron flux in quadrant i and ϕ_i denotes the neutron flux in quadrant i.

Initially, the reactor was assumed to be operating on full power. It was also assumed that initially each RR is equally at 66.7% in position, ARs are fully in and SRs and shut-off rods are fully out, which is the critical configuration of the equilibrium core of AHWR. For a control voltage with positive magnitude, the corresponding RR moves into the core and for a negative control voltage, it moves out of the core. The regulating rod is stationary when the control voltage applied to it is zero. The transients are described in the following subsections. In each case, the reactor is at steady–state for the initial 50 seconds.

3.5.1 Case I: Movement of RR in Quadrant–I

This simulation involves movement of RR located in Quadrant-I. At time $t = 50$ s, control signal of 1 V is applied to RR drive and maintained for 8 s. Corresponding RR moves linearly into the reactor core, as governed by (3.22) and reaches 71.14% in position. Then, control signal is made 0 V to hold the RR at the new position. After 3 s, the RR is driven out linearly to nominal position by applying a control signal of -1 V. Again after 3 s, an outward movement followed by inward movement back to its

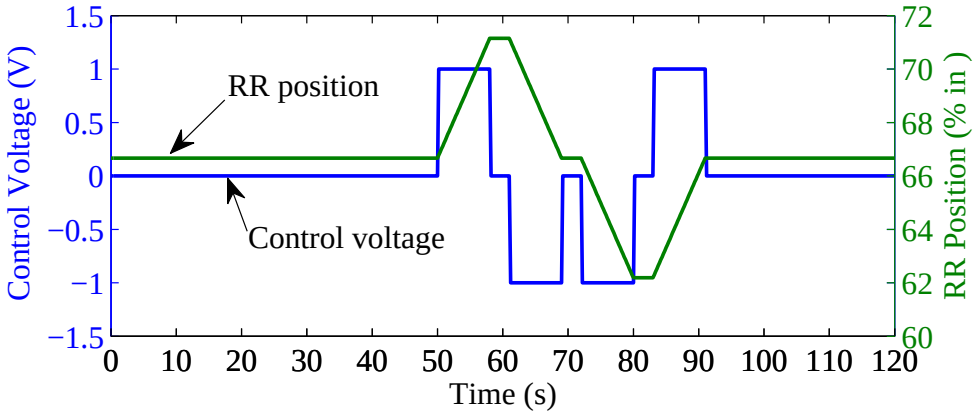

Figure 3.7: Position of RR corresponding to applied control signal.

nominal position is simulated.

Fig. 3.7 shows the applied control voltage to RR drive and corresponding position of the RR in the core during the applied transient. Fig. 3.8 shows the core average flux alongwith error in core average flux computed using nodal method, taking computations from 128 node scheme as reference. Fig. 3.9 and Fig. 3.10 show the average values of flux in Quadrants-I, II, III and IV of the reactor alongwith error.

3.5.2 Case II: Differential Movement of 2 RRs

Scenarios in which the flux/power distribution in the reactor core undergoes variations, despite of the total power remaining constant are of great significance in spatial reactor control applications. In order to assess the validity of the space–time kinetics model under such conditions, a transient involving simultaneous counter-movement of two diagonally opposite RRs was simulated. At time t=50 s, the RR in Quadrant-III was driven linearly into the reactor core from its nominal position under a signal of 1 V, while the RR at the diagonally opposite lattice location in Quadrant-I was driven out simultaneously at the same speed under a signal of -1 V. Fig. 3.11 shows the position of RRs in the core during the applied transient.

Fig. 3.12 shows the core average flux alongwith error in core average flux computed using nodal method, taking computations from 128 node scheme as reference. Fig. 3.13

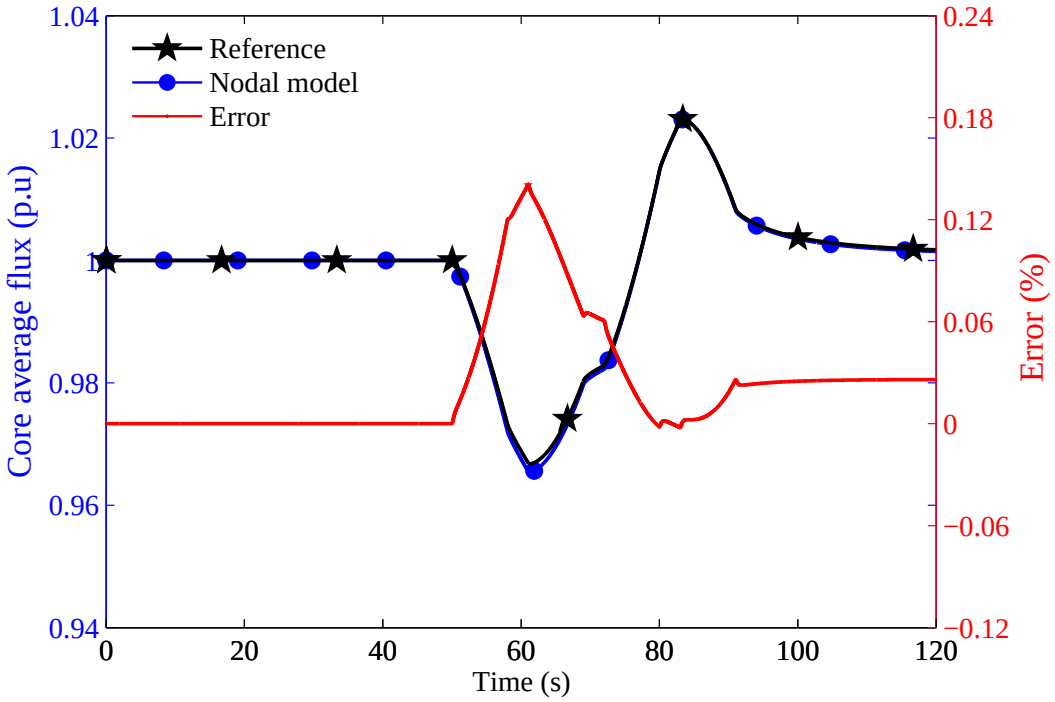

Figure 3.8: Core average flux alongwith error (%) during the transient involving the movement of RR in Quadrant-I.

Table 3.8: L_2- norm of error in fluxes

S.No	Test case	L_2- norm of error in				
		Core average flux	Quadrant -I flux	Quadrant -II flux	Quadrant -III flux	Quadrant -IV flux
1	Case-I	0.1072	0.1014	0.1490	0.1557	0.0907
2	Case-II	2.5997	3.6277	1.9373	1.7581	3.1031

and Fig. 3.14 shows the average values of flux in Quadrants-I, II, III and IV of the reactor alongwith error. To quantify the accuracy of the AHWR model developed, L_2 norm of the error vector $\boldsymbol{e}_{\phi_i}$ was computed for both the test cases and this is shown in Table 3.8. The L_2 norm is defined as

$$|e_{\phi_i}|_{L_2} = \sqrt{e_{\phi_i}^{2\ (1)} + e_{\phi_i}^{2\ (2)} + \cdots + e_{\phi_i}^{2\ (k)}}, \quad i = I, II, III, IV, \tag{3.41}$$

where k is the number of observations made.

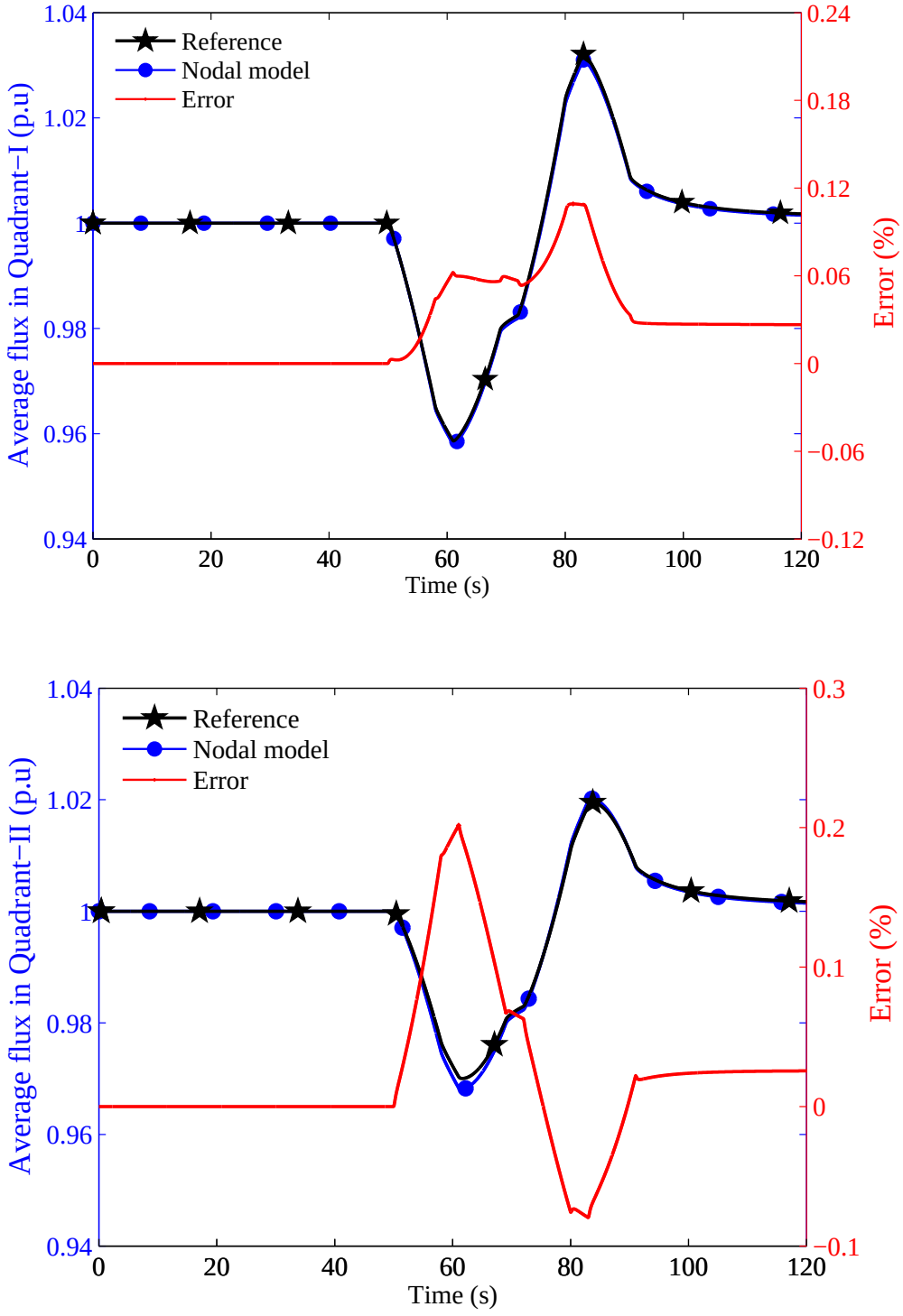

Figure 3.9: Average flux in Quadrants I and II during the movement of RR in quadrant I.

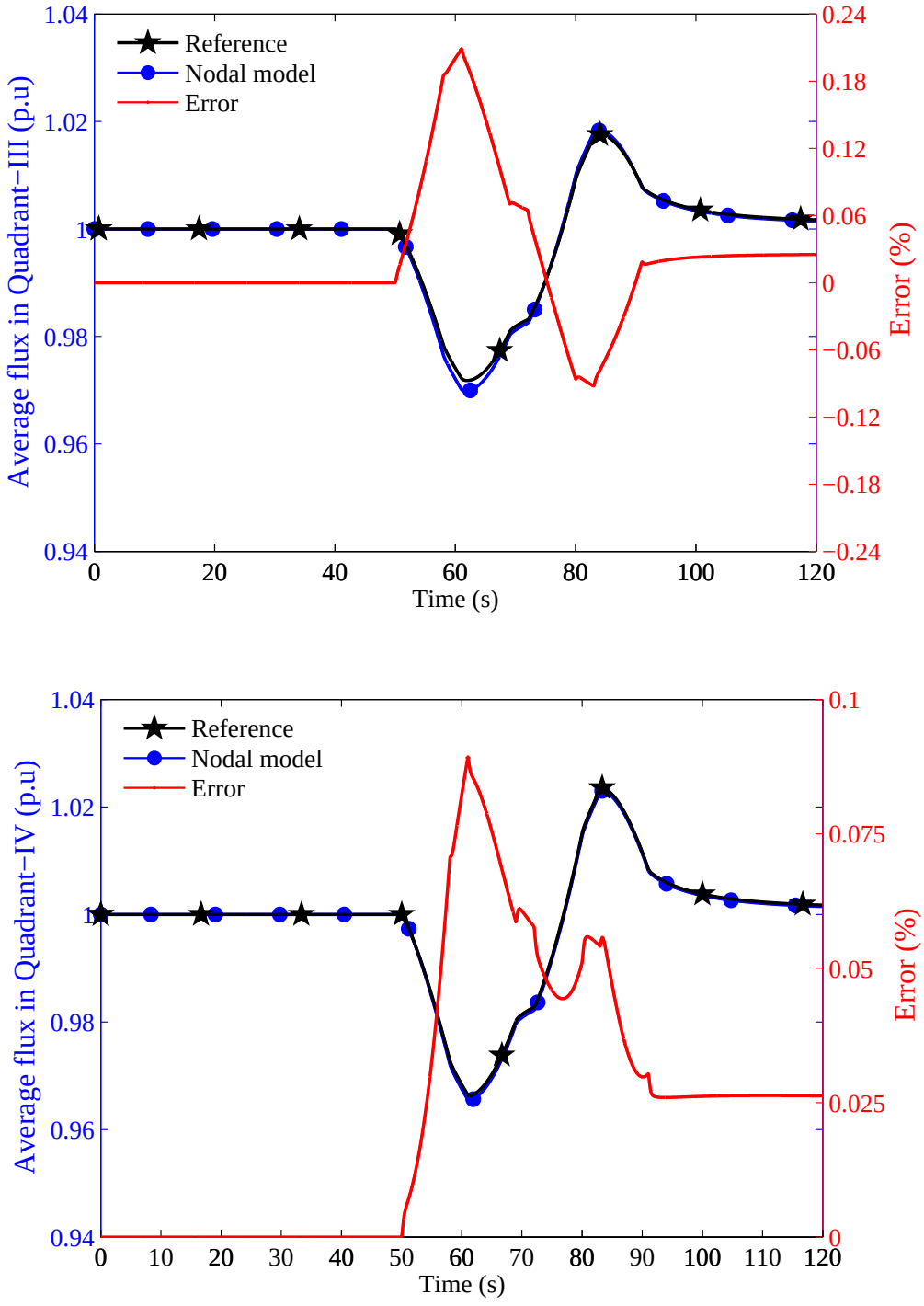

Figure 3.10: Average flux in Quadrants III and IV during the movement of RR in quadrant I.

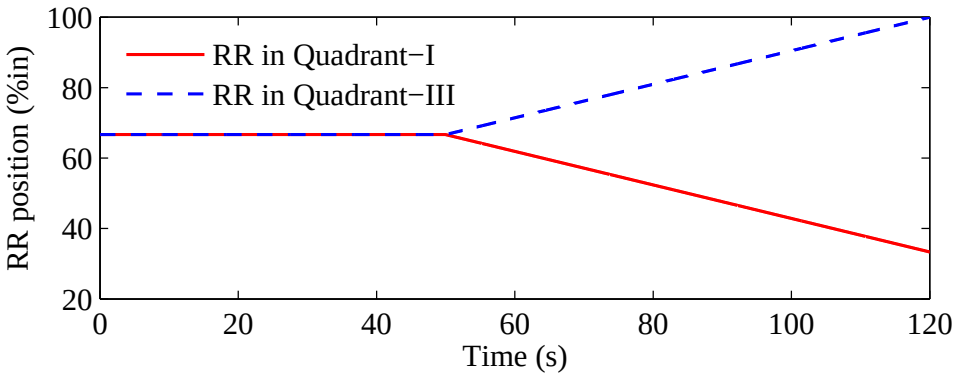

Figure 3.11: Position of RRs in Quadrant-I and Quadrant-III during the transient involving differential movement of RRs.

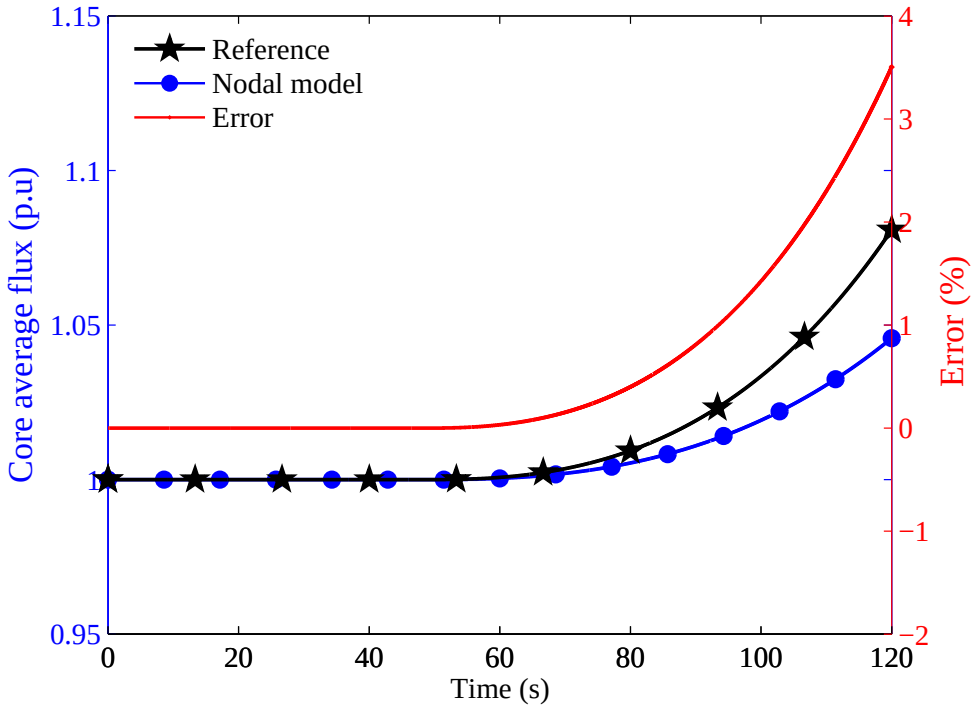

Figure 3.12: Core average flux alongwith error (%) during the transient involving differential movement of RRs.

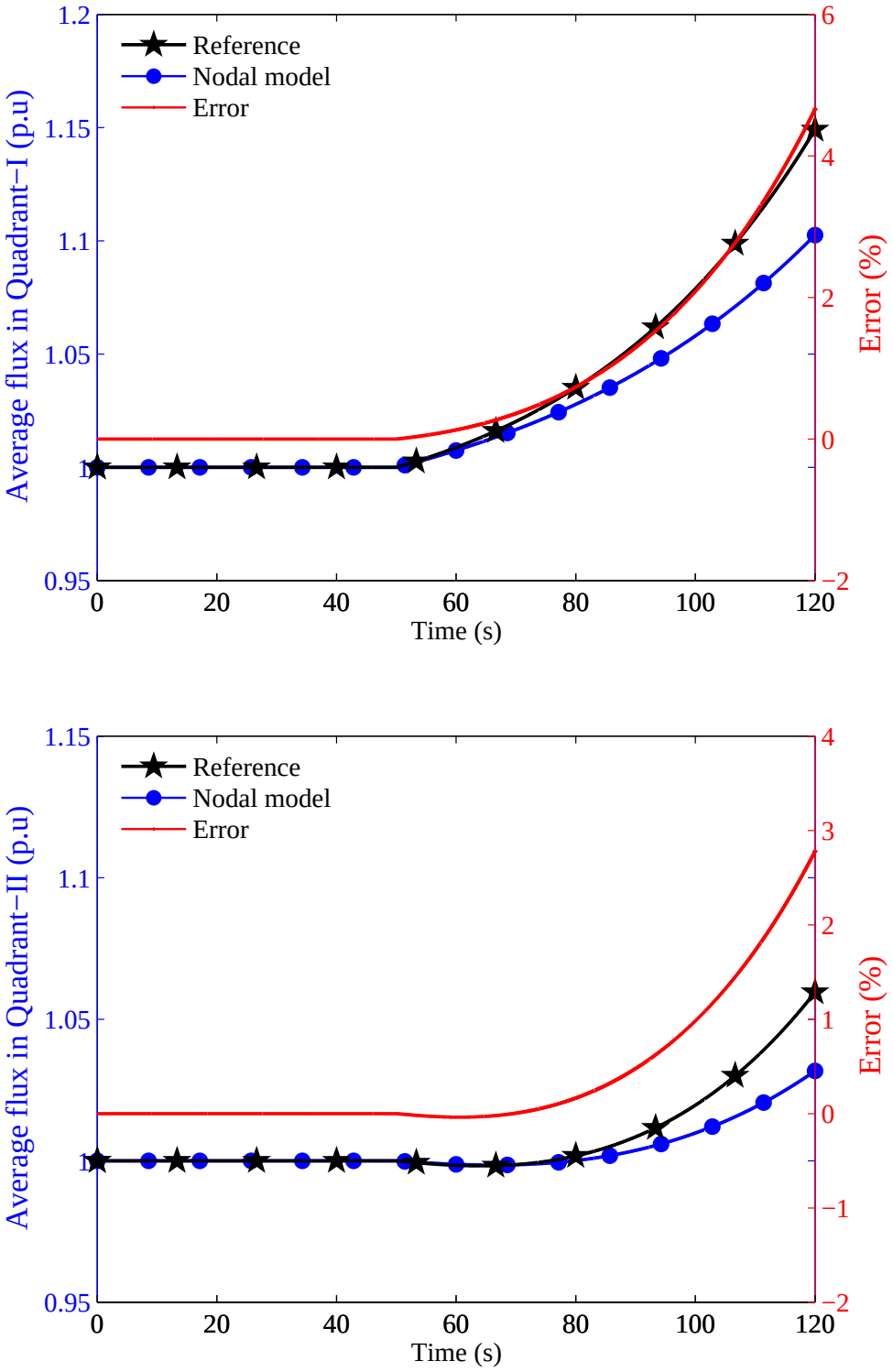

Figure 3.13: Average flux in Quadrants I and II during the transient involving differential movement of RRs.

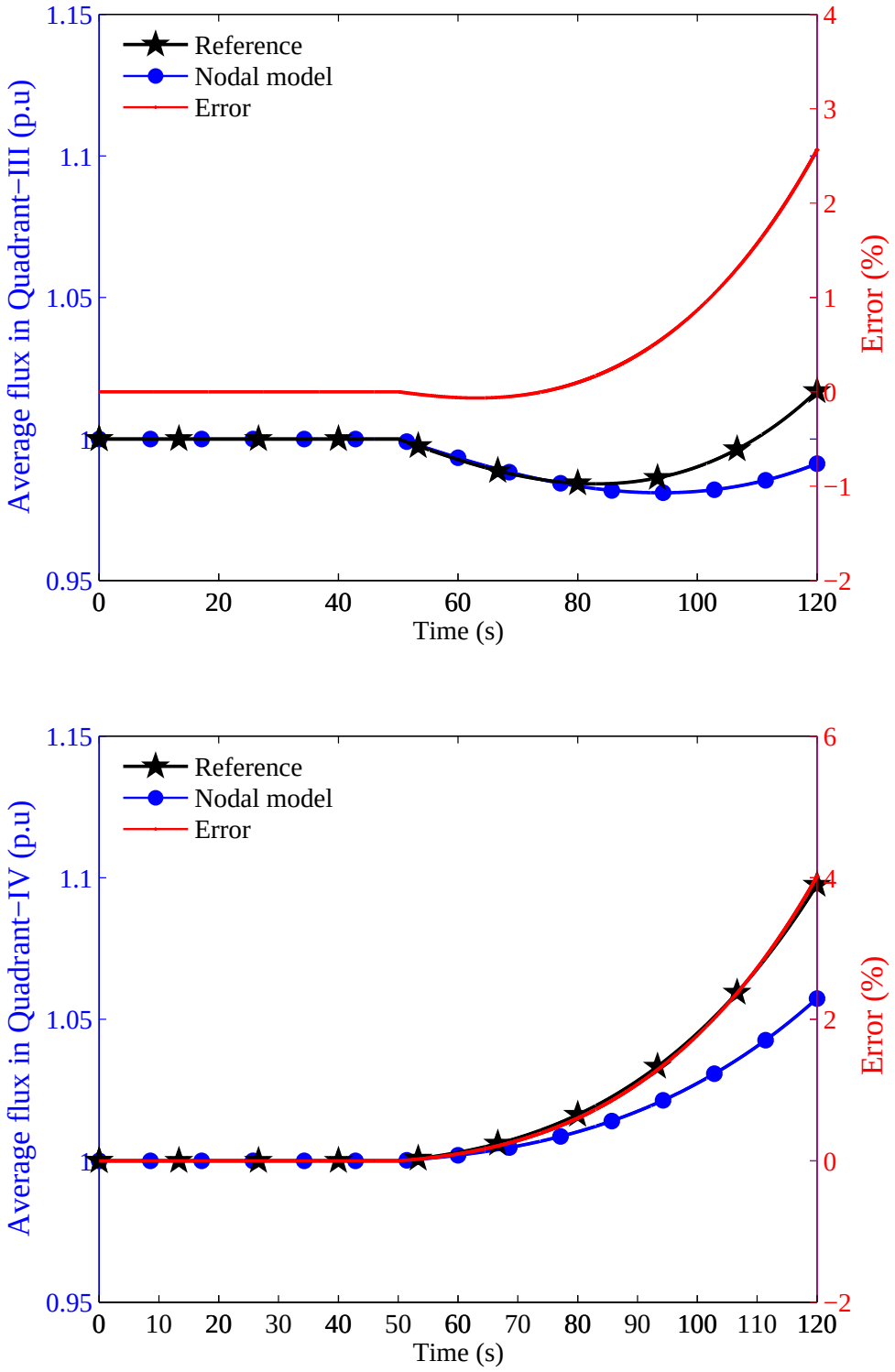

Figure 3.14: Average flux in Quadrants III and IV during the transient involving differential movement of RRs.

3.6 Discussion

In this chapter, a nonlinear dynamic model which represents time–dependent behavior of AHWR has been presented. The dynamic behavior of the model has also been validated for core average flux and Quadrant fluxes using a high fidelity model based on 128-node scheme of AHWR. From the simulations, it can be concluded that for a considerable perturbation around the steady–state operating point, the core average flux and reconstructed fluxes in all the quadrants from the AHWR model are found to be in good agreement with the reference values. As a result of this, AHWR model with 128-node scheme is suitable for generation of accurate detector fluxes which can be used as real time plant data and reference model with 17-node scheme is suitable for estimation of detailed flux distribution in the reactor core using Kalman filtering technique.

Chapter 4

Theory of Model Reduction Techniques

Complex large–scale systems usually require high dimensional models to represent them accurately. Analysis, simulation and design methods based on such high order models may eventually lead to complicated control strategies requiring very complex logic or large amounts of computation. The development of state–space methods has made it feasible to design a control system for high order linear systems. When the order of the system becomes very high, however, special algebraic techniques for performing the design calculations are required to permit the calculations to be performed at a reasonable cost in a typical digital computer. Moreover, a control system designed for a very high order linear system is likely to be more complicated than it would be reasonable to build. Because of their importance on systems analysis and in the design of controllers or observers, model reduction methods have received considerable attention over the past few decades. Among the various classes of model reduction methods, modal techniques have gained significant interest since they permit explicit formulation. *i.e.*, the reduced order model is derived directly from the linear large–scale

Parts of this chapter were published in *2015 IEEE international Conference on Industrial Instrumentation and Control Applications (ICIC)*, Pune, India and in *Annals of Nuclear Energy*, Vol. 102.

system through algebraic relationships. This chapter presents the theory of some of the model order reduction techniques *viz.* Davison's, Marshall's, singular perturbation analysis and balanced truncation.

4.1 Formulation of Model Order Reduction Problem

Classic and modern control theories are usually concerned with analyzing and synthesizing systems described by ordinary differential equations (ODE) that often represent physical laws governing the dynamics of the given system. The linearization of higher nonlinear ODEs about an equilibrium, leads to the well-known representation of a linear-time invariant (LTI) system. Consider a large–scale dynamical system described by the LTI model

$$\begin{aligned} \dot{\mathbf{x}}(t) &= \mathbf{A}\mathbf{x}(t) + \mathbf{B}\mathbf{u}(t), \\ \mathbf{y}(t) &= \boldsymbol{\Psi}\mathbf{x}(t), \end{aligned} \tag{4.1}$$

where $\mathbf{x}(t) \in \mathbb{R}^n$, $\mathbf{u}(t) \in \mathbb{R}^m$, and $\mathbf{y}(t) \in \mathbb{R}^p$ are the state, input and output vectors respectively; $\mathbf{A} \in \mathbb{R}^{n\times n}$, $\mathbf{B} \in \mathbb{R}^{n\times m}$ and $\boldsymbol{\Psi} \in \mathbb{R}^{p\times n}$ are system, input and output matrices respectively. For the rest of this thesis, assume the notion of large–scale system represented by (4.1) in state–space form as $\mathbf{G} := \left[\begin{array}{c|c} \mathbf{A} & \mathbf{B} \\ \hline \boldsymbol{\Psi} & \mathbf{0} \end{array}\right]$. The same $\mathbf{G}$ is also used to denote the Transfer Function (TF) corresponding to (4.1). From the context there would be no ambiguity. The transfer function from $\mathbf{u}$ to $\mathbf{y}$ is $\mathbf{G}(s) := \boldsymbol{\Psi}(s\mathbf{I} - \mathbf{A})^{-1}\mathbf{B}$. The order n of the LTI system ranges from a few tens to several hundred for large–scale systems. The increase in dimension and the desire to control the multi-input/multi-output systems triggered the need of application of model order reduction. The intent of model order reduction is to obtain a simplified lower order, model which preserves the input and output behavior of the system.

The reduced order model of order $r < n$, has the same response characteristics as

that of the original model with far less storage requirements and much lower evaluation time. The resulting model given by,

$$\dot{\mathbf{x}}_r(t) = \mathbf{A}_r\mathbf{x}_r(t) + \mathbf{B}_r\mathbf{u}(t), \tag{4.2}$$

$$\mathbf{y}_r(t) = \boldsymbol{\Psi}_r\mathbf{x}_r(t) \tag{4.3}$$

might be used to replace the original description in simulation studies or it might be used to design a reduced order controller or observer. The application of Davison's technique, Marshall's technique, singular perturbation analysis and balanced truncation has been explored in this thesis and these techniques are described briefly in the following sections.

4.2 Davison's Technique

Davison [14] proposed one of the first structured approach to model order reduction. It approximates the original order n of the system to r by neglecting the eigenvalues of the original system that are farthest from the origin and retains only the dominant eigenvalues and hence the dominant time constants of the original system are present in the reduced order model. Initially the system states are rearranged in such a manner that the eigenvectors corresponding to the states to be retained from (4.1) are placed first.

The essence of this modal approach to model reduction consists of neglecting the dynamics associated with fast modes, *i.e.*, those which die out quickly when perturbed. Hence, it is useful to partition the above relationships in terms of dominant and non-dominant modes, as well as important and less important state variables. Let the state vector $\mathbf{x}$ be partitioned into dominant and non-dominant parts as $\mathbf{x}_1$, which are considered to be retained and $\mathbf{x}_2$, which are to be ignored. Therefore the partitioned

form of (4.1) is

$$\begin{bmatrix} \dot{\mathbf{x}_1} \\ \dot{\mathbf{x}_2} \end{bmatrix} = \begin{bmatrix} \mathbf{A}_{11} & \mathbf{A}_{12} \\ \mathbf{A}_{21} & \mathbf{A}_{22} \end{bmatrix} \begin{bmatrix} \mathbf{x}_1 \\ \mathbf{x}_2 \end{bmatrix} + \begin{bmatrix} \mathbf{B}_1 \\ \mathbf{B}_2 \end{bmatrix} \mathbf{u}, \tag{4.4}$$

$$\mathbf{y} = \begin{bmatrix} \boldsymbol{\Psi}_1 & \boldsymbol{\Psi}_2 \end{bmatrix} \begin{bmatrix} \mathbf{x}_1 \\ \mathbf{x}_2 \end{bmatrix}, \tag{4.5}$$

where $\mathbf{x}_1 \in \mathbb{R}^r$, $\mathbf{x}_2 \in \mathbb{R}^{n-r}$. Further consider the representation of the system (4.4), (4.5) by the equivalent diagonal form (the eigenvalues of the system are assumed to be distinct).

$$\begin{bmatrix} \dot{\mathbf{z}}_1 \\ \dot{\mathbf{z}}_2 \end{bmatrix} = \begin{bmatrix} \tilde{\mathbf{A}}_1 & 0 \\ 0 & \tilde{\mathbf{A}}_2 \end{bmatrix} \begin{bmatrix} \mathbf{z}_1 \\ \mathbf{z}_2 \end{bmatrix} + \begin{bmatrix} \tilde{\mathbf{B}}_1 \\ \tilde{\mathbf{B}}_2 \end{bmatrix} \mathbf{u}, \tag{4.6}$$

$$\mathbf{y} = \begin{bmatrix} \tilde{\boldsymbol{\Psi}}_1 & \tilde{\boldsymbol{\Psi}}_2 \end{bmatrix} \begin{bmatrix} \mathbf{z}_1 \\ \mathbf{z}_2 \end{bmatrix}, \tag{4.7}$$

where $\mathbf{z}_1 \in \mathbb{R}^r$, $\mathbf{z}_2 \in \mathbb{R}^{n-r}$ are the states in diagonal system representation,

$$\tilde{\mathbf{A}}_1 = \text{diag.} \begin{bmatrix} \mu_1 & \mu_2 & \cdots & \mu_r \end{bmatrix}, \tag{4.8}$$

$$\tilde{\mathbf{A}}_2 = \text{diag.} \begin{bmatrix} \mu_r & \mu_{r+2} & \cdots & \mu_n \end{bmatrix} \tag{4.9}$$

and the eigenvalues μ_i, $i = 1, 2, \ldots, r$ are to be retained in approximate model. Let

$$\mathbf{x} = \boldsymbol{V}\mathbf{z} = \begin{bmatrix} \boldsymbol{V}_{11} & \boldsymbol{V}_{12} \\ \boldsymbol{V}_{21} & \boldsymbol{V}_{22} \end{bmatrix} \begin{bmatrix} \mathbf{z}_1 \\ \mathbf{z}_2 \end{bmatrix} \tag{4.10}$$

be the required linear transformation for obtaining the diagonal form representation such that $Re(\mu_1) \leq Re(\mu_2) \leq \ldots Re(\mu_n)$. The matrix $\boldsymbol{V}$ is called modal matrix whose columns are the corresponding right eigenvectors of $\mathbf{A}$.

According to Davison's method [14], the modes in $\mathbf{z}_2$ are non-dominant and therefore can be ignored. Thus setting $\mathbf{z}_2 = \mathbf{0}$ in (4.10) gives reduced order model (4.2), (4.3) where

$$\mathbf{A}_r = \boldsymbol{V}_{11}\tilde{\mathbf{A}}_1\boldsymbol{V}_{11}^{-1}, \tag{4.11}$$

$$\mathbf{B}_r = \boldsymbol{V}_{11}\tilde{\mathbf{B}}_1, \tag{4.12}$$

$$\boldsymbol{\Psi}_r = \tilde{\boldsymbol{\Psi}}_1\boldsymbol{V}_{11}^{-1}, \tag{4.13}$$

$$\text{and} \qquad \mathbf{x}_2 = \boldsymbol{V}_{21}\boldsymbol{V}_{11}^{-1}\mathbf{x}_1. \tag{4.14}$$

Thus, the original nth order model is approximated by rth order model. The first r state variables of the original model are approximated by the state variables of the reduced order model and the $(n-r)$ state variables are expressed in terms of the first r state variables by (4.14).

4.3 Marshall's Technique

Marshall [77] proposed an alternate method for the computation of reduced order model. This method assumes that $\dot{\mathbf{z}}_2 = 0$ in (4.6), which then yields

$$\dot{\mathbf{z}}_1 = \tilde{\mathbf{A}}_1\mathbf{z}_1 + \tilde{\mathbf{B}_1}\mathbf{u} \tag{4.15}$$

$$\text{and} \qquad \mathbf{0} = \tilde{\mathbf{A}}_2\mathbf{z}_2 + \tilde{\mathbf{B}_2}\mathbf{u}. \tag{4.16}$$

From (4.10), we have $\mathbf{z} = \boldsymbol{V}^{-1}x = \begin{bmatrix} \boldsymbol{U}_{11} & \boldsymbol{U}_{12} \\ \boldsymbol{U}_{21} & \boldsymbol{U}_{22} \end{bmatrix} \begin{bmatrix} \mathbf{x}_1 \\ \mathbf{x}_2 \end{bmatrix}$. Then from (4.16), we obtain

$$\mathbf{x}_2 = -\boldsymbol{U}_{22}^{-1}\boldsymbol{U}_{21}\mathbf{x}_1 - \boldsymbol{U}_{22}^{-1}\tilde{\mathbf{A}}_2^{-1}\tilde{\mathbf{B}_2}\mathbf{u}. \tag{4.17}$$

Substituting the solution of $\mathbf{x}_2$ from (4.17) into (4.4), the reduced order model is obtained as (4.2) and (4.3), where

$$\mathbf{A}_r = \mathbf{A}_{11} - \mathbf{A}_{12}\boldsymbol{U}_{22}^{-1}\boldsymbol{U}_{21}, \tag{4.18}$$

$$\mathbf{B}_r = \mathbf{B}_1 - \mathbf{A}_{12}\boldsymbol{U}_{22}^{-1}\tilde{\mathbf{A}}_2^{-1}\tilde{\mathbf{B}}_2, \tag{4.19}$$

$$\text{and} \qquad \mathbf{x}_2 = -\boldsymbol{U}_{22}^{-1}(\boldsymbol{U}_{21}\mathbf{x}_1 + \tilde{\mathbf{A}}_2^{-1}\tilde{\mathbf{B}}_1\mathbf{u}). \tag{4.20}$$

Again the original nth order model is approximated by rth order model. The first r state variables of the original model are approximated by the state variables of the reduced order model and the $(n-r)$ state variables are expressed in terms of the first r state variables by (4.20).

Remark 1: Methods based on retaining of dominant modes such as Davison's and Marshall's technique require diagonalization of the model. However, they differ in the procedure for obtaining reduced order models. Davison's method neglects the modes which are farther from the origin of s-plane. Whereas, Marshall's technique assumes that the fast modes decay rapidly. Davison's method does not provide the steady–state response of the original system and this drawback can be overcome in Marshall's method by exciting the modes in the reduced order model differently from those of original system. Both the methods can be applicable to only special case which provide non-degenerate eigenvectors. When the system matrix $\mathbf{A}$ under consideration has repeated eigenvalues and degenerate eigenvectors, it cannot be transformed into a pure diagonal form. An advantage of modal truncation methods (Davison's and Marshall's) is that the poles of the reduced-order system are also poles of the original system; however, selection of dominant eigenvalues is a difficult task for the systems having narrow spaced eigenvalues. One major disadvantage of the modal methods (Davison's and Marshall's) is that they require involved with the computation of eigenvalues and eigenvectors of the original high order model. This procedure is computationally cumbersome and may fail when the eigenvalues of the system are widely separated.

4.4 Singular Perturbation Analysis

In Linear time invariant models of large–scale systems, the interaction of slow and fast modes is common a feature and it leads the mathematical models to be ill-conditioned in control design. Singular perturbation analysis [60] provides a simple means to obtain approximate solutions to the original system as well as it alleviates the high dimensionality problem. This method is based on the assumption that the system can be separated into two subsystems: fast and slow. Singular perturbation method provides reduced order model, first by ignoring the fast modes of the system, then improves its quality of the approximation by reintroducing their effect as 'boundary layer' corrections calculated in separate time–scales.

In this method both the slow and fast modes are retained, but analysis and design problems are solved in two stages. By a suitable regrouping of the state variables, the original higher order system can be expressed into standard singularly perturbed form in which the derivatives of some of the states are multiplied by a small positive scalar ε, *i.e.*,

$$\dot{\mathbf{x}}_1 = \mathbf{A}_{11}\mathbf{x}_1 + \mathbf{A}_{12}\mathbf{x}_2 + \mathbf{B}_1\mathbf{u}, \quad \mathbf{x}_1(0) = \mathbf{x}_{10}, \tag{4.21}$$

$$\varepsilon\dot{\mathbf{x}}_2 = \mathbf{A}_{21}\mathbf{x}_1 + \mathbf{A}_{22}\mathbf{x}_2 + \mathbf{B}_2\mathbf{u}, \quad \mathbf{x}_2(0) = \mathbf{x}_{20} \tag{4.22}$$

$$\text{and} \qquad \mathbf{y} = \acute{\boldsymbol{\Psi}}_1\mathbf{x}_1 + \acute{\boldsymbol{\Psi}}_2\mathbf{x}_2. \tag{4.23}$$

where the n_1 dimensional state vector $\mathbf{x}_1$ is predominantly slow and the n_2 dimensional state vector $\mathbf{x}_2$ contains fast transients superimposed on a slowly varying "quasi–steady–state", *i.e.*, $\|\dot{\mathbf{x}}_2\| >> \|\dot{\mathbf{x}}_1\|$. The order of the system represented by (4.21) and (4.22) is $n_1 + n_2$. $\mathbf{u}$ is the m dimensional input vector and $\mathbf{y}$ is the p dimensional output vector. The scaling parameter $\varepsilon > 0$ represents the speed ratio of the slow versus fast phenomena. Let $\mu(\mathbf{A}) = \{\mu_1, \mu_2, \ldots, \mu_n\}$ be the set of eigenvalues of system (4.21)–(4.23). An important characteristic of the system described by (4.21)–(4.23) is that

the eigenvalues are found in two widely separated clusters: n_2 eigenvalues are of large magnitude while n_1 are of small magnitude. By setting the parasitic parameter $\varepsilon = 0$ in (4.22), the order of the system in (4.21), (4.22) reduces from $n_1 + n_2$ to n_1 because the differential equation (4.22) degenerates into algebraic equation as

$$\mathbf{0} = \mathbf{A}_{21}\bar{\mathbf{x}}_1 + \mathbf{A}_{22}\bar{\mathbf{x}}_2 + \mathbf{B}_2\mathbf{u}$$

where $\bar{\mathbf{x}}_1$, $\bar{\mathbf{x}}_2$ are the variables of the system (4.21), (4.22) when $\varepsilon = 0$. If $\mathbf{A}_{22}^{-1}$ exists, then the solution of $\bar{\mathbf{x}}_2$ into (4.21) results in reduced order model of order n_1 as

$$\dot{\mathbf{x}}_S = \mathbf{A}_S\mathbf{x}_S + \mathbf{B}_S\mathbf{u}_S, \tag{4.24}$$

$$\mathbf{y}_S = \boldsymbol{\Psi}_S\mathbf{x}_S + \mathbf{N}_S\mathbf{u}_S, \tag{4.25}$$

where

$$\mathbf{x}_S = \bar{\mathbf{x}}_1, \tag{4.26}$$

$$\mathbf{u}_S = \bar{\mathbf{u}}, \tag{4.27}$$

$$\mathbf{A}_S = \mathbf{A}_{11} - \mathbf{A}_{12}\mathbf{A}_{22}^{-1}\mathbf{A}_{21}, \tag{4.28}$$

$$\mathbf{B}_S = \mathbf{B}_1 - \mathbf{A}_{12}\mathbf{A}_{22}^{-1}\mathbf{B}_2, \tag{4.29}$$

$$\boldsymbol{\Psi}_S = \acute{\boldsymbol{\Psi}}_1 - \acute{\boldsymbol{\Psi}}_2\mathbf{A}_{22}^{-1}\mathbf{A}_{21}, \tag{4.30}$$

$$\mathbf{N}_S = -\acute{\boldsymbol{\Psi}}_2\mathbf{A}_{22}^{-1}\mathbf{B}_2, \tag{4.31}$$

and a fast subsystem of order n_2 given by

$$\varepsilon\dot{\mathbf{x}}_F = \mathbf{A}_{22}\mathbf{x}_F + \mathbf{B}_2\mathbf{u}_F, \tag{4.32}$$

$$\mathbf{y}_F = \acute{\boldsymbol{\Psi}}_2\mathbf{x}_F, \tag{4.33}$$

where

$$\mathbf{x}_F = \mathbf{x}_2 - \bar{\mathbf{x}}_2, \tag{4.34}$$

$$\mathbf{u}_F = \mathbf{u} - \bar{\mathbf{u}}. \tag{4.35}$$

Therefore, eigenvalues of original system are $\mu(\mathbf{A}) = \mu(\mathbf{A}_S) \cup \mu(\frac{\mathbf{A}_{22}}{\varepsilon})$.

Remark 2: In control theory singular perturbation approach also provides model order reduction first by neglecting the fast phenomena. It is then improves the approximation by reintroducing their effect as 'boundary layer' correction calculated in separate time–scales. The approach makes use of the standard singularly perturbed form representation as (4.21–4.22). Then, the model reduction is achieved by setting $\varepsilon = 0$ and substituting the solution of states whose derivatives were multiplied with ε, in terms of other state variables. This approach to model order reduction is similar to the "dominant mode" technique which neglect "high frequency " parts and retains low frequency parts of the dynamical system.

4.4.1 Two-Time-Scale Decomposition of Singularly Perturbed Systems

The main purpose of the singular perturbation approach to analysis and design is to handle the ill-conditioning resulting from the interaction of slow and fast dynamic modes. The system described by (4.21)–(4.23), can be converted into block diagonal form as,

$$\begin{bmatrix} \dot{\mathbf{x}}_S \\ \dot{\mathbf{x}}_F \end{bmatrix} = \begin{bmatrix} \mathbf{A}_S & \mathbf{0} \\ \mathbf{0} & \mathbf{A}_F \end{bmatrix} \begin{bmatrix} \mathbf{x}_S \\ \mathbf{x}_F \end{bmatrix} + \begin{bmatrix} \mathbf{B}_S \\ \mathbf{B}_F \end{bmatrix} \mathbf{u} \tag{4.36}$$

and corresponding observations as

$$\mathbf{y} = \begin{bmatrix} \boldsymbol{\Psi}_S & \boldsymbol{\Psi}_F \end{bmatrix} \begin{bmatrix} \mathbf{x}_S \\ \mathbf{x}_F \end{bmatrix}, \tag{4.37}$$

such that $\mu(\mathbf{A}) = \mu(\mathbf{A}_S) \cup \mu(\mathbf{A}_F)$, where $\mu(\mathbf{A})$ denotes the set of eigenvalues of $\mathbf{A}$. The similarity transformation that is applied to the system given by (4.21)–(4.23) to obtain the system given by (4.36)–(4.37), is

$$\begin{bmatrix} \mathbf{x}_S \\ \mathbf{x}_F \end{bmatrix} = \begin{bmatrix} \mathbf{I}_{n_1} - \varepsilon\mathbf{M}\mathbf{L} & -\varepsilon\mathbf{M} \\ \mathbf{L} & \mathbf{I}_{n_2} \end{bmatrix} \begin{bmatrix} \mathbf{x}_1 \\ \mathbf{x}_2 \end{bmatrix}, \tag{4.38}$$

in which $\mathbf{I}_{n_1}$ and $\mathbf{I}_{n_2}$ respectively denote n_1 and n_2 dimensional identity matrices, and $\mathbf{L}$ and $\mathbf{M}$ respectively satisfy,

$$\varepsilon\dot{\mathbf{L}} = \mathbf{A}_{22}\mathbf{L} - \mathbf{A}_{21} - \varepsilon\mathbf{L}(\mathbf{A}_{11} - \mathbf{A}_{12}\mathbf{L}) \tag{4.39}$$

$$\text{and} \quad \varepsilon\dot{\mathbf{M}} = -\mathbf{M}(\mathbf{A}_{22} + \varepsilon\mathbf{L}\mathbf{A}_{12}) + \mathbf{A}_{12} + \varepsilon(\mathbf{A}_{11} - \mathbf{A}_{12}\mathbf{L})\mathbf{M}. \tag{4.40}$$

$\mathbf{L}$ in (4.39) and $\mathbf{M}$ in (4.40) can be determined respectively by iterative solution of [63]

$$\mathbf{L}_{k+1} = \mathbf{A}_{22}^{-1}\mathbf{A}_{21} + \varepsilon\mathbf{A}_{22}^{-1}\mathbf{L}_k(\mathbf{A}_{11} - \mathbf{A}_{12}\mathbf{L}_k), \tag{4.41}$$

$$\begin{aligned} \mathbf{M}_{k+1} = \varepsilon[(\mathbf{A}_{11} - \mathbf{A}_{12}\mathbf{L}_k)\mathbf{M}_k - \mathbf{M}_k\mathbf{L}_k\mathbf{A}_{12}]\mathbf{A}_{22}^{-1} \\ + \mathbf{A}_{12}\mathbf{A}_{22}^{-1}, \end{aligned} \tag{4.42}$$

$$\mathbf{L}_0 = \mathbf{A}_{22}^{-1}\mathbf{A}_{21}, \quad \mathbf{M}_0 = \mathbf{A}_{12}\mathbf{A}_{22}^{-1}, \quad k = 0, 1, 2, ... \tag{4.43}$$

The matrices in (4.36) and (4.37) are related to those in (4.21)–(4.23) as

$$\left.\begin{aligned} \mathbf{A}_S &= \mathbf{A}_{11} - \mathbf{A}_{12}\mathbf{L}, \quad \mathbf{A}_F = \frac{\mathbf{A}_{22}}{\varepsilon} + \mathbf{L}\mathbf{A}_{12}, \\ \mathbf{B}_S &= (\boldsymbol{I}_{n_1} - \varepsilon\mathbf{M}\mathbf{L})\mathbf{B}_1 - \mathbf{M}\mathbf{B}_2, \\ \mathbf{B}_F &= \mathbf{L}\mathbf{B}_1 + \frac{\mathbf{B}_2}{\varepsilon}, \quad \boldsymbol{\Psi}_S = \boldsymbol{\Psi}_1 - \boldsymbol{\Psi}_2\mathbf{L}, \\ \text{and} \quad \boldsymbol{\Psi}_F &= \varepsilon\boldsymbol{\Psi}_1\mathbf{M} + \boldsymbol{\Psi}_2(\mathbf{I}_{n_2} - \varepsilon\mathbf{L}\mathbf{M}). \end{aligned}\right\} \tag{4.44}$$

The system represented by (4.36) and (4.37) can be discretized to obtain

$$\begin{bmatrix} \mathbf{x}_{S,k} \\ \mathbf{x}_{F,k} \end{bmatrix} = \begin{bmatrix} \boldsymbol{\Phi}_S & 0 \\ 0 & \boldsymbol{\Phi}_F \end{bmatrix} \begin{bmatrix} \mathbf{x}_{S,k-1} \\ \mathbf{x}_{F,k-1} \end{bmatrix} + \begin{bmatrix} \boldsymbol{\Gamma}_S \\ \boldsymbol{\Gamma}_F \end{bmatrix} \mathbf{u}_{k-1}, \tag{4.45}$$

$$\mathbf{y}_k = \begin{bmatrix} \boldsymbol{\Psi}_S & \boldsymbol{\Psi}_F \end{bmatrix} \begin{bmatrix} \mathbf{x}_{S,k} \\ \mathbf{x}_{F,k} \end{bmatrix}. \tag{4.46}$$

where $\boldsymbol{\Phi}_S = e^{\mathbf{A}_S\tau}$, $\boldsymbol{\Phi}_F = e^{\mathbf{A}_F\tau}$, $\boldsymbol{\Gamma}_S = \int_0^\tau e^{\mathbf{A}_S\mu}\mathbf{B}_S d\mu$, $\boldsymbol{\Gamma}_F = \int_0^\tau e^{\mathbf{A}_F\mu}\mathbf{B}_F d\mu$, and $\tau = t_k - t_{k-1}$ is the sampling duration. For $\tau > \varepsilon$, the system represented by (4.45) also exhibits two-time-scale behavior, *i.e.*, the eigenvalues of $\boldsymbol{\Phi}_F$ will be located close to the origin of the z-plane while those of $\boldsymbol{\Phi}_S$ will be located close to the periphery of the unit circle.

Remark 3: The block diagonalization technique of singular perturbation approach described in subsection 4.4.1 alleviates both dimensionality and stiffness difficulties. The decomposition of two-time-scale systems into separate slow and fast subsystems suggests that separate controller/observer law can be designed for each subsystem and then combined into a composite controller/observer law for the original system.

4.5 Balanced Truncation Method

For the state–space models represented by (4.1), a methodology for deriving reduced-order model is proposed in terms of realization in balanced co-ordinates by Moore [81].

Most of the balanced truncation methods available in literature can only be applied if the system is stable. But realistic models, which are used for system analysis and design may not be stable. Hence, the straightforward application of balanced truncation methods is not possible. Therefore, model reduction of unstable system can be treated by first separating the stable and unstable parts of the system, and then reducing the stable part using balanced truncation methods.

4.5.1 Model decomposition into stable and unstable subsystems

For the purpose of this thesis, stable means the open left half of the complex s-plane *i.e.,* $\boldsymbol{\mu} \in \mathbb{C}^- :\Rightarrow Re(\boldsymbol{\mu}) < 0$; unstable means right half of the complex s-plane including the imaginary axis *i.e.,* $\boldsymbol{\mu} \in \bar{\mathbb{C}}^+ :\Rightarrow Re(\boldsymbol{\mu}) \geq 0$. Different approaches for decomposition into stable and unstable subsystems were reported in [5, 57, 86, 99, 137]. Here, we consider the application of decomposition algorithm given in [86]. It is briefly introduced in the following.

The system represented by (4.1) can be converted into block triangular form as

$$\mathbf{G}_t := \left[\begin{array}{c|c} \mathbf{E}^T\mathbf{A}\mathbf{E} & \mathbf{E}^T\mathbf{B} \\ \hline \boldsymbol{\Psi}\mathbf{U} & \mathbf{0} \end{array}\right] = \left[\begin{array}{c|c} \mathbf{A}_t & \mathbf{B}_t \\ \hline \boldsymbol{\Psi}_t & \mathbf{0} \end{array}\right], \tag{4.47}$$

where

$$\mathbf{A}_t = \begin{array}{c} k \\ n-k \end{array}\!\!\left[\begin{array}{c|c} \overset{k}{\mathbf{A}_{t_{11}}} & \overset{n-k}{\mathbf{A}_{t_{12}}} \\ \hline \mathbf{0} & \mathbf{A}_{t_{22}} \end{array}\right]; \mathbf{B}_t = \begin{array}{c} k \\ n-k \end{array}\!\!\left[\begin{array}{c} \mathbf{B}_{t_1} \\ \hline \mathbf{B}_{t_2} \end{array}\right];$$

$$\boldsymbol{\Psi}_t = \left[\begin{array}{c|c} \overset{k}{\boldsymbol{\Psi}_{t_{11}}} & \overset{n-k}{\boldsymbol{\Psi}_{t_{12}}} \end{array}\right],$$

where $\mathbf{A}_{t_{11}}$, $\mathbf{A}_{t_{12}}$, $\mathbf{A}_{t_{22}}$, $\mathbf{B}_{t_1}$, $\mathbf{B}_{t_2}$, $\boldsymbol{\Psi}_{t_{11}}$ and $\boldsymbol{\Psi}_{t_{12}}$ are respectively $k \times k$, $k \times (n-k)$, $(n-k) \times (n-k)$, $k \times m$, $(n-k) \times m$, $p \times k$ and $p \times (n-k)$ submatrices, obtained by partitioning $\mathbf{A}_t$, $\mathbf{B}_t$ and $\boldsymbol{\Psi}_t$ as indicated.

A similarity transformation that is applied to the system given by (4.1) to obtain the system (4.47) is

$$\mathbf{x} = \mathbf{E}\mathbf{x}_t, \tag{4.48}$$

where $\mathbf{E}$ is an orthogonal similarity transformation that brings $\mathbf{A}$ to the real Schur form such that the diagonal elements of $\mathbf{A}_t$ are are the real parts of the eigenvalues of $\mathbf{A}$ arranged in order of increasing values of the real part. Further, k is the number of stable poles present in $\mathbf{G}$. By another transformation, the system represented by (4.47) can be converted into block diagonal form as

$$\mathbf{G}_d := \left[\begin{array}{c|c} \mathbf{F}^{-1}\mathbf{A}_t\mathbf{F} & \mathbf{F}^{-1}\mathbf{B}_t \\ \hline \boldsymbol{\Psi}_t\mathbf{F} & \mathbf{0} \end{array}\right] = \left[\begin{array}{c|c} \check{\mathbf{A}} & \check{\mathbf{B}} \\ \hline \check{\boldsymbol{\Psi}} & \mathbf{0} \end{array}\right], \tag{4.49}$$

where

$$\check{\mathbf{A}} = \begin{array}{c} \\ n-k \end{array}\overset{\begin{array}{cc} k & n-k \end{array}}{\left[\begin{array}{c|c} \mathbf{A}_s & \mathbf{0} \\ \hline \mathbf{0} & \mathbf{A}_{us} \end{array}\right]}\begin{array}{c} k \\ \\ \end{array}; \check{\mathbf{B}} = \begin{array}{c} \\ n-k \end{array}\overset{\begin{array}{c} k \end{array}}{\left[\begin{array}{c} \mathbf{B}_s \\ \hline \mathbf{B}_{us} \end{array}\right]}\begin{array}{c} k \\ \\ \end{array};$$

$$\check{\boldsymbol{\Psi}} = \left[\begin{array}{cc} k & n-k \\ \boldsymbol{\Psi}_s & \boldsymbol{\Psi}_{us} \end{array}\right],$$

with $\boldsymbol{\mu}(\mathbf{A}_s) := \boldsymbol{\mu}(\mathbf{A}) \subset \mathbb{C}^-$, $\mathbf{A}_s \in \mathbb{R}^{k\times k}$, $\boldsymbol{\mu}(\mathbf{A}_{us}) := \boldsymbol{\mu}(\mathbf{A}) \subset \bar{\mathbb{C}}^+$, and $\mathbf{A}_{us} \in \mathbb{R}^{(n-k)\times(n-k)}$. Note that $\mathbf{A}_s$, $\mathbf{A}_{us}$, $\mathbf{B}_s$, $\mathbf{B}_{us}$, $\boldsymbol{\Psi}_s$ and $\boldsymbol{\Psi}_{us}$ are respectively $k \times k$, $(n-k)\times(n-k)$, $k \times m$, $(n-k)\times m$, $p \times k$ and $p \times (n-k)$ submatrices, obtained by partitioning $\check{\mathbf{A}}$, $\check{\mathbf{B}}$ and $\check{\boldsymbol{\Psi}}$ as indicated,

The second stage transform that is applied to the system given by (4.47) to obtain the system (4.49) is

$$\mathbf{x}_t = \begin{bmatrix} \mathbf{I}_k & \mathbf{S} \\ \mathbf{0} & \mathbf{I}_{n-k} \end{bmatrix} \begin{bmatrix} \mathbf{x}_s \\ \mathbf{x}_{us} \end{bmatrix} = \mathbf{F} \begin{bmatrix} \mathbf{x}_s \\ \mathbf{x}_{us} \end{bmatrix}, \tag{4.50}$$

where $\mathbf{S}$ is the solution of the Sylvester equation

$$\mathbf{A}_{t_{11}}\mathbf{S} - \mathbf{S}\mathbf{A}_{t_{22}} + \mathbf{A}_{t_{12}} = \mathbf{0}. \tag{4.51}$$

Therefore, the system (4.1) can be written in decoupled form as

$$\mathbf{G} := \mathbf{G}_{-} + \mathbf{G}_{+}, \tag{4.52}$$

where $\mathbf{G}_{-} := (\mathbf{A}_s, \mathbf{B}_s, \boldsymbol{\Psi}_s, \mathbf{0})$ is stable and $\mathbf{G}_{+} := (\mathbf{A}_{us}, \mathbf{B}_{us}, \boldsymbol{\Psi}_{us}, \mathbf{0})$ is unstable.

4.5.2 State-Space Balancing Algorithm

Two quantities, reachability and observability Gramians play a major role in obtaining system balancing transformation. For a linear system represented by (4.1), they are defined respectively as follows:

$$\mathbf{W}_R := \int_0^\infty e^{\mathbf{A}\tau}\mathbf{B}\mathbf{B}^T e^{\mathbf{A}^T\tau} d\tau \tag{4.53}$$

$$\mathbf{W}_O := \int_0^\infty e^{\mathbf{A}^T\tau}\boldsymbol{\Psi}^T\boldsymbol{\Psi} e^{\mathbf{A}\tau} d\tau \tag{4.54}$$

Assuming that the pair $(\mathbf{A}_s, \mathbf{B}_s)$ is reachable and $(\boldsymbol{\Psi}_s, \mathbf{A}_s)$ is observable, the *reachability Gramian* $\mathbf{W}_R$ and *observability Gramian* $\mathbf{W}_O$ of $\mathbf{G}_{-}$ can be obtained by the solution of the following algebraic Lyapunov equations [70]:

$$\mathbf{A}_s\mathbf{W}_R + \mathbf{W}_R\mathbf{A}_s^T + \mathbf{B}_s\mathbf{B}_s^T = 0, \tag{4.55}$$

$$\mathbf{A}_s^T\mathbf{W}_O + \mathbf{W}_O\mathbf{A}_s + \boldsymbol{\Psi}_s^T\boldsymbol{\Psi}_s = 0. \tag{4.56}$$

The goal of balancing is to find a co-ordinate transformation such that in the new co-ordinate system the reachability and the observability Gramians both are diagonal and equal. In balanced co-ordinate system $\mathbf{G}_{-}$ can be represented as

$$\mathbf{G}_{-}^{bal} := \left[\begin{array}{c:c} \mathbf{T}^{-1}\mathbf{A}_s\mathbf{T} & \mathbf{T}^{-1}\mathbf{B}_s \\ \hdashline \boldsymbol{\Psi}_s\mathbf{T} & \mathbf{0} \end{array}\right] = \left[\begin{array}{c:c} \mathbf{A}_{bal} & \mathbf{B}_{bal} \\ \hdashline \boldsymbol{\Psi}_{bal} & \mathbf{0} \end{array}\right], \tag{4.57}$$

where

$$\mathbf{A}_{bal} = \begin{array}{c} \\ r \\ k-r \end{array} \begin{array}{c} \begin{array}{cc} r & k-r \end{array} \\ \left[\begin{array}{c|c} \mathbf{A}_{bal}^{(11)} & \mathbf{A}_{bal}^{(12)} \\ \hline \mathbf{A}_{bal}^{(21)} & \mathbf{A}_{bal}^{(22)} \end{array}\right] \end{array}; \mathbf{B}_{bal} = \begin{array}{c} \\ r \\ k-r \end{array} \begin{array}{c} \\ \left[\begin{array}{c} \mathbf{B}_{bal}^{(1)} \\ \hline \mathbf{B}_{bal}^{(2)} \end{array}\right] \end{array};$$

$$\boldsymbol{\Psi}_{bal} = \begin{array}{c} \\ \left[\begin{array}{cc} r & k-r \\ \boldsymbol{\Psi}_{bal}^{(1)} & \boldsymbol{\Psi}_{bal}^{(2)} \end{array}\right] \end{array},$$

where $\mathbf{A}_{bal}^{(11)}$, $\mathbf{A}_{bal}^{(12)}$, $\mathbf{A}_{bal}^{(21)}$, $\mathbf{A}_{bal}^{(22)}$, $\mathbf{B}_{bal}^{(1)}$, $\mathbf{B}_{bal}^{(2)}$, $\boldsymbol{\Psi}_{bal}^{(1)}$ and $\boldsymbol{\Psi}_{bal}^{(2)}$ are respectively $r \times r$, $r \times (k-r)$, $(k-r) \times r$, $(k-r) \times (k-r)$, $r \times m$, $(r-k) \times m$, $p \times r$ and $p \times (k-r)$ submatrices, obtained by partitioning $\mathbf{A}_{bal}$, $\mathbf{B}_{bal}$ and $\boldsymbol{\Psi}_{bal}$ as indicated. Further, r is the number of states which are to be retained in $\mathbf{G}_{-}^{bal}$. The procedure for obtaining $\mathbf{G}_{-}^{bal}$ and selection of r are discussed in the following.

A similarity transformation to obtain $\mathbf{G}_{-}^{bal}$ from $\mathbf{G}_{-}$ is

$$\mathbf{x}_s = \mathbf{T}\mathbf{x}_{s_b}, \tag{4.58}$$

where $\mathbf{T} \in \mathbb{R}^{k \times k}$ is nonsingular. Following [70], an algorithm for computation of balancing transformation is as follows:

(1) Compute the Gramians $\mathbf{W}_R$ and $\mathbf{W}_O$ for $\mathbf{G}_{-}$.

(2) Compute the Cholesky factors of $\mathbf{W}_R$ and $\mathbf{W}_O$ *i.e.,* $\mathbf{W}_R = \boldsymbol{L}_R \boldsymbol{L}_R^T$, $\quad \mathbf{W}_O = \boldsymbol{L}_O \boldsymbol{L}_O^T$, where $\boldsymbol{L}_R$ and $\boldsymbol{L}_O$ denote lower triangular Cholesky factors.

(3) Compute SVD of product of Cholesky factors, *i.e.,* $\boldsymbol{L}_O^T \boldsymbol{L}_R = \mathbf{U}\boldsymbol{\Sigma}\mathbf{V}^T$

(4) Finally, a co-ordinate transformation that results in balanced realization can be obtained as

$$\mathbf{T} = \boldsymbol{L}_R \mathbf{V} \boldsymbol{\Sigma}^{-1/2}. \tag{4.59}$$

$\mathbf{G}_{-}^{bal}$ is asymptotically stable and is in balanced realization form with

$$\overline{\mathbf{W}}_R = \overline{\mathbf{W}}_O = \text{diag.} \begin{bmatrix} \boldsymbol{\Sigma}_1 & \boldsymbol{\Sigma}_2 \end{bmatrix}, \tag{4.60}$$

where

$$\boldsymbol{\Sigma}_1 = \text{diag. } [\boldsymbol{\sigma}_1 \ \boldsymbol{\sigma}_2 \ \ldots \ \boldsymbol{\sigma}_r], \quad \boldsymbol{\Sigma}_2 = \text{diag. } [\boldsymbol{\sigma}_{r+1} \ \boldsymbol{\sigma}_{r+2} \ \ldots \ \boldsymbol{\sigma}_k],$$

$\boldsymbol{\sigma}_r > \boldsymbol{\sigma}_{r+1}$ and $\boldsymbol{\sigma}_i > 0$, $i = 1, 2, \ldots, k$, $\boldsymbol{\sigma}_i$ are the Hankel singular values of $\mathbf{G}_-^{bal}$. One usually tries to choose r so that we have $\boldsymbol{\sigma}_r \gg \boldsymbol{\sigma}_{r+1}$, in addition to other criteria like desired accuracy and sought order of the reduced order model. Therefore, the system (4.1) can be represented in additive TF form as

$$\mathbf{G}(s) := \mathbf{G}_+(s) + \mathbf{G}_-^{bal}(s), \tag{4.61}$$

where $\mathbf{G}_-^{bal} := (\mathbf{A}_{bal}, \mathbf{B}_{bal}, \boldsymbol{\Psi}_{bal}, \mathbf{0})$ is balanced and stable. Let

$$\begin{bmatrix} \mathbf{x}_1 \\ \mathbf{x}_2 \\ \mathbf{x}_3 \end{bmatrix} = \begin{bmatrix} \boldsymbol{\eta}_{11} & \boldsymbol{\eta}_{12} & \boldsymbol{\eta}_{13} \\ \boldsymbol{\eta}_{21} & \boldsymbol{\eta}_{22} & \boldsymbol{\eta}_{23} \\ \boldsymbol{\eta}_{31} & \boldsymbol{\eta}_{32} & \boldsymbol{\eta}_{33} \end{bmatrix} \begin{bmatrix} \mathbf{x}_{us} \\ \mathbf{x}_{s_{b1}} \\ \mathbf{x}_{s_{b2}} \end{bmatrix} \tag{4.62}$$

where $\mathbf{x}_{us} \in \mathbb{R}^{n-k}$, $\mathbf{x}_{s_{b1}} \in \mathbb{R}^r$, and $\mathbf{x}_{s_{b2}} \in \mathbb{R}^{k-r}$ be a similarity transformation to obtain (4.61) from (4.1). Hankel singular values for the system are defined as the square roots of the eigenvalues of the product $\mathbf{W}_R\mathbf{W}_O$. The balanced basis has the property that the states which are difficult to reach are simultaneously difficult to observe. The states in $\mathbf{G}_-^{bal}$ corresponding to the largest singular values are most important in the input-output behavior. Truncation of the states corresponding to the smaller Hankel singular values *i.e.,* $\boldsymbol{\Sigma}_2$ will result in a reduced order model $\widehat{\mathbf{G}}_r$ whose input-output behavior closely approximates the behavior of the original model. More precisely, the H_∞ norm of the difference between full-order system $\mathbf{G}$ and the reduced order system $\widehat{\mathbf{G}}_r$ is upper bounded by twice the sum of the neglected Hankel singular values [2] and given as

$$\|\mathbf{G} - \widehat{\mathbf{G}}_r\|_{H_\infty} \leqslant 2(\boldsymbol{\sigma}_{r+1} + \cdots + \boldsymbol{\sigma}_k). \tag{4.63}$$

Therefore, a reduced order model for the system (4.1) can be obtained as

$$\bar{\mathbf{G}}_r := \left[\begin{array}{c|c} \mathbf{A}_r & \mathbf{B}_r \\ \hline \boldsymbol{\Psi}_r & \mathbf{0} \end{array}\right], \tag{4.64}$$

where

$$\mathbf{A}_r = \begin{array}{c} \\ n-k \\ r \end{array} \begin{array}{c} \begin{array}{cc} n-k & r \end{array} \\ \left[\begin{array}{c|c} \mathbf{A}_{us} & \mathbf{0} \\ \hline \mathbf{0} & \mathbf{A}_{bal}^{(11)} \end{array}\right] \end{array}; \quad \mathbf{B}_r = \begin{array}{c} \\ n-k \\ r \end{array} \begin{array}{c} \\ \left[\begin{array}{c} \mathbf{B}_{us} \\ \hline \mathbf{B}_{bal}^{(1)} \end{array}\right] \end{array};$$

$$\boldsymbol{\Psi}_r = \begin{array}{c} \begin{array}{cc} n-k & r \end{array} \\ \left[\begin{array}{c|c} \boldsymbol{\Psi}_{us} & \boldsymbol{\Psi}_{bal}^{(1)} \end{array}\right] \end{array}.$$

Reduced order model of (4.1) in terms of original co-ordinate system can be obtained by setting $\mathbf{x}_{s_{b2}} = \mathbf{0}$ in (4.62) as

$$\dot{\tilde{\mathbf{x}}} = \boldsymbol{\Lambda}\mathbf{A}_r\boldsymbol{\Lambda}^{-1}\tilde{\mathbf{x}} + \boldsymbol{\Lambda}\mathbf{B}_r\mathbf{u}, \tag{4.65}$$

$$\mathbf{y} = \boldsymbol{\Psi}_r\boldsymbol{\Lambda}^{-1}\tilde{\mathbf{x}}, \tag{4.66}$$

where $\tilde{\mathbf{x}} = \begin{bmatrix} \mathbf{x}_1 \\ \mathbf{x}_2 \end{bmatrix}$, $\boldsymbol{\Lambda} = \begin{bmatrix} \boldsymbol{\eta}_{11} & \boldsymbol{\eta}_{12} \\ \boldsymbol{\eta}_{21} & \boldsymbol{\eta}_{22} \end{bmatrix}$. Moreover, from (4.62) we have

$$\mathbf{x}_3 = \boldsymbol{\xi} \begin{bmatrix} \mathbf{x}_1 \\ \mathbf{x}_2 \end{bmatrix}, \text{ where } \boldsymbol{\xi} = \begin{bmatrix} \boldsymbol{\eta}_{31} & \boldsymbol{\eta}_{32} \end{bmatrix} \boldsymbol{\Lambda}^{-1}. \tag{4.67}$$

Thus, the original n th order model represented by (4.1) is reduced to $(n-k+r)$ th order model. The state variables of the reduced order model are defined as the first $(n-k+r)$ state variables of the original model. Though we do not need the remaining $(k-r)$ state variables of original model, if they are required in an application, they can be expressed in terms of the first $(n-k+r)$ state variables by using (4.67).

Remark 4: : Model reduction by balanced truncation requires balancing the whole system $\mathbf{G}_-$ followed by truncation. The Lyapunov equations (4.55) and (4.56) play a

prominent role in obtaining system balancing transformation $\mathbf{T}$ and are required to be solved to obtain $\mathbf{W}_R$ and $\mathbf{W}_O$. The Bartels-Stewart and Hammarling methods are direct standard methods for the solution of Lyapunov equations of small to moderate size. These methods rely on initial Schur decomposition of $\mathbf{A}_s$ followed by additional factorization schemes. In general and especially for large-scale systems, it is unwise to solve for $\mathbf{W}_R$ and $\mathbf{W}_O$ directly since these require arithmetic operations of order N^3 representing computational complexity and storage of order N^2, where N is the original system order. This approach may turn out to be numerically inefficient and ill-conditioned as the Gramians $\mathbf{W}_R$ and $\mathbf{W}_O$ often have numerically low rank *i.e.*, the eigenvalues of $\mathbf{W}_R$ and $\mathbf{W}_O$ decay rapidly. However, results on low rank approximations to the solutions of Lyapunov equations based on iterative methods (SVD-Krylov methods) make the balanced truncation model reduction approach feasible for large-scale systems [2, 4, 93].

Chapter 5

Application of Model Order Reduction Techniques to Space–Time Kinetics Model of AHWR

In chapter-3, the dynamical model describing the time–dependent core neutronics behavior of the AHWR has been derived. This complex nonlinear mathematical model (core neutronics and control rod dynamic equations) can be linearized around steady–state operating point to obtain a linear model for the purpose of estimation. An important characteristic of this nodal method based model, is that the order depends on the number of nodes into which the reactor spatial domain is divided. A rigorous model with more number of nodes will give good accuracy in online monitoring and control, but its order is also very high. At the same time, nuclear reactor models often exhibit simultaneous presence of dynamics of different speeds. Such behavior leads to

Parts of this chapter were published in *2015 IEEE international Conference on Industrial Instrumentation and Control Applications (ICIC)*, Pune, India and in *Annals of Nuclear Energy*, Vol. 102.

a mathematical model with multiple time-scales, which may be susceptible to numerical ill-conditioning in flux mapping studies. Hence, there is a strong motivation for obtaining a suitable reduced order model which alleviates the high dimensionality and numerical ill-conditioning problems in computations.

This chapter presents the derivation of an estimation model for flux distribution studies in the AHWR and also the comparative study between different reduced order models of AHWR, namely, Davison's technique, Marshall's technique, singular perturbation analysis and balanced truncation, by comparing their performances relative to each other and with the original model.

5.1 Derivation of Estimation Model

The system of nonlinear equations (3.18)–(3.22) is linearized around the steady–state operating point (ϕ_{h0}, C_{h0}, H_{j0}), by considering a small perturbation in neutron flux level, delayed neutron precursor concentration (for simplicity, only one group of delayed neutron precursors is considered instead of six groups), RR position and the input voltages to RR drives, denoted respectively by $\delta\phi_h$, δC_h, δH_h and $\delta\vartheta_l$ around the operating point. Now from (3.18)–(3.20) and (3.22), we have

$$\frac{d}{dt}\Big(\frac{\delta\phi_h}{\phi_{h0}}\Big) = \Big[-\omega_{hh}\upsilon_h + \frac{\rho_{h0}}{\ell_h} - \frac{\beta}{\ell_h}\Big]\frac{\delta\phi_h}{\phi_{h0}} + \sum_{k=1}^{N_h}\omega_{hk}\upsilon_h\Big(\frac{\phi_{k0}}{\phi_{h0}}\Big)\frac{\delta\phi_k}{\phi_{k0}} + \frac{\beta}{\ell_h}\frac{\delta C_h}{C_{h0}} - \frac{10.234\times10^{-6}\times\phi_{h0}}{\ell_h}\delta H_h, \tag{5.1}$$

$$h = 1, 2, 3, ..., Z_p,$$

$$\frac{d}{dt}\Big(\frac{\delta C_h}{C_{h0}}\Big) = \lambda\frac{\delta\phi_h}{\phi_{h0}} - \lambda\frac{\delta C_h}{C_{h0}}, \quad h = 1, 2, 3, \ldots, Z_p \tag{5.2}$$

$$\frac{d}{dt}\Big(\frac{\delta\phi_h}{\phi_{h0}}\Big) = -\omega_{hh}\upsilon_h\frac{\delta\phi_h}{\phi_{h0}} + \sum_{k=1}^{N_h}\omega_{hk}\upsilon_h\Big(\frac{\phi_{k0}}{\phi_{h0}}\Big)\frac{\delta\phi_k}{\phi_{k0}}, \tag{5.3}$$

$$h = Z_p + 1, \ldots, Z_p + Z_r,$$

$$\frac{d\delta H_l}{dt} = K_{RR}\delta\vartheta_l, \quad l = 2, 4, 6, 8. \tag{5.4}$$

where δ denotes the deviation from respective steady–state values. In (5.1), the term δH_l denoting the deviation in position of the lth RR from that corresponding to the critical configuration, will be present only if the node h contains the RR-l. Now, let us define the state vector as

$$\mathbf{x} := \begin{bmatrix} \mathbf{x}_{\phi_C}^T & \mathbf{x}_C^T & \mathbf{x}_{\phi_R}^T & \mathbf{x}_H^T \end{bmatrix}^T \tag{5.5}$$

where

$$\mathbf{x}_{\phi_C} := \begin{bmatrix} \delta\phi_1/\phi_{1_0} & ... & \delta\phi_{17}/\phi_{17_0} \end{bmatrix}^T, \tag{5.6}$$

$$\mathbf{x}_C := \begin{bmatrix} \delta C_1/C_{1_0} & ... & \delta C_{17}/\phi_{17_0} \end{bmatrix}^T, \tag{5.7}$$

$$\mathbf{x}_{\phi_R} := \begin{bmatrix} \delta\phi_{18}/\phi_{18_0} & ... & \delta\phi_{59}/\phi_{59_0} \end{bmatrix}^T, \tag{5.8}$$

$$\mathbf{x}_H := \begin{bmatrix} \delta H_2 & \delta H_4 & \delta H_6 & \delta H_8 \end{bmatrix}^T. \tag{5.9}$$

In (5.5), $\mathbf{x}_{\phi_C}$ and $\mathbf{x}_C$ denote the state vectors corresponding to the deviation in normalized neutron flux and associated deviation in precursors' concentration in the core nodes respectively. $\mathbf{x}_{\phi_R}$ denotes state vector corresponding to the deviation in normalized neutron flux in reflector nodes, $\mathbf{x}_H$ denotes the state vector corresponding to the deviation in the position of RRs.

Also, define the input vector as

$$\mathbf{u} = \begin{bmatrix} \delta\vartheta_2 & \delta\vartheta_4 & \delta\vartheta_6 & \delta\vartheta_8 \end{bmatrix}^T. \tag{5.10}$$

As already introduced, $\delta\vartheta_l$ denotes deviation of applied to lth RR. Then, the system of equations (5.1)–(5.4) which constitute the estimation model can be represented in standard linear state–space form of (4.1). The system matrix $\mathbf{A}$ of size 80×80, is

expressed as,

$$\mathbf{A} = \begin{bmatrix} \mathbf{A}_{\phi_C\phi_C} & \mathbf{A}_{\phi_C C} & \mathbf{A}_{\phi_C\phi_R} & \mathbf{A}_{\phi_C H} \\ \mathbf{A}_{C\phi_C} & \mathbf{A}_{CC} & \mathbf{0} & \mathbf{0} \\ \mathbf{A}_{\phi_R\phi_C} & \mathbf{0} & \mathbf{A}_{\phi_R\phi_R} & \mathbf{0} \\ \mathbf{0} & \mathbf{0} & \mathbf{0} & \mathbf{0} \end{bmatrix}, \tag{5.11}$$

the input matrix is given as

$$\mathbf{B} = \begin{bmatrix} \mathbf{0} & \mathbf{0} & \mathbf{0} & \mathbf{B}_H^T \end{bmatrix}^T, \tag{5.12}$$

and the output matrix is given as

$$\boldsymbol{\Psi} = \begin{bmatrix} \boldsymbol{\kappa}_{\mathrm{DV}} & \mathbf{0} & \mathbf{0} & \mathbf{0} \end{bmatrix} \tag{5.13}$$

where

$$\mathbf{A}_{\phi_C\phi_C}(i,j) := \begin{cases} -\omega_{ij} v_i + \frac{\rho_{i0}}{\ell_i} - \frac{\beta}{\ell_i} & \text{if } (i = j) \\ \omega_{ij} v_i \frac{\phi_{j0}}{\phi_{i0}} & \text{if } (i \neq j) \end{cases}$$

$$\mathbf{A}_{\phi_C C} := -\beta \times \text{diag.} \begin{bmatrix} \frac{1}{\ell_1} & \frac{1}{\ell_2} & \ldots & \frac{1}{\ell_{Z_p}} \end{bmatrix}$$

$$\mathbf{A}_{\phi_C\phi_R}(i,j) := \begin{cases} -\omega_{ij} v_i & \text{if } (i = j) \\ \omega_{ij} v_i \frac{\phi_{j0}}{\phi_{i0}} & \text{if } (i \neq j) \end{cases}$$

$$\mathbf{A}_{\phi_C H}(i,j) := \begin{cases} -10.234 \times 10^{-6} \times \frac{\phi_{i0}}{\ell_h} & \text{for } (i = 2,4,6,8), \\ & j = i/2 \\ 0 & \text{otherwise.} \end{cases}$$

$$\mathbf{A}_{C\phi_C} := \text{diag.} \begin{bmatrix} \lambda_1 & \lambda_2 & \cdots & \lambda_{Z_p} \end{bmatrix}$$

$$\mathbf{A}_{CC} := -\text{diag.} \begin{bmatrix} \lambda_1 & \lambda_2 & \cdots & \lambda_{Z_p} \end{bmatrix}$$

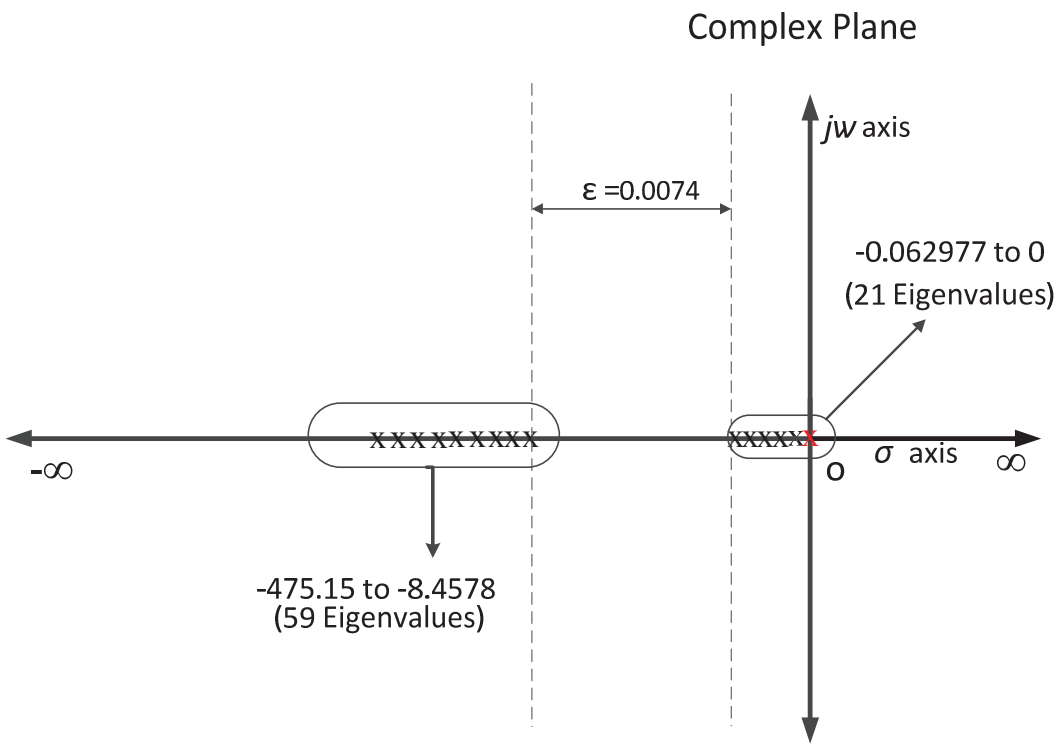

Figure 5.1: Eigenvalue spectrum of the linear model.

$$\mathbf{A}_{\phi_R\phi_R}(i,j) := \begin{cases} -\omega_{ij} v_i & \text{if } (i=j) \\ \omega_{ij} v_i \frac{\phi_{j0}}{\phi_{i0}} & \text{if } (i \neq j) \end{cases}$$

$$\mathbf{A}_{\phi_R\phi_C} := A^T_{\phi_C\phi_R}$$

$$\mathbf{B}_H := \text{diag.} \begin{bmatrix} K_{RR} & K_{RR} & K_{RR} & K_{RR} \end{bmatrix}.$$

The neutronic parameters and necessary data under full power operation are given in Chapter-3. The eigenvalues of the system matrix **A** of AHWR are shown in Table 5.1 and the spectrum of eigenvalue is shown in Fig. 5.1. It has 5 eigenvalues at the origin of complex s-plane and the remaining 75 eigenvalues in the left half of s-plane out of which 16 are of the order 10^{-1}, and the rest very large in magnitude.

Table 5.1: Eigenvalues of **A**

S.No	**Eigenvalue**	**S.No**	**Eigenvalue**
1	0	41	$-1.6369e+02$
2	0	42	$-1.6501e+02$
3	0	43	$-1.6833e+02$
4	0	44	$-1.7116e+02$
5	$-7.1761e-14$	45	$-1.7161e+02$
6	$-5.1852e-02$	46	$-1.7600e+02$
7	$-5.2002e-02$	47	$-1.8084e+02$
8	$-5.8369e-02$	48	$-1.8486e+02$
9	$-5.8821e-02$	49	$-1.9477e+02$
10	$-5.9777e-02$	50	$-2.0282e+02$
11	$-6.0480e-02$	51	$-2.0345e+02$
12	$-6.0863e-02$	52	$-2.0394e+02$
13	$-6.1191e-02$	53	$-2.0886e+02$
14	$-6.1958e-02$	54	$-2.0934e+02$
15	$-6.2035e-02$	55	$-2.1248e+02$
16	$-6.2324e-02$	56	$-2.3111e+02$
17	$-6.2514e-02$	57	$-2.3124e+02$
18	$-6.2553e-02$	58	$-2.3218e+02$
19	$-6.2712e-02$	59	$-2.3271e+02$
20	$-6.2951e-02$	60	$-2.4075e+02$
21	$-6.2977e-02$	61	$-2.4168e+02$
22	$-8.4578e+00$	62	$-2.5542e+02$
23	$-3.8195e+01$	63	$-2.5569e+02$
24	$-3.8778e+01$	64	$-2.6274e+02$
25	$-6.8742e+01$	65	$-2.6306e+02$
26	$-7.6403e+01$	66	$-2.6394e+02$
27	$-9.2359e+01$	67	$-2.6511e+02$
28	$-9.5878e+01$	68	$-2.7631e+02$
29	$-1.0271e+02$	69	$-2.7746e+02$
30	$-1.0577e+02$	70	$-2.7786e+02$
31	$-1.0861e+02$	71	$-3.0219e+02$
32	$-1.1391e+02$	72	$-3.0289e+02$
33	$-1.2358e+02$	73	$-3.2666e+02$
34	$-1.2424e+02$	74	$-3.2689e+02$
35	$-1.3989e+02$	75	$-3.7870e+02$
36	$-1.4226e+02$	76	$-3.9074e+02$
37	$-1.4783e+02$	77	$-3.9924e+02$
38	$-1.4838e+02$	78	$-4.1423e+02$
39	$-1.4978e+02$	79	$-4.7040e+02$
40	$-1.6005e+02$	80	$-4.7515e+02$

Table 5.2: Eigenvalues of $\mathbf{A}_M$

S.No	Eigenvalue	S.No	Eigenvalue
1	$-3.3497e-14$	39	$-1.6833e+02$
2	$-5.1852e-02$	40	$-1.7116e+02$
3	$-5.2002e-02$	41	$-1.7161e+02$
4	$-5.8369e-02$	42	$-1.7600e+02$
5	$-5.8821e-02$	43	$-1.8084e+02$
6	$-5.9777e-02$	44	$-1.8486e+02$
7	$-6.0480e-02$	45	$-1.9477e+02$
8	$-6.0863e-02$	46	$-2.0282e+02$
9	$-6.1191e-02$	47	$-2.0345e+02$
10	$-6.1958e-02$	48	$-2.0394e+02$
11	$-6.2035e-02$	49	$-2.0886e+02$
12	$-6.2324e-02$	50	$-2.0934e+02$
13	$-6.2514e-02$	51	$-2.1248e+02$
14	$-6.2553e-02$	52	$-2.3111e+02$
15	$-6.2712e-02$	53	$-2.3124e+02$
16	$-6.2951e-02$	54	$-2.3218e+02$
17	$-6.2977e-02$	55	$-2.3271e+02$
18	$-8.4578e+00$	56	$-2.4075e+02$
19	$-3.8195e+01$	57	$-2.4168e+02$
20	$-3.8778e+01$	58	$-2.5542e+02$
21	$-6.8742e+01$	59	$-2.5569e+02$
22	$-7.6403e+01$	60	$-2.6274e+02$
23	$-9.2359e+01$	61	$-2.6306e+02$
24	$-9.5878e+01$	62	$-2.6394e+02$
25	$-1.0271e+02$	63	$-2.6511e+02$
26	$-1.0577e+02$	64	$-2.7631e+02$
27	$-1.0861e+02$	65	$-2.7746e+02$
28	$-1.1391e+02$	66	$-2.7786e+02$
29	$-1.2358e+02$	67	$-3.0219e+02$
30	$-1.2424e+02$	68	$-3.0289e+02$
31	$-1.3989e+02$	69	$-3.2666e+02$
32	$-1.4226e+02$	70	$-3.2689e+02$
33	$-1.4783e+02$	71	$-3.7870e+02$
34	$-1.4838e+02$	72	$-3.9074e+02$
35	$-1.4978e+02$	73	$-3.9924e+02$
36	$-1.6005e+02$	74	$-4.1423e+02$
37	$-1.6369e+02$	75	$-4.7040e+02$
38	$-1.6005e+02$	76	$-4.7515e+02$

5.2 Model Order Reduction of AHWR Space–Time Kinetics Model

In this Section, for the estimation model of AHWR derived in the previous Section, various model order reduction techniques, *viz.*, Davison's and Marshall's dominant mode retention techniques, model decomposition into slow and fast subsystems based on singular perturbation analysis and balanced truncation technique have been applied to obtain a reduced order model from the original high order model.

For the study in this section, we define the output vector as $\mathbf{y} = \begin{bmatrix} \mathbf{y}_1 & \cdots & \mathbf{y}_{17} \end{bmatrix}^T$, where $\mathbf{y}_i = \delta\phi_i/\phi_{i_0}$ denotes the corresponding deviation in nodal flux. Therefore, output matrix is given as

$$\boldsymbol{\Psi} = \begin{bmatrix} \boldsymbol{\Psi}_{\phi_C} & \mathbf{0} & \mathbf{0} & \mathbf{0} \end{bmatrix}, \tag{5.14}$$

and $\boldsymbol{\Psi}_{\phi_C} := \mathbf{I}_{Z_p}$, where $\mathbf{I}_{Z_p}$ denotes an Identity matrix.

From Table 5.1, it is evident that, there are multiple eigenvalues at the origin of the complex s-plane. Hence, diagonalization of the estimation model is not possible. However, this difficulty is overcome by rewriting the dynamics of the original system. State vector (5.5) is regrouped and the dynamics of original system are rewritten such that the control rod dynamics are decoupled. The decoupled set of equations are:

$$\dot{\mathbf{x}}_M = \mathbf{A}_M\mathbf{x}_M + \mathbf{B}_M\mathbf{x}_H, \tag{5.15}$$

$$\mathbf{y} = \boldsymbol{\Psi}_M\mathbf{x}_M, \tag{5.16}$$

$$\text{and} \qquad \dot{\mathbf{x}}_H = \mathbf{B}_H\mathbf{u} \tag{5.17}$$

where $\mathbf{x}_M = \begin{bmatrix} \mathbf{x}_C^T & \mathbf{x}_{\phi_R}^T & \mathbf{x}_{\phi_C}^T \end{bmatrix}^T$ is of order 76 and $\mathbf{B}_M = \begin{bmatrix} \mathbf{0} & \mathbf{0} & \mathbf{A}_{\phi_C H}^T \end{bmatrix}^T$,

$$\mathbf{A}_M = \begin{bmatrix} \mathbf{A}_{CC} & \mathbf{0} & \mathbf{A}_{C\phi_C} \\ \mathbf{0} & \mathbf{A}_{\phi_R\phi_R} & \mathbf{A}_{\phi_R\phi_C} \\ \mathbf{A}_{\phi_C C} & \mathbf{A}_{\phi_C\phi_R} & \mathbf{A}_{\phi_C\phi_C} \end{bmatrix}, \tag{5.18}$$

and

$$\boldsymbol{\Psi}_M = \begin{bmatrix} \mathbf{0} & \mathbf{0} & \boldsymbol{\Psi}_{\phi_C} \end{bmatrix}. \tag{5.19}$$

Eigenvalues of $\mathbf{A}_M$ are shown in Table 5.2. It can be verified that all the eigenvalues of $\mathbf{A}_M$ are distinct. In fact, eigenvalues of $\mathbf{A}_M$ are approximately equal to the 76 eigenvalues of $\mathbf{A}$, listed at S.No 5 to 80 in Table 5.1. Now the model reduction techniques discussed in Section 4.2 and Section 4.3 can be directly applied to the 76th order model, given by (5.15) and (5.16), for obtaining the simplified models. Finally, by augmenting the control rod dynamics the simplified model for AHWR can be represented as,

$$\dot{\mathbf{x}}_R = \begin{bmatrix} \dot{\mathbf{x}}_r \\ \dot{\mathbf{x}}_H \end{bmatrix} = \begin{bmatrix} \mathbf{A}_r & \mathbf{B}_r \\ \mathbf{0} & \mathbf{0} \end{bmatrix} \begin{bmatrix} \mathbf{x}_r \\ \mathbf{x}_H \end{bmatrix} + \begin{bmatrix} \mathbf{0} \\ \mathbf{B}_H \end{bmatrix} \mathbf{u}, \tag{5.20}$$

$$\mathbf{y} = \begin{bmatrix} \boldsymbol{\Psi}_r & \mathbf{0} \end{bmatrix} \begin{bmatrix} \mathbf{x}_r \\ \mathbf{x}_H \end{bmatrix}. \tag{5.21}$$

5.2.1 Reduced Model Based on Davison's Technique

First consider the application of Davison's technique discussed in Section 4.2 to the estimation model given by (5.15) and (5.16) so as to retain the 17 eigenvalues of $\mathbf{A}_M$, listed at S.No 1 to 17 in Table 5.2. However, the reduced order model thus obtained does not yield satisfactory approximation as deviation between responses of the original system and simplified model are seem to be large. Therefore, another state $\delta\phi_1/\phi_{1_0}$ has been included in the reduced order model to achieve the satisfactory transient performance with respect to original model. Thus, eigenvalue -8.4578 (S.No. 18) has also been retained in the simplified model. By substituting the matrices $\mathbf{A}_r, \mathbf{B}_r$ and $\boldsymbol{\Psi}_r$ in (5.20) and (5.21) thus obtained, the following simplified model of order 22 is obtained for AHWR.

$$\dot{\mathbf{x}}_R = \mathbf{A}_{\mathrm{d}}\mathbf{x}_R + \mathbf{B}_{\mathrm{d}}\mathbf{u}. \tag{5.22}$$

$$\mathbf{y}_{\mathrm{d}} = \boldsymbol{\Psi}_{\mathrm{d}}\mathbf{x}_R, \tag{5.23}$$

where $\mathbf{x}_R = \begin{bmatrix} \mathbf{x}_C^T & \delta\phi_1/\phi_{1_0} & \mathbf{x}_H^T \end{bmatrix}^T$ is the reduced state vector of order 22×1. $\mathbf{A}_\mathrm{d}$, $\mathbf{B}_\mathrm{d}$ and $\boldsymbol{\Psi}_\mathrm{d}$ are corresponding system, input and output matrices of the AHWR simplified model obtained by the application of Davison's technique. The eigenvalues retained in simplified model are the first 22 eigenvalues of the original system shown in Table 5.1.

5.2.2 Reduced Model Based on Marshall's Technique

The Marshall's technique discussed in Section 4.3 can be applied to the estimation model given by (5.15) and (5.16) so as to retain the 17 eigenvalues of $\mathbf{A}$, listed at S.No 5 to 21 in Table 5.1. By substituting the matrices $\mathbf{A}_r, \mathbf{B}_r$ and $\boldsymbol{\Psi_r}$ in (5.20) and (5.21) thus obtained, the following simplified model of order 21 is obtained for AHWR.

$$\dot{\mathbf{x}}_R = A_\mathrm{m}\mathbf{x}_R + \mathbf{B}_\mathrm{m}\mathbf{u}, \tag{5.24}$$

$$\mathrm{y}_m = \boldsymbol{\Psi}_\mathrm{m}\mathbf{x}_R, \tag{5.25}$$

where $\mathbf{x}_R = \begin{bmatrix} \mathbf{x}_C^T & \mathbf{x}_H^T \end{bmatrix}^T$ is the reduced state vector of order 21×1. $\mathbf{A}_\mathrm{m}$, $\mathbf{B}_\mathrm{m}$ and $\boldsymbol{\Psi}_\mathrm{m}$ are corresponding system input and output matrices of the AHWR simplified model obtained by the application of Marshall's technique. The eigenvalues retained in simplified model are the first 21 eigenvalues of the original system shown in Table 5.1.

5.2.3 Reduced Model Based on Singular Perturbation Analysis

An observation of the eigenvalues of the system matrix $\mathbf{A}$ reveals that the eigenvalues fall into two distinct clusters. First cluster has 21 eigenvalues consisting of 5 eigenvalues at the origin and the other 16 eigenvalues ranging from -6.2977×10^{-2} to -5.1852×10^{-2} and the second one is of 59 eigenvalues ranging from -4.751×10^{2} to -8.4578. The distance between these two eigenvalue clusters, computed by dividing the largest absolute value of the slow (first) group by the smallest absolute value of the fast (second) group, is $\varepsilon = 0.0074$. This indicates the presence of two-time-scales in the estimation

model. It would therefore, be possible to decompose the model into a slow subsystem of order 21 and a fast subsystem of order 59, by the application of the method presented in Section 4.4. For carrying out this, the following regrouping of states is suggested:

$$\mathbf{x}_1 = \begin{bmatrix} \mathbf{x}_H^T & \mathbf{x}_C^T \end{bmatrix}^T \tag{5.26}$$

$$\mathbf{x}_2 = \begin{bmatrix} \mathbf{x}_{\phi_R}^T & \mathbf{x}_{\phi_C}^T \end{bmatrix}^T \tag{5.27}$$

The sub matrices $\mathbf{A}_{11}$, $\mathbf{A}_{12}$, $\mathbf{A}_{21}$, $\mathbf{A}_{22}$, $\mathbf{B}_1$, $\mathbf{B}_2$, $\acute{\boldsymbol{\Psi}}_1$ and $\acute{\boldsymbol{\Psi}}_2$ in (4.21), (4.22) and (4.23) are obtained by appropriate rearrangement and partitioning of matrices $\mathbf{A}$, $\mathbf{B}$ and $\boldsymbol{\Psi}$ which are given respectively by (5.11), (5.12) and (5.14). Using these, a slow subsystem of order 21 with $\mathbf{A}_S$, $\mathbf{B}_S$, $\boldsymbol{\Psi}_S$ and $\mathbf{N}_S$ represented by (4.24) and (4.25) is obtained and it can be considered as the simplified model of the AHWR.

5.2.4 Reduced Model Based on Balanced Truncation

The balanced truncation technique discussed in Section 4.5 can also be applied to the AHWR model for obtaining the reduced order model with lesser dimension than the original. The model has 80 states, 4 inputs and 17 outputs. The presence of the five eigenvalues at the origin restricts the straightforward application of the state-space balancing method described in Section 4.5.1. Therefore, we carry out stable and unstable decomposition of the AHWR model described by (5.11) and (5.12) to obtain an unstable subsystem of order 5 and a stable subsystem of order 75. Thereafter, we calculate the similarity transformation $\mathbf{T}$ in (4.58) was calculated such that the reachability and observability Gramians in the transformed co-ordinate system are diagonal and equal. Corresponding Hankel singular values of $\mathbf{G}$ are shown in Table 5.3. Fig. 5.2 shows the Hankel singular values, which represent the "energy" of each state in the balanced system of AHWR. Before applying the truncation of the system $\mathbf{G}_-^{bal}$, it is necessary to determine the partitioning of the Hankel singular values. We consider the first five Hankel singular

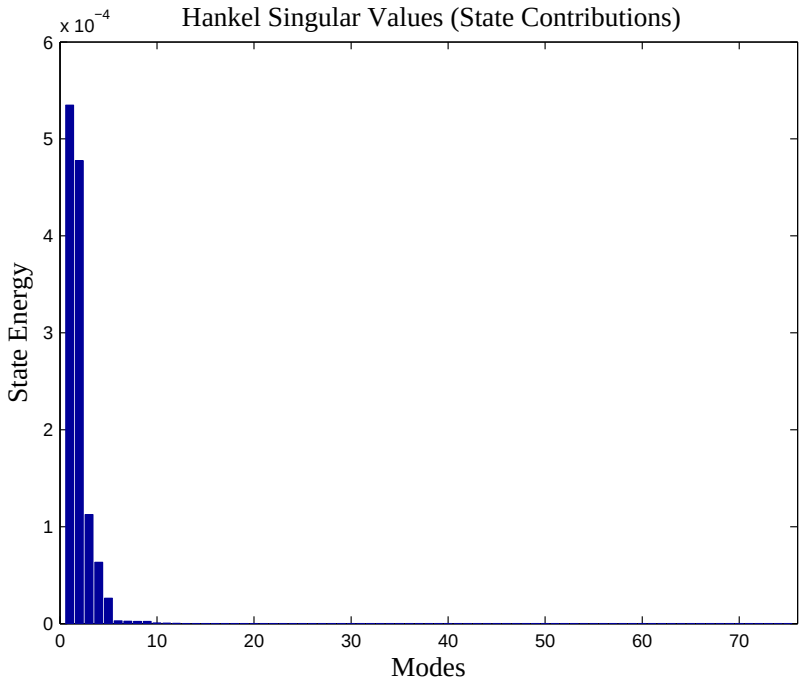

Figure 5.2: Hankel Singular Values.

values as listed in Table 5.3 because the ratio $\boldsymbol{\sigma}_1/\boldsymbol{\sigma}_6$ is considerably larger than $\boldsymbol{\sigma}_1/\boldsymbol{\sigma}_5$, $\boldsymbol{\sigma}_1/\boldsymbol{\sigma}_4$, ..., *etc.* Hence, the order of $\widehat{\mathbf{G}}_r$ is 5 and considering unstable dynamics also an approximate model of order 10 is obtained. The eigenvalues of the reduced order system matrix $\mathbf{A}_r$ of AHWR are shown in Table 5.4. As regards, 5 unstable eigenvalues, the remaining 4 eigenvalues from those of order 10^{-2} have been retained while the one from the larger ones has also been retained. In the overall, balanced truncation results into retaining unstable dynamics, slow stable dynamics and fast dynamics. It is also evident that the eigenvalues of $\mathbf{A}_r$ also fall into two distinct clusters. First cluster has 9 eigenvalues consisting of 5 eigenvalues at the origin and other four, ranging from -0.0601 to -0.0529 and the second cluster has only one eigenvalue, *i.e.,* -8.5034. Thus, the reduced order model also possesses two-time-scale property. The distance between these clusters, ε_r, of the reduced order model is 0.0071, which is almost equal to ε of the original model.

Table 5.3: Hankel Singular Values

S. No.	HSV
1	$5.3482e-04$
2	$4.7748e-04$
3	$1.1243e-04$
4	$6.3352e-05$
5	$2.6254e-05$
6	$2.8352e-06$
7	$2.5019e-06$
8	$2.3118e-06$
9	$2.2158e-06$
10	$6.2689e-07$
11	$5.6801e-07$
12	$2.0409e-07$
13	$1.8819e-07$
14	$1.3690e-07$
15	$1.2165e-07$
16	$6.7644e-08$
17-75	$< 1.0000e-09$

Table 5.4: Eigenvalues of reduced system matrix $\mathbf{A}_r$ based on Balanced Truncation

S. No.	Eigenvalue
1.	0
2	0
3	0
4	0
5	$-1.2223e-16$
6	$-5.2867e-02$
7	$-5.3016e-02$
8	$-5.9551e-02$
9	$-6.0083e-02$
10	$-8.5034e+00$

5.3 Comparison of Different Reduced Order Models with the Application of Space-Time Kinetics Model of AHWR

As already stated, due to the interaction of slow and fast dynamics present in AHWR, the mathematical model describing its dynamics exhibits the multiple time-scales bringing in susceptibility to numerical ill-conditioning in control design and analysis. In previous Section, a systematic method has been suggested to handle the numerical ill-conditioning occurring in the computations due to the presence of the slow control rod dynamics by decoupling the higher order model into very slow and fast models. Model order reduction techniques based on Davison's and Marshall's dominant mode retention are then applied to retain the slow dynamics. Finally the reduced order model was formulated by augmenting the control rod dynamics. Model decomposition into slow and fast subsystems based on singular perturbation analysis has also been explored by suggesting regrouping of state variables.

In this section, comparison of the performance characteristics of different reduced order models of AHWR obtained from Davison's, Marshall's, singular perturbation analysis and balanced truncation methods, relative to each other and with the performance characteristics of the original higher order model has been presented. To illustrate the dynamic behavior of different reduced order linear models, the open loop response for a short–time control relevant transient is presented here. Response obtained by the simulation of original 80th order model is considered as reference. In simulation, the reactor was assumed to be initially operating at full power and each RR is at 66.7% in position. At time $t = 0$ s, control signal of 1 V is applied to RR drive in node 2 and maintained for 5 s, under which the RR moved linearly into the reactor core. After a short interval of 5 s, the control signal is made -1 V and is maintained at this level for 10 s. Then the control voltage is made 1 V for 5 s to bring back the RR to its nominal

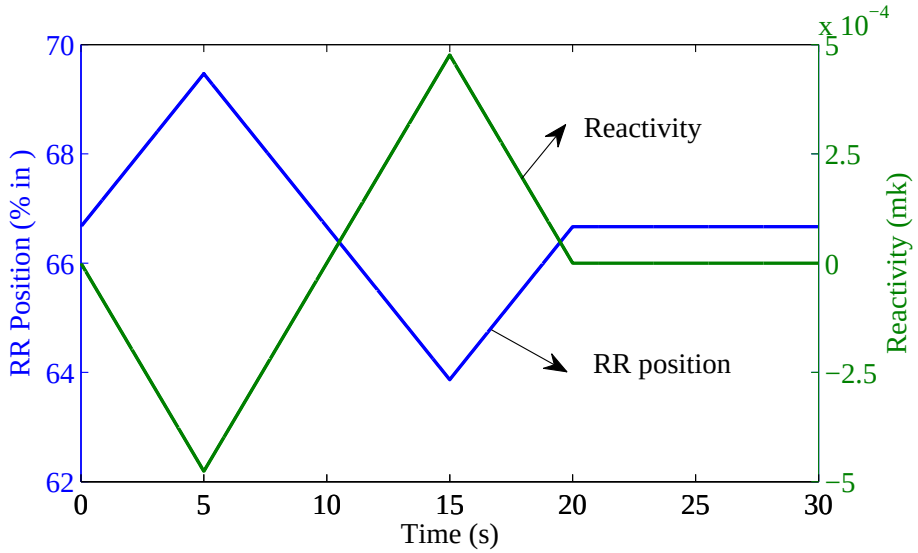

Figure 5.3: Position of RR and reactivity introduced during the movement of RR.

position. Fig. 5.3 shows the position of RR and, the reactivity introduced by it during the transient. From the deviations in the nodal fluxes, the deviation in the core average flux is calculated as

$$\delta\phi_{avg} = \frac{\sum_{i=1}^{17} \delta\phi_i V_i}{\sum_{i=1}^{17} V_i}, \tag{5.28}$$

where V_i denotes the volume of i^{th} node. To characterize the accuracy of approximation of the reduced order models, we compute the error using

$$e_{y_i} = (y_{i_{ref}} - y_i) \times 100, \quad i = 1, 2, \ldots, 17, \tag{5.29}$$

where $y_{i_{ref}}$ denotes the reference value of deviation in flux in node i and y_i denotes the approximate value of deviation in flux in node i. Accuracy analysis as described earlier has also been carried out to determine the error in the approximation. We also quantified the error in approximation for different simplified models by computing the L_2-norm (3.41) of the error defined by (5.29) and this is shown in Table 5.5. Fig. 5.4 compares the L_2-norm of error vector for all the 17-nodes of the AHWR. Plot for

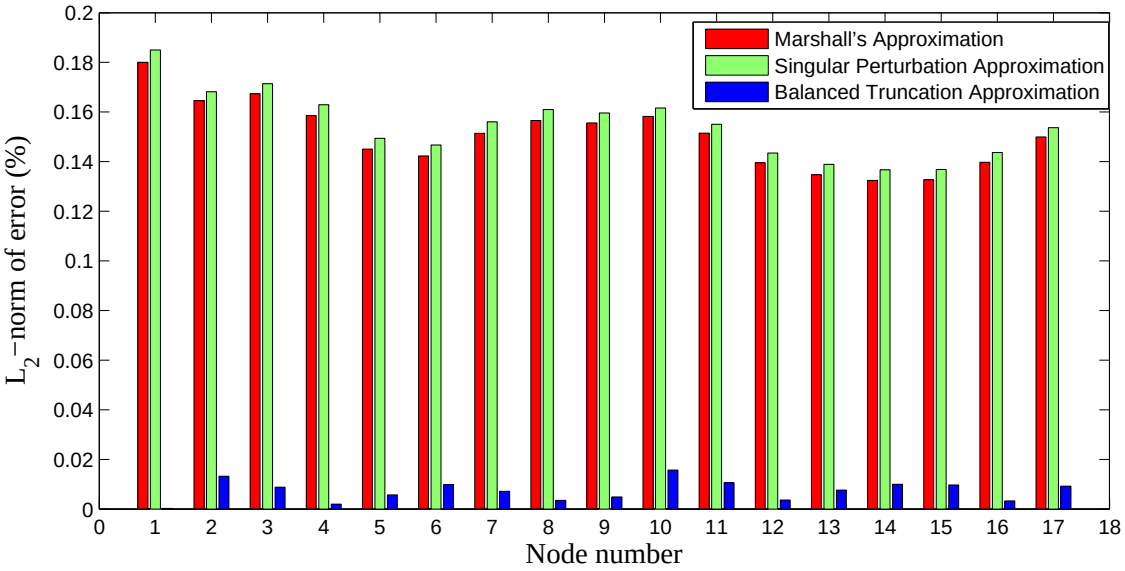

Figure 5.4: Comparison of L_2-norm of the error (%) in deviation in neutron fluxes in all the 17 nodes of the AHWR.

Table 5.5: Error (%) in deviation in fluxes

Method	**Order of Simplified model**	**L_2-norm of error in**			
		Core average flux	**Node-2 flux**	**Node-10 flux**	**Node-14 flux**
Davison's technique	22	0.0954	3.7349	1.9481	1.0641
Marshall's technique	21	0.1518	0.1646	0.1582	0.1324
Singular perturbation analysis	21	0.1559	0.1682	0.1616	0.1347
Balanced truncation technique	10	0.1680×10^{-3}	0.0132	0.0157	0.0099

Davison's approach has not been shown, as it yields large error compared to other methods.

The response of different reduced order models shown in Fig. 5.5 reveals that the core average flux obtained from the approximate models is nearly same as that of the original model. Fig. 5.6 shows the variation of flux in node 2, from the respective equilibrium value. Fig. 5.7 shows the variation of neutron flux in node 10, which is neighboring to node 2. Fig. 5.8 shows the variation of neutron flux in node 14 which is far away from node 2. The comparison of responses makes it clear that Davison's technique fails to reproduce the accurate response characteristics as that of original model in node 2, 10 and 14 with the reduced order model obtained by retaining first 22 eigenvalues of **A**. Marshall's, singular perturbation and balanced truncation methods

Table 5.6: Comparison of computation time, computational cost and memory requirement for simplified models

(a) Computation time for simplified models

Method	Order of the Simplified model	Computation time in (s)		
		Algorithm	Simulation	Total
Davison's technique	22	0.0203	0.1569	0.1772
Marshall's technique	21	0.0174	0.1493	0.1667
Singular perturbation analysis	21	0.0025	0.1849	0.1874
Balanced truncation technique	10	0.3169	0.0823	0.3992
Original model	80	NA	0.3328	0.3328

(b) Computational cost and memory requirement for simplified models

Method	Number of FLOPs (Mega FLOPs)	Memory requirement (MB)
Davison's technique	3.8	441.90
Marshall's technique	5.5	489.64
Singular perturbation analysis	2.2	140.58
Balanced truncation technique	17.2	1192.77

yield better approximation for deviation in core average flux as well as nodal fluxes with the order of 21, 21 and 10 respectively, compared to the Davison's technique. However, the application of Davison's and Marshall's method increases computational burden in obtaining approximate model in reactor applications due to the presence of multiple eigenvalues at origin of the complex s-plane, whereby the diagonalization of AHWR space–time kinetics model is difficult. Balanced truncation method requires the decomposition of stable and unstable dynamics while singular perturbation technique requires reordering of state variables and block diagonalization. Singular perturbation and balanced truncation methods preserve the two-time-scale property of the model, however, transient response of balanced truncation method is marginally superior to the singular perturbation method. It may be noted from the Table 5.5 that the error in approximation using the balanced truncation approach is far lower in comparison with other methods.

We compare the computation time and memory for the different model order reduction techniques. The computation was performed on Matlab R2015b and Windows-7,

64 bit computer with intel(R) Core(TM) i3-4130 CPU @ 3.40 GHz processor and 4 GB RAM memory. The computation time for processing the model reduction algorithm is just a one-time requirement and can be performed off-line, while simulation is to be carried for different situations and multiple cases may be studied. Hence, comparison of simulation time would be appropriate. Nevertheless, the Table 5.5(a) gives a comparison of algorithm processing time as well as simulation time, for balanced truncation and other methods. Although the total computation time for balanced truncation approach is slightly higher compared to the original model, simulation time is very less compared to the original method as well as the other methods.

Also, the number of floating point operations (FLOPs) and memory requirement are given in Table 5.5(b) for the different methods. Balanced truncation approach requires the solution of two Lyapunov equations followed by a SVD. Both these steps involve arithmetic operations of order N^3 representing computational complexity and storage of order N^2. Hence, it results into large computational cost and memory requirement. Singular perturbation analysis is the most efficient requiring the minimum memory as well as FLOPs while the balanced truncation method is the least efficient with requirement of about 17.2 Mega FLOPs and 1192.7 MB memory. However, the most important thing is its feasibility of working in reduced order modeling of AHWR space–time kinetics.

5.4 Discussion

For the AHWR system, various model order reduction techniques, *viz.*, Davison's and Marshall's dominant mode retention techniques; balanced truncation technique and model decomposition into slow and fast subsystems based on singular perturbation analysis, have been applied. Among these, Davison's and Marshall's techniques require diagonalization and balanced truncation technique requires a modal decomposition into unstable and stable subsystems. Also, it is essential for model order reduction based on Davison's and Marshall's techniques, to identify the modes to retain and those to

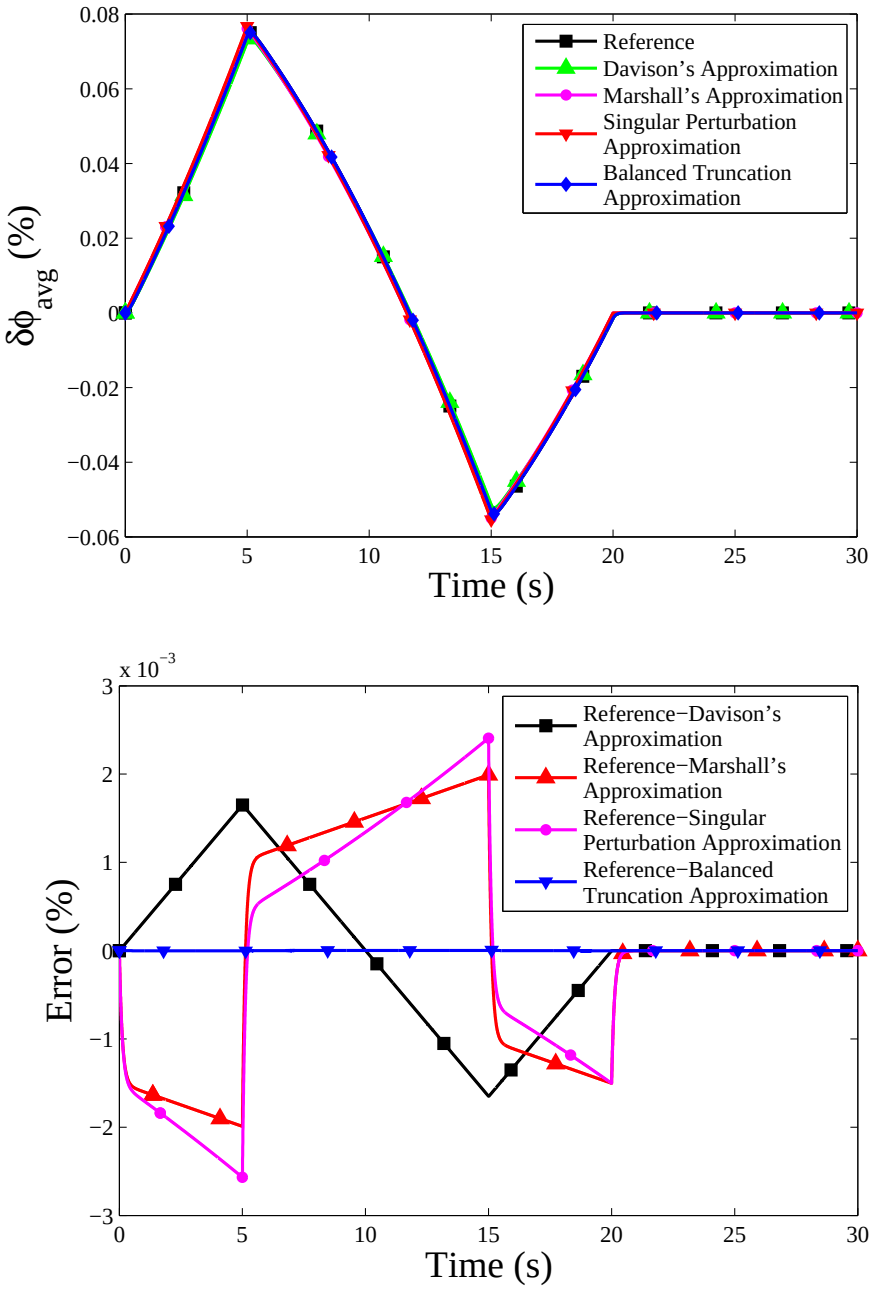

Figure 5.5: Comparison of core average flux during the movement of RR.

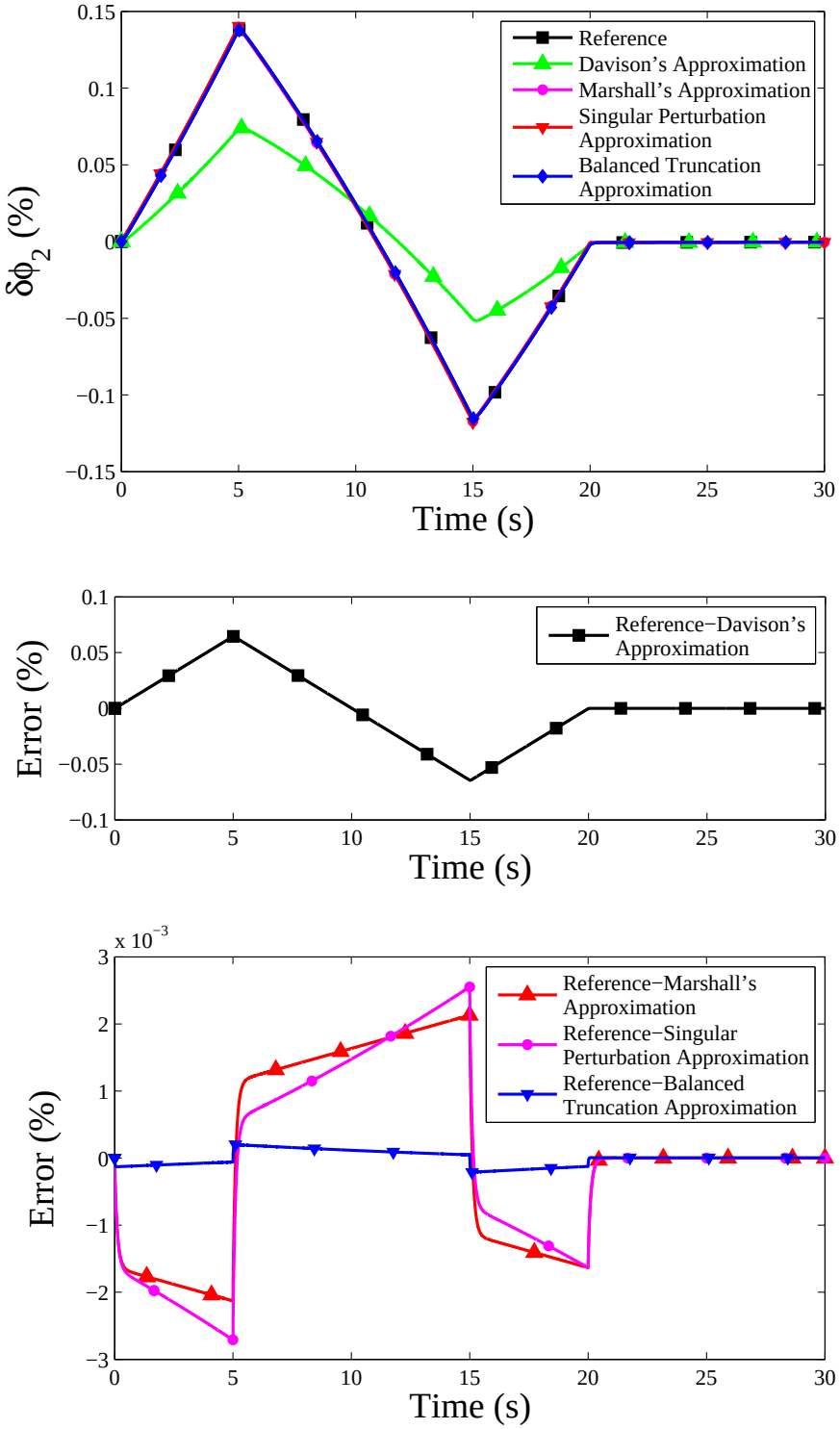

Figure 5.6: Comparison of neutron flux in node-2 during the movement of RR.

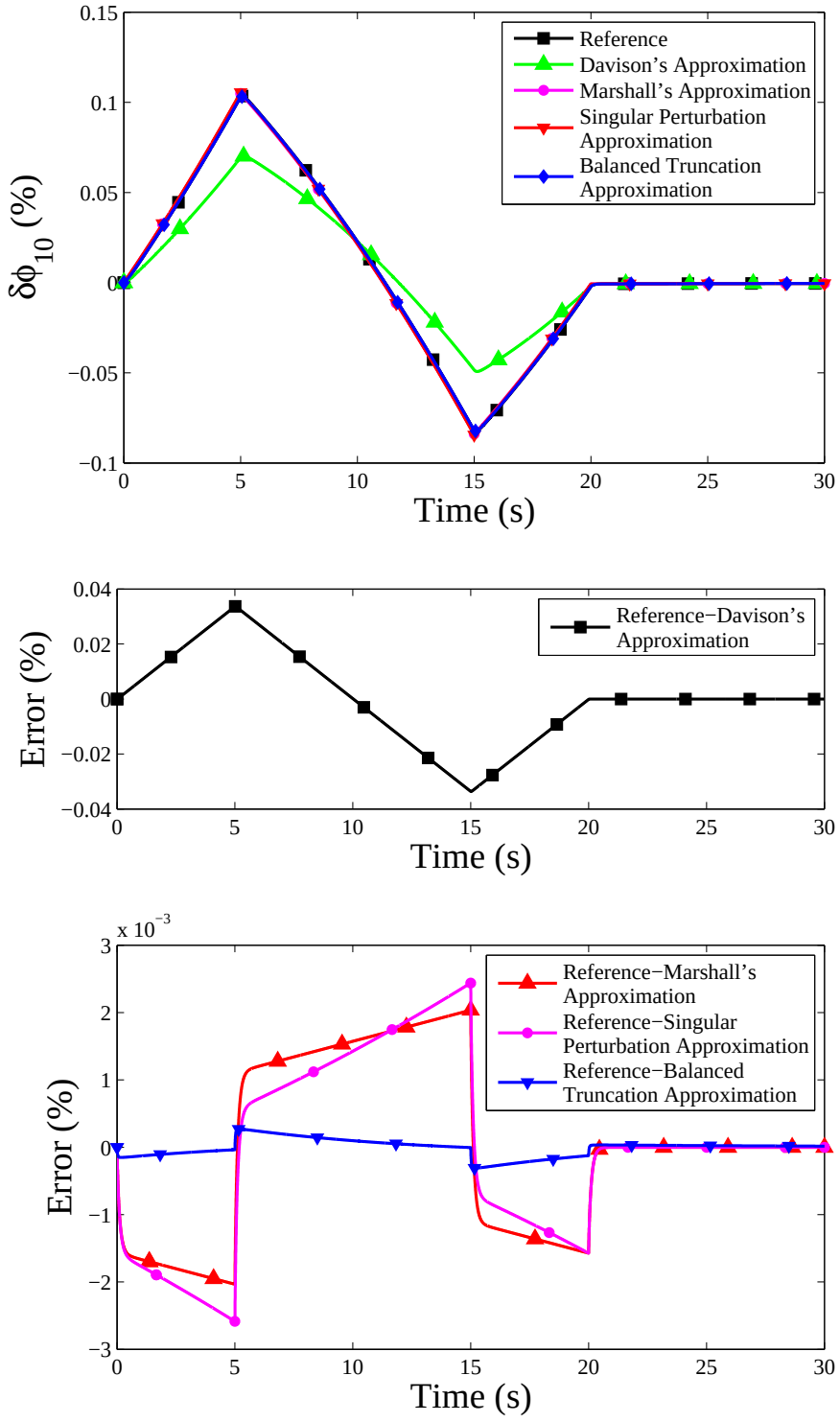

Figure 5.7: Comparison of neutron flux in node-10 during the movement of RR.

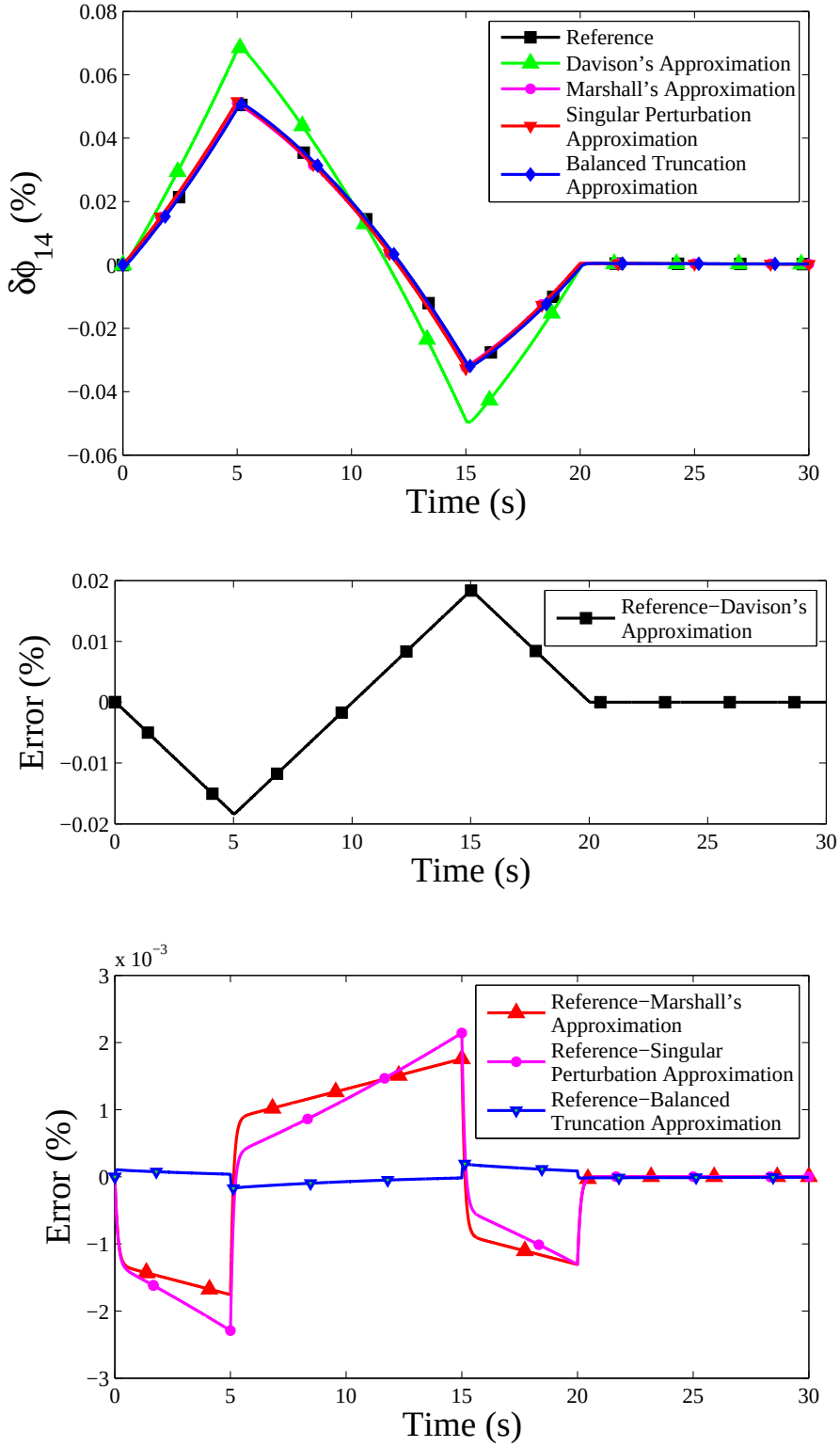

Figure 5.8: Comparison of neutron flux in node-14 during the movement of RR.

truncate/reduce. In contrast, singular perturbation techniques require a decomposition of the state-space systems into fast/slow subsystems using block diagonalization methods. Davison's and Marshall's techniques result into a simplified model that retains the slowly varying dynamics while the application of singular perturbation analysis and two-time-scale methods decompose the model into two subsystems *viz.*, slow and fast, thus providing better approximation of dynamics of the system. Quite similar to this, application of balanced truncation yields a reduced model in which both the slow and fast dynamic characteristics are simultaneously retained yielding good accuracy in approximation of high order model by reduced order model.

The order of reduced order model obtained by the application of Davison's technique is 22, while that obtained using Marshall's and singular perturbation techniques both is 21 each, but the balanced truncation technique is the most effective in model reduction yielding the reduced model of order 10 only. The transient response of simplified models based on Marshall's, singular perturbation and balanced truncation techniques were in good agreement with the transient response of the original high order model.

In summary, we have proposed a novel approach for the application of balanced truncation technique to nuclear reactor systems which have a nontrivial unstable part based on stable and unstable decomposition. This is accomplished easily while the direct application of balanced truncation for model order reduction is not feasible. The computation involved in obtaining a balanced basis is typically considered too high and this method has not been adequately used in model order reduction applications. However, our work shows that the computation is required to be done off-line and only once. The computation time is only marginally higher, but the advantages outweigh the marginally higher computation time. It is evidenced that the final reduced order model based on the balanced truncation method is of much lower order in spite of negligible error between the response of the original system and that obtained from the reduced order model. This provides significant advantage from a practical perspective because a lower-order controller or estimator needs to be designed for the purpose of controlling

the AHWR. In general, the singular perturbation and balanced truncation methods are expected to perform better in cases where time-scales are widely separated.

Chapter 6

A Two-time-scale approach for Discrete-Time Kalman Filter Design and application to AHWR Flux Mapping

In this chapter, the task of flux-mapping in THE AHWR has been formulated as linear stochastic estimation problem and a solution is obtained by Kalman filtering technique. It utilizes estimation model derived in Section 5.1 and available detector measurements corrupted with white Gaussian noise. However, direct implementation of the DKF algorithm to this high-order stiff estimation model is not feasible as the designing procedure is accompanied by serious numerical ill-conditioning caused by the simultaneous presence of slow and fast phenomena typically present in a nuclear reactor. In particular, the set of recursive equations for computation of DKF gains, as a solution to weighted least squares problem, is ill-conditioned. Consequently, serious numerical difficulties are expected if the DKF gain matrix is to be computed on the basis of the full order Riccati equation. By using the reduced models based on Davison's technique, Marshall's tech-

A part of this chapter was published in *IEEE Transactions on Nuclear Science*, Vol. 63(1) .

nique, singular perturbation analysis and balanced truncation, the estimation model of lower order can be obtained. Trying all these would be of enormous effort. However, an attempt has been made to apply the singular perturbation technique which fortunately is found to work well for the AHWR flux mapping. This chapter presents the proposed novel technique to address the numerical ill-conditioning problems in full order design by decoupling the DKF equations according to the order of the slow and fast subsystems. Finally this technique has been applied for estimation of detailed mesh, channel quadrant and core average fluxes in the AHWR.

6.1 Discrete-Time Kalman Filter Algorithm

The DKF is an optimal recursive data processing algorithm [34, 78], also known as Linear Quadratic Estimator which uses a series of measurements observed over time, containing noise (random variations) and other model inaccuracies, and produces estimates of unknown states that tend to be more precise than those based on a single measurement alone. From Bayesian point of view, DKF propagates the conditional probability density of the desired quantities (mean and covariance), conditioned on the knowledge of the past measurements and updates it when new measurements are available [118]. Consider a general linear discrete time-invariant stochastic system represented by,

$$\mathbf{x}_k = \mathbf{\Phi}\mathbf{x}_{k-1} + \mathbf{\Gamma}\mathbf{u}_{k-1} + \boldsymbol{w}_{k-1}, \tag{6.1}$$

$$\text{and} \quad \mathbf{y}_k = \mathbf{\Psi}\mathbf{x}_k + \boldsymbol{v}_k, \tag{6.2}$$

where k is the discrete-time instant, $\mathbf{x} \in \mathbb{R}^n$ is the state vector, $\mathbf{u} \in \mathbb{R}^m$ is the input vector and $\mathbf{y} \in \mathbb{R}^p$ is the output vector. $\mathbf{\Phi} \in \mathbb{R}^{n\times n}$, $\mathbf{\Gamma} \in \mathbb{R}^{n\times m}$ and $\mathbf{\Psi} \in \mathbb{R}^p$ denote the state transition, input and output matrices respectively. Also, $\boldsymbol{w}_k$ and $\boldsymbol{v}_k$ are random vectors representing respectively the process and measurement noise sequences, assumed to be independent, zero mean, with Gaussian probability distribution and known covariances

$\mathbf{Q}$ and $\mathbf{R}$ respectively, *i.e.*,

$$\begin{aligned}
&\boldsymbol{w}_k \sim N(0, \mathbf{Q}), \quad E[\boldsymbol{w}(t_k)] = \mathbf{0}, \quad E[\boldsymbol{w}(t_k)\boldsymbol{w}^T(t_j)] = \mathbf{Q}\delta_{kj}, \\
&\boldsymbol{v}_k \sim N(0, \mathbf{R}), \quad E[\boldsymbol{v}(t_k)] = \mathbf{0}, \quad E[\boldsymbol{v}(t_k)\boldsymbol{v}^T(t_j)] = \mathbf{R}\delta_{kj}, \\
&E[\boldsymbol{v}(t_k)\boldsymbol{w}^T(t_j)] = \mathbf{0},
\end{aligned}$$

where $\mathbf{Q}$ is positive-semidefinite matrix and $\mathbf{R}$ is positive-definite matrix. $E[\cdot]$ is expectation operator and δ_{kj} is the Kronecker delta function; *i.e.*, $\delta_{kj} = 1$ if $k = j$, and $\delta_{kj} = 0$ if $k \neq j$. The initial state $\mathbf{x}_0$ is also a Gaussian random variable, independent of the noise processes, with $\mathbf{x}_0 \sim N(\hat{\mathbf{x}}_0, \mathbf{P}_0)$. Therefore $E[\mathbf{x}_0] = \hat{\mathbf{x}}_0, E[(\mathbf{x} - \hat{\mathbf{x}}_0)(\mathbf{x} - \hat{\mathbf{x}}_0)^T] = \mathbf{P}_0$, where $\hat{\mathbf{x}}$ is the state estimate, $\mathbf{P}$ is the covariance of the error in the state estimate. The DKF equations for the above system fall into two groups, namely time update equations and the measurement update equations, discussed in following subsections.

6.1.1 Time Update Equations

These equations, also known as state and covariance prediction equations, project forward (in time) the current state and error covariance estimates to obtain *a priori* estimates for the next step, *i.e.*,

$$\hat{\mathbf{x}}_k^- = \boldsymbol{\Phi}\hat{\mathbf{x}}_{k-1} + \boldsymbol{\Gamma}\mathbf{u}_{k-1}, \tag{6.3}$$

$$\text{and} \quad \mathbf{P}_k^- = \boldsymbol{\Phi}\mathbf{P}_{k-1}\boldsymbol{\Phi}^T + \mathbf{Q}. \tag{6.4}$$

6.1.2 Measurement Update Equations

These equations incorporate a new measurement $\mathbf{y}_k$ into *a priori* estimate to obtain an improved *a posteriori* estimate, *i.e.*,

$$\mathbf{K}_k = \mathbf{P}_k^-\boldsymbol{\Psi}^T[\boldsymbol{\Psi}\mathbf{P}_k^-\boldsymbol{\Psi}^T + \mathbf{R}]^{-1}, \tag{6.5}$$

$$\hat{\mathbf{x}}_k = \hat{\mathbf{x}}_k^- + \mathbf{K}_k[\mathbf{y}_k - \boldsymbol{\Psi}\hat{\mathbf{x}}_k^-], \tag{6.6}$$

$$\text{and} \quad \mathbf{P}_k = [\boldsymbol{I} - \boldsymbol{K}_k\Psi]\mathbf{P}_k^-, \tag{6.7}$$

where $\mathbf{K}_k$ is the Kalman gain, which incorporates the the discrepancy between the actual measurement ($\mathbf{y}_k$) and predicted measurement ($\boldsymbol{\Psi}\hat{\mathbf{x}}_k^-$) as shown in (6.6).

6.2 Two-time-scale approach for Discrete-Time Kalman Filter design

Direct implementation of the DKF algorithm to a high order stiff system, such as the nuclear reactor is not feasible due to numerical ill-conditioning. However, utilizing the block diagonalized model, the time and measurement update equations discussed in Section 6.1, can be decoupled according to the order n_1 of the slow and order n_2 of the fast subsystems. A high order stochastic system such as the one represented by (6.1) and (6.2); possessing two-time-scale behavior can be represented into linear singularly perturbed form and block-diagonalized as described in Sec. 4.4.1, to obtain

$$\begin{bmatrix} \mathbf{x}_{S,k} \\ \mathbf{x}_{F,k} \end{bmatrix} = \begin{bmatrix} \boldsymbol{\Phi}_S & 0 \\ 0 & \boldsymbol{\Phi}_F \end{bmatrix} \begin{bmatrix} \mathbf{x}_{S,k-1} \\ \mathbf{x}_{F,k-1} \end{bmatrix} + \begin{bmatrix} \boldsymbol{\Gamma}_S \\ \boldsymbol{\Gamma}_F \end{bmatrix} \mathbf{u}_{k-1} + \begin{bmatrix} \boldsymbol{w}'_{S,k-1} \\ \boldsymbol{w}'_{F,k-1} \end{bmatrix}, \tag{6.8}$$

$$\mathbf{y}_k = \begin{bmatrix} \boldsymbol{\Psi}_S & \boldsymbol{\Psi}_F \end{bmatrix} \begin{bmatrix} \mathbf{x}_S \\ \mathbf{x}_F \end{bmatrix} + \begin{bmatrix} \boldsymbol{v}_{S,k-1} \\ \boldsymbol{v}_{F,k-1} \end{bmatrix} \tag{6.9}$$

where the additional terms $\boldsymbol{w}'_S$, $\boldsymbol{v}_S$ and $\boldsymbol{v}_F$ follow from (6.1) and (6.2). The matrices $\mathbf{P}$ and $\mathbf{Q}$ appearing in (6.4) can also be partitioned according to the orders of the slow

and fast subsystems and from (6.4), we have

$$\begin{aligned}\mathbf{P}_k^- &= \begin{bmatrix} \mathbf{P}_{11,k}^- & \mathbf{P}_{12,k}^- \\ \mathbf{P}_{12,k}^{-^T} & \mathbf{P}_{22,k}^- \end{bmatrix} \\ &= \begin{bmatrix} \mathbf{\Phi}_S & \mathbf{0} \\ \mathbf{0} & \mathbf{\Phi}_F \end{bmatrix} \begin{bmatrix} \mathbf{P}_{11,k-1} & \mathbf{P}_{12,k-1} \\ \mathbf{P}_{12,k-1}^T & \mathbf{P}_{22,k-1} \end{bmatrix} \begin{bmatrix} \mathbf{\Phi}_S^T & \mathbf{0} \\ \mathbf{0} & \mathbf{\Phi}_F^T \end{bmatrix} \\ &\qquad + \begin{bmatrix} \mathbf{Q}_{11} & \mathbf{Q}_{12} \\ \mathbf{Q}_{12}^T & \mathbf{Q}_{22} \end{bmatrix}. \end{aligned} \tag{6.10}$$

Thus, we have

$$\mathbf{P}_{11,k}^- = \mathbf{\Phi}_S \mathbf{P}_{11,k} \mathbf{\Phi}_S^T + \mathbf{Q}_{11}, \tag{6.11}$$

$$\mathbf{P}_{22,k}^- = \mathbf{\Phi}_F \mathbf{P}_{22,k} \mathbf{\Phi}_F^T + \mathbf{Q}_{22}, \tag{6.12}$$

$$\text{and} \quad \mathbf{P}_{12,k}^- = \mathbf{\Phi}_S \mathbf{P}_{12,k} \mathbf{\Phi}_F^T + \mathbf{Q}_{12}. \tag{6.13}$$

Similarly, the Kalman gain $\mathbf{K}_k$ in (6.6) can also be partitioned into slow subsystem Kalman gain $\mathbf{K}_{S,k}$ and fast subsystem Kalman gains $\mathbf{K}_{F,k}$ and (6.5) can be written as

$$\begin{aligned}\mathbf{K}_k = \begin{bmatrix} \mathbf{K}_{S,k} \\ \mathbf{K}_{F,k} \end{bmatrix} &= \begin{bmatrix} \mathbf{P}_{11,k}^- & \mathbf{P}_{12,k}^- \\ \mathbf{P}_{12,k}^{-^T} & \mathbf{P}_{22,k}^- \end{bmatrix} \begin{bmatrix} \mathbf{\Psi}_S^T \\ \mathbf{\Psi}_F^T \end{bmatrix} \times \\ &\left\{ \begin{bmatrix} \mathbf{\Psi}_S^T \\ \mathbf{\Psi}_F^T \end{bmatrix}^T \begin{bmatrix} \mathbf{P}_{11,k}^- & \mathbf{P}_{12,k}^- \\ \mathbf{P}_{12,k}^{-^T} & \mathbf{P}_{22,k}^- \end{bmatrix} \begin{bmatrix} \mathbf{\Psi}_S^T \\ \mathbf{\Psi}_F^T \end{bmatrix} + \mathbf{R} \right\}^{-1}. \end{aligned} \tag{6.14}$$

Hence,

$$\mathbf{K}_{S,k} = (\mathbf{P}_{11,k}^- \mathbf{\Psi}_S^T + \mathbf{P}_{12,k}^- \mathbf{\Psi}_F^T) \mathbf{Y}^{-1} \tag{6.15}$$

$$\text{and} \quad \mathbf{K}_{F,k} = (\mathbf{P}_{12,k}^{-^T} \mathbf{\Psi}_S^T + \mathbf{P}_{22,k}^- \mathbf{\Psi}_F^T) \mathbf{Y}^{-1}. \tag{6.16}$$

where

$$\mathbf{Y} = \boldsymbol{\Psi}_S \mathbf{P}^-_{11,k} \boldsymbol{\Psi}_S^T + 2\boldsymbol{\Psi}_S \mathbf{P}^-_{12,k} \boldsymbol{\Psi}_F^T + \boldsymbol{\Psi}_F \mathbf{P}^-_{22,k} \boldsymbol{\Psi}_F^T + \mathbf{R} \tag{6.17}$$

and

$$\mathbf{P}_k = \begin{bmatrix} \mathbf{P}_{11,k} & \mathbf{P}_{12,k} \\ \mathbf{P}_{12,k}^T & \mathbf{P}_{22,k} \end{bmatrix} = \left\{ \begin{bmatrix} \mathbf{I}_{n1} & \mathbf{0} \\ \mathbf{0} & \mathbf{I}_{n2} \end{bmatrix} - \begin{bmatrix} \mathbf{K}_{S,k} \\ \mathbf{K}_{F,k} \end{bmatrix} \begin{bmatrix} \boldsymbol{\Psi}_S^T \\ \boldsymbol{\Psi}_F^T \end{bmatrix}^T \right\} \times \begin{bmatrix} \mathbf{P}^-_{11,k} & \mathbf{P}^-_{12,k} \\ \mathbf{P}^{-^T}_{12,k} & \mathbf{P}^-_{22,k} \end{bmatrix}, \tag{6.18}$$

which yields:

$$\mathbf{P}_{11,k} = (\mathbf{I}_{n1} - \mathbf{K}_{S,k}\boldsymbol{\Psi}_S)\mathbf{P}^-_{11,k} - \mathbf{K}_{S,k}\boldsymbol{\Psi}_F \mathbf{P}^{-^T}_{12,k}, \tag{6.19}$$

$$\mathbf{P}_{22,k} = (\mathbf{I}_{n2} - \mathbf{K}_{F,k}\boldsymbol{\Psi}_F)\mathbf{P}^-_{22,k} - \mathbf{K}_{F,k}\boldsymbol{\Psi}_S \mathbf{P}^-_{12,k}, \tag{6.20}$$

$$\text{and } \mathbf{P}_{12,k} = (\mathbf{I}_{n1,n2} - \mathbf{K}_{S,k}\boldsymbol{\Psi}_S)\mathbf{P}^-_{12,k} - \mathbf{K}_{S,k}\boldsymbol{\Psi}_F \mathbf{P}^-_{22,k}. \tag{6.21}$$

Note that covariance equation of time update step is decoupled into three equations given by (6.11)–(6.13); measurement update step is decoupled into three equations given by (6.19)–(6.21), and Kalman gain equation is decoupled into two equations given by (6.15)–(6.16). Hence the proposed DKF algorithm for singularly perturbed system has total ten equations.

6.3 Application to AHWR Flux Mapping

In chapter 5, the estimation model of the AHWR was obtained and a state regrouping was suggested whereby the model is readily put into standard singularly perturbed form. Now, the system, input and output matrices given by (5.11)–(5.13) are partitioned into block matrices according to the new state vectors defined. Thus in (4.21)–(4.23) we have:

$$\mathbf{A}_{11} = \begin{bmatrix} \mathbf{0} & \mathbf{0} \\ \mathbf{0} & \mathbf{A}_{CC} \end{bmatrix}; \qquad \mathbf{A}_{12} = \begin{bmatrix} \mathbf{0} & \mathbf{0} \\ \mathbf{0} & \mathbf{A}_{C\phi_C} \end{bmatrix};$$

$$\mathbf{A}_{21} = \begin{bmatrix} \mathbf{0} & \mathbf{0} \\ \mathbf{A}_{\phi_C H} & \mathbf{A}_{\phi_C C} \end{bmatrix}; \mathbf{A}_{22} = \begin{bmatrix} \mathbf{A}_{\phi_R\phi_R} & \mathbf{A}_{\phi_R\phi_C} \\ \mathbf{A}_{\phi_C\phi_R} & \mathbf{A}_{\phi_C\phi_C} \end{bmatrix};$$

$$\mathbf{B}_1 = \begin{bmatrix} \mathbf{B}_H^T & \mathbf{0} \end{bmatrix}^T; \qquad \mathbf{B}_2 = \begin{bmatrix} \mathbf{0} & \mathbf{0} \end{bmatrix}^T;$$

$$\boldsymbol{\Psi}_1 = \begin{bmatrix} \mathbf{0} & \mathbf{0} \end{bmatrix}; \qquad \boldsymbol{\Psi}_2 = \begin{bmatrix} 0 & \boldsymbol{\kappa}_{\mathrm{DV}} \end{bmatrix}.$$

Now, the full order system is block diagonalized using the similarity transformation (4.38), in which the $\mathbf{L}$ and $\mathbf{M}$ matrices for the transformation are obtained by the iterative solution of (4.41) and (4.42) respectively. Thereafter $\mathbf{A}_S$, $\mathbf{A}_F$, $\mathbf{B}_S$, $\mathbf{B}_F$, $\boldsymbol{\Psi}_S$ and $\boldsymbol{\Psi}_F$ of the decoupled system represented by (4.36)–(4.37) are obtained by (4.44). It is observed that 59 magnitude wise largest eigenvalues of $\mathbf{A}$ are equal to eigenvalues of $\mathbf{A}_F$, and the remaining 21 eigenvalues are equal to eigenvalues of $\mathbf{A}_S$. This confirms that the estimation model is decoupled into slow and fast subsystems of order 21 and 59 respectively.

Now the method presented in Section 6.2 has been applied for flux mapping in the core of AHWR. Estimation model represented by (4.36)–(4.37) is discretized for sampling time $\tau = 0.2$ s for which the discrete-time system is observed to possess two-time-scale property. The eigenvalues of discretized system are given in Table 6.1. From the Table 6.1 , it is evident that discretized model has 21 (S.No.60-S.No.80) eigenvalues on/around the periphery of the unit circle, and the rest 59 (S.No.1-S.No.59) are inside the unit circle, which indicates the two-time-scale property in the discrete model.

The effectiveness of the Kalman filtering technique for flux mapping has been examined in three cases. In the first case, decay of non-zero initial condition is observed. The states of the estimation model are non-zero while the reactor is assumed to be at steady–state. In the second, the movement of one or multiple RRs is simulated. Finally in the third case, xenon-induced spatial oscillation is considered. These cases are

elaborated in the following subsections.

SPND signals (measurements) were generated under the same transient situations from a separate set of off-line computations using a 128-node scheme as shown in Fig. 3.4, for the first two cases, and the 17-node scheme as shown in Fig. 3.3 for the third case. From the operational 540 MWe PHWR units 3 and 4 of Tarapur Atomic Power Station (TAPS), India, it was revealed that noise in the signals of detectors takes normal probability distribution with a standard deviation of nearly 2 % [79]. Hence, measurement noise of the order of 2 % has been assumed for each SPND. This noise is equivalent to 2 % random fluctuations around the full power steady state–value in each detector.

Using the methodology described in Section 3.4, reference flux values have been generated for 22950 volume elements, 452 fuel channels, 4 quadrants and the core average flux denoted respectively as ϕ_V, $\boldsymbol{\phi}_Z$, $\boldsymbol{\phi}_Q$ and $\boldsymbol{\phi}_G$. The state estimation is carried out using the DKF algorithm with

$$\mathbf{Q} = 0.1 \times \mathbf{I}_{80} \quad \text{and} \quad \mathbf{R} = \mathbf{I}_{200}$$

where $\mathbf{I}_{80}$ and $\mathbf{I}_{200}$ denote identity matrices of size 80 and 200 respectively. Estimates for fluxes in 22950 volume elements are obtained as

$$\hat{\boldsymbol{\phi}}_V = \boldsymbol{\kappa}_V \hat{\mathbf{x}}_{\boldsymbol{\phi}_C}, \tag{6.22}$$

where $\boldsymbol{\kappa}_V$ denotes the weighting matrix for flux reconstruction. Now, from the estimates of flux in 22950 volume elements, the average values of channel fluxes are obtained as

$$\hat{\phi}_Z = \sum_{i \in Z} \hat{\phi}_{V_i} V_i \Big/ \sum_{i \in Z} V_i, \tag{6.23}$$

where V_i denotes the volume of the ith mesh box, Z denotes fuel channels in core, as

Table 6.1: Eigenvalues of discrete-time model for $\tau = 0.2$

S.No	Eigenvalue	S.No	Eigenvalue
1	$8.9824e-21$	41	$1.2527e-14$
2	$1.1967e-20$	42	$9.7747e-14$
3	$2.2928e-20$	43	$1.2944e-13$
4	$3.1010e-20$	44	$1.4448e-13$
5	$5.3019e-20$	45	$4.3960e-13$
6	$7.6267e-19$	46	$7.0621e-13$
7	$8.2310e-19$	47	$1.6174e-11$
8	$8.7412e-19$	48	$1.8456e-11$
9	$9.2210e-19$	49	$1.2773e-10$
10	$9.4823e-19$	50	$3.6852e-10$
11	$1.2429e-19$	51	$6.4999e-10$
12	$2.2956e-19$	52	$1.1980e-09$
13	$3.3126e-19$	53	$4.7009e-09$
14	$3.3126e-19$	54	$9.5022e-09$
15	$3.2213e-19$	55	$2.3107e-07$
16	$6.9401e-19$	56	$1.0695e-06$
17	$6.9401e-19$	57	$4.2831e-04$
18	$8.3220e-19$	58	$4.8134e-04$
19	$1.5295e-18$	59	$1.8423e-01$
20	$1.5295e-18$	60	$9.8748e-01$
21	$1.6051e-18$	61	$9.8749e-01$
22	$1.6051e-18$	62	$9.8754e-01$
23	$2.1275e-18$	63	$9.8757e-01$
24	$2.1275e-18$	64	$9.8758e-01$
25	$2.2904e-18$	65	$9.8761e-01$
26	$2.2904e-18$	66	$9.8767e-01$
27	$3.0038e-18$	67	$9.8768e-01$
28	$4.7078e-18$	68	$9.8784e-01$
29	$4.7078e-18$	69	$9.8790e-01$
30	$4.9702e-18$	70	$9.8798e-01$
31	$6.3127e-18$	71	$9.8812e-01$
32	$1.0917e-17$	72	$9.8830e-01$
33	$8.7525e-17$	73	$9.8839e-01$
34	$1.9767e-16$	74	$9.8965e-01$
35	$5.1624e-15$	75	$9.8968e-01$
36	$1.2425e-15$	76	$1.0000e+00$
37	$1.3603e-15$	77	$1.0000e+00$
38	$2.3955e-15$	78	$1.0000e+00$
39	$4.6504e-15$	79	$1.0000e+00$
40	$6.0565e-15$	80	$1.0000e+00$

Table 6.2: Test cases and description

S. No.	Test case	Description
1	1 RR	Movement of RR in Q-I, other 3 RRs are stationary
2	2 RR	Simultaneous movement of RRs in Q-I and Q-III, other 2 RRs are stationary
3	4 RR	Simultaneous movement of RRs in Q-I, Q-II, Q-III and Q-IV
4	2 RR-D	Simultaneous movement of RRs in Q-I and Q-III in opposite directions, other 2 RRs are stationary

shown in Fig. 3.3. Similarly, the estimated values of quadrant fluxes are computed from

$$\hat{\phi}_Q = \sum_{i \in Q} \hat{\phi}_{V_i} V_i \Big/ \sum_{i \in Q} V_i, \tag{6.24}$$

where Q = I, II, III and IV. Estimated value of core average flux is computed as

$$\hat{\phi}_G = \sum_{i=1}^{10848} \hat{\phi}_{V_i} V_i \Big/ \sum_{i=1}^{10848} V_i. \tag{6.25}$$

The values of these quantities, as determined using DKF algorithm are compared with their respective reference values for assessment of reconstruction accuracy.

6.4 Computation of Error

To characterize the performance of the DKF, we compute relative errors in estimation of flux in 22950 volume elements, 452 coolant channels and 4 quadrants, and also the error in the estimation of the core average flux, respectively using

$$e_{V_{i_{\text{rel}}}} = \frac{\hat{\phi}_{V_i} - \phi_{V_i}}{\phi_{V_i}} \times 100, \quad i = 1, 2, ..., 22950; \tag{6.26}$$

$$e_{Z_{i_{\text{rel}}}} = \frac{\hat{\phi}_{Z_i} - \phi_{Z_i}}{\phi_{Z_i}} \times 100, \quad i = 1, 2, ..., 452; \tag{6.27}$$

$$e_{Q_{i_{\text{rel}}}} = \frac{\hat{\phi}_{Q_i} - \phi_{Q_i}}{\phi_{Q_i}} \times 100, \quad i = I, II, III, IV; \tag{6.28}$$

$$\text{and} \quad e_{G_{\text{rel}}} = \frac{\hat{\phi}_G - \phi_G}{\phi_G} \times 100. \tag{6.29}$$

Root Mean Square (RMS) percentage error in flux is also calculated for volume elements and coolant channels using

$$e_{V_{\text{RMS}}} = \sqrt{\frac{1}{22950} \sum_{i=1}^{22950} (\hat{\phi}_{V_i} - \phi_{V_i})^2} \times 100; \tag{6.30}$$

$$\text{and} \quad e_{Z_{\text{RMS}}} = \sqrt{\frac{1}{452} \sum_{i=1}^{452} (\hat{\phi}_{Z_i} - \phi_{Z_i})^2} \times 100. \tag{6.31}$$

6.4.1 Response of DKF to Non-Zero Initial Condition of Estimation Model

The reactor is assumed to be under steady–state full power operation such that the delayed neutron precursor concentrations in different nodes are in equilibrium with the respective nodal flux levels and RRs are at 66.7% in position, which corresponds to critical core configuration. As already stated, SPND signals were generated from off-line computations using the 128 node scheme. At steady–state, their signals are constant but measurement noise of 2% has been introduced for each detector.

The initial estimate for neutron flux in node 1 of AHWR core is assumed to be deviating from the actual value by 10% while the state estimates for neutron flux in the remaining nodes, $\mathbf{x}_C$, $\mathbf{x}_{\phi_R}$, and $\mathbf{x}_H$ are assumed to be identical to their actual values. Now, the DKF algorithm is processed using the values of $\mathbf{Q}$ and $\mathbf{R}$ as mentioned earlier. The values of estimated neutron flux and delayed neutron precursor concentrations in node 1, 2 and 15 of AHWR are shown in Fig. 6.1, 6.2 and 6.3 respectively. The estimated states gradually approach zero in short duration of time. Such a response is considered to be satisfactory.

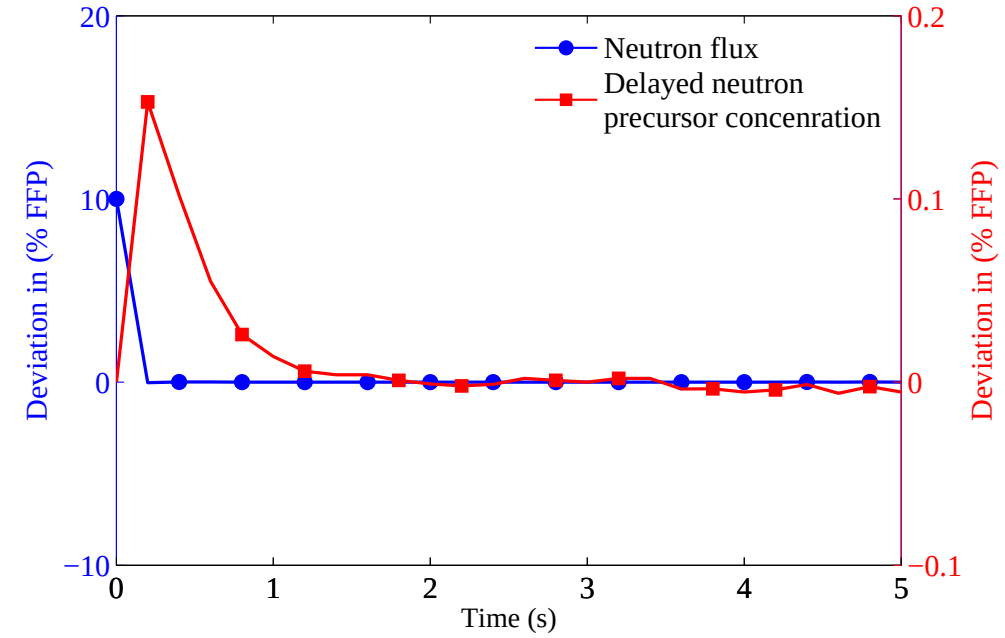

Figure 6.1: Variation in the estimated values of neutron flux and delayed neutron precursor concentration in Node 1.

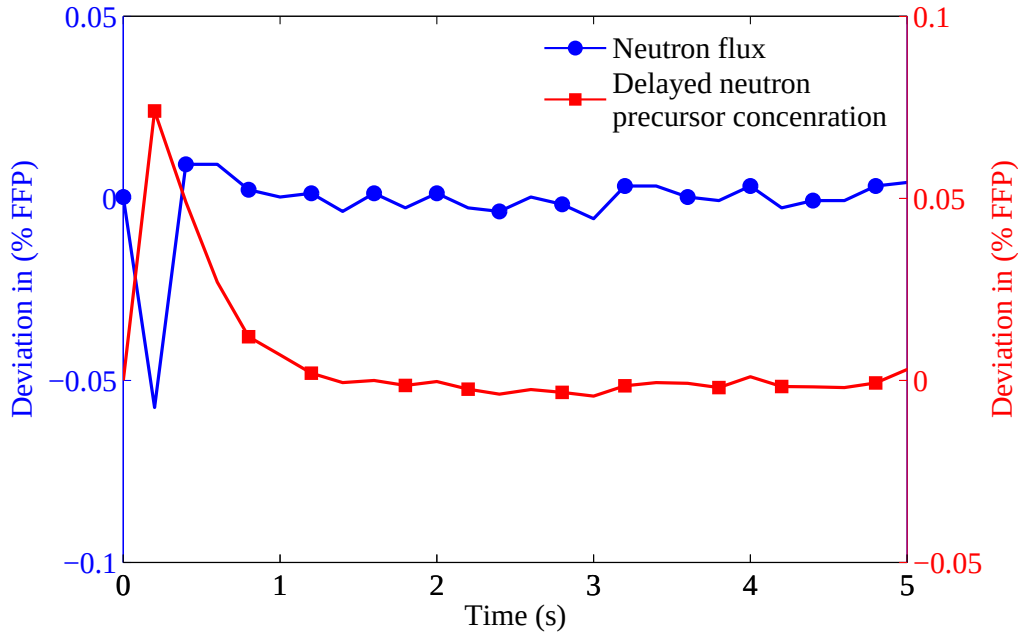

Figure 6.2: Variation in the estimated values of neutron flux and delayed neutron precursor concentration in Node 2.

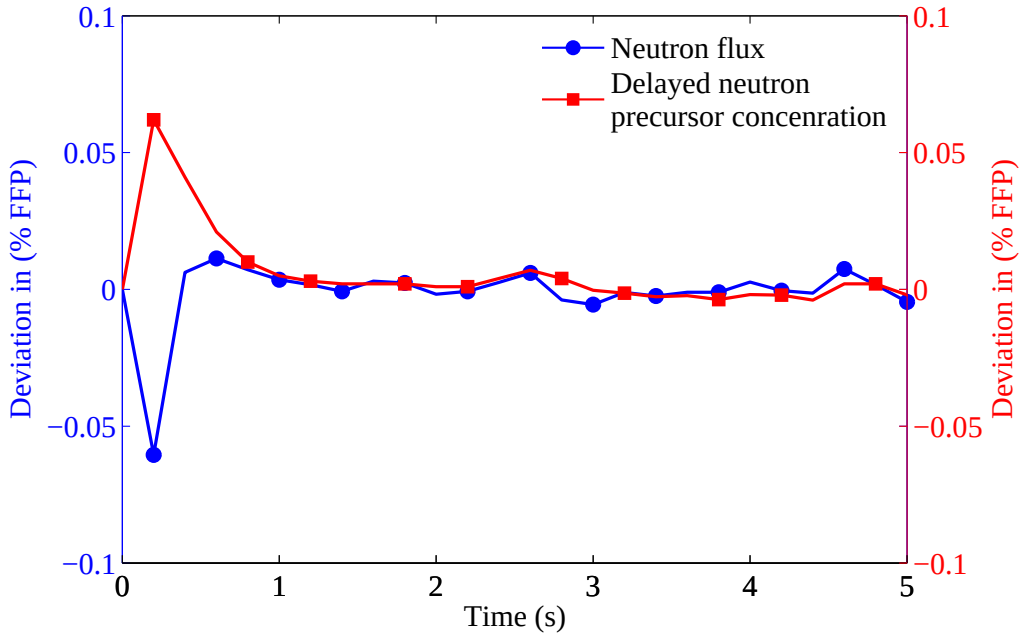

Figure 6.3: Variation in the estimated values of neutron flux and delayed neutron precursor concentration in Node 15.

Table 6.3: Maximum RMS error in estimation of flux in the transient involving movement RR

S.No.	Parameter	Error (%)
1	RMS error in estimation of fluxes in 22950 mesh boxes, $e_{z_{rms}}$	0.3040
2	RMS error in estimation of fluxes in 452 fuel channels, $e_{v_{rms}}$	0.3381
3	RMS error in estimation of fluxes in 4 quadrants	0.1592

6.4.2 Movement of Regulating Rods

This simulation involves movement of one or multiple RRs as listed in Table 6.2. At steady–state full power operation, RRs are at 66.7% in position. In each case, the reactor is at steady–state for the initial 50 seconds. At time $t = 50$ s, control signal of 1 V is applied to RR drive and maintained for 8 s. Corresponding RRs move linearly into the reactor core, as governed by (3.22) and reach 71.14% in position. Then, control signal is made 0 V to hold the RRs at the new position. After 3 s, the RR is driven out linearly to nominal position by applying a control signal of -1 V. Again after 3 s, an outward movement followed by inward movement back to its nominal position is simulated.

First, movement of RR located in Quadrant-I is considered. Fig. 6.4 shows the

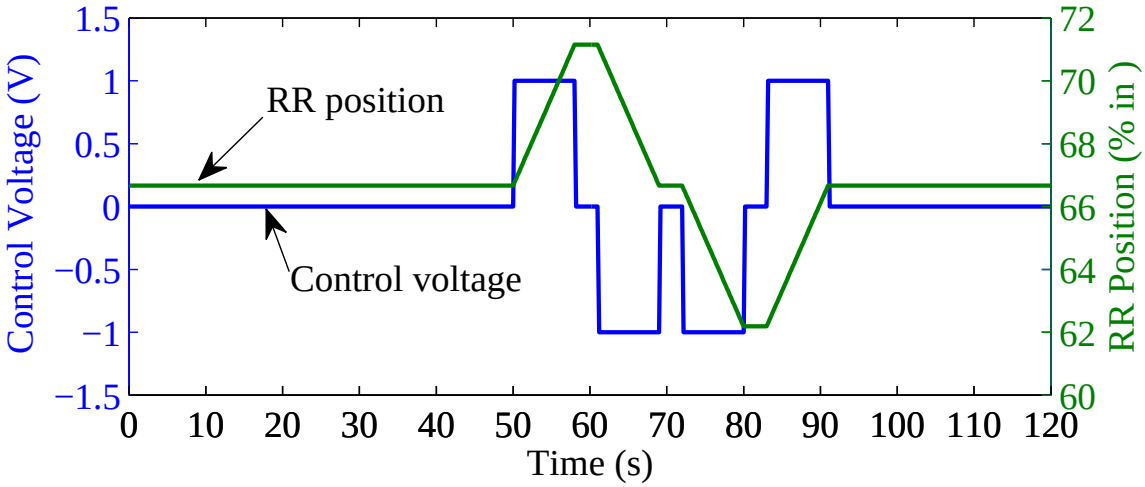

Figure 6.4: Position of RR corresponding to applied control signal.

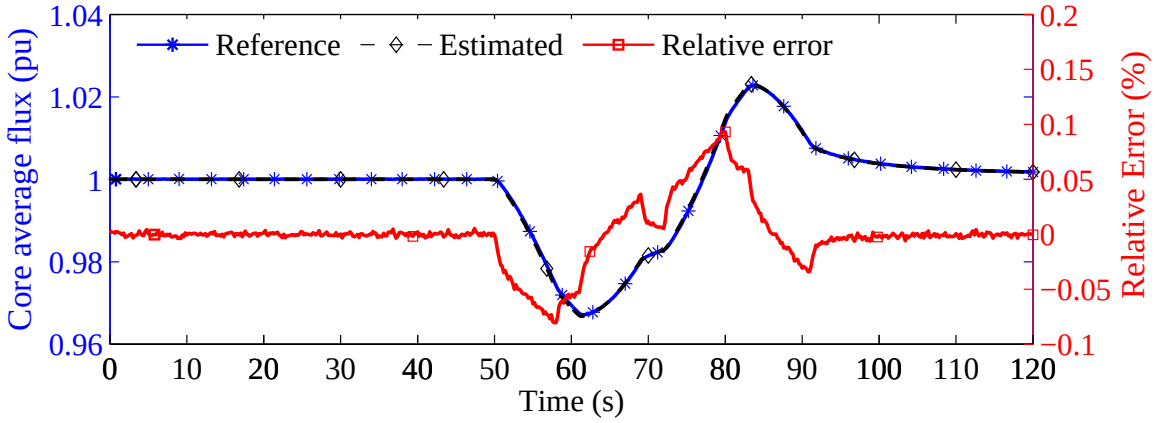

Figure 6.5: Core average flux alongwith relative error (%) during the transient involving the movement of RR in Quadrant-I.

Table 6.4: Maximum RMS error (%) in fluxes

Test Case	**Quadrants** (4)	**Channels**		**All Mesh boxes (22950)**
		Fuel locations (452)	**All locations (513)**	
1 RR*	0.1939	0.3381	0.3457	0.3040
2 RR*	0.2431	0.4320	0.4404	0.3946
4 RR*	0.3406	0.5647	0.5766	0.5112
2 RR-D#	0.2861	0.5014	0.5139	0.4410

* Max. RMS error occurred at $t = 80$ s.
# Max. RMS error occurred at $t = 58$ s.

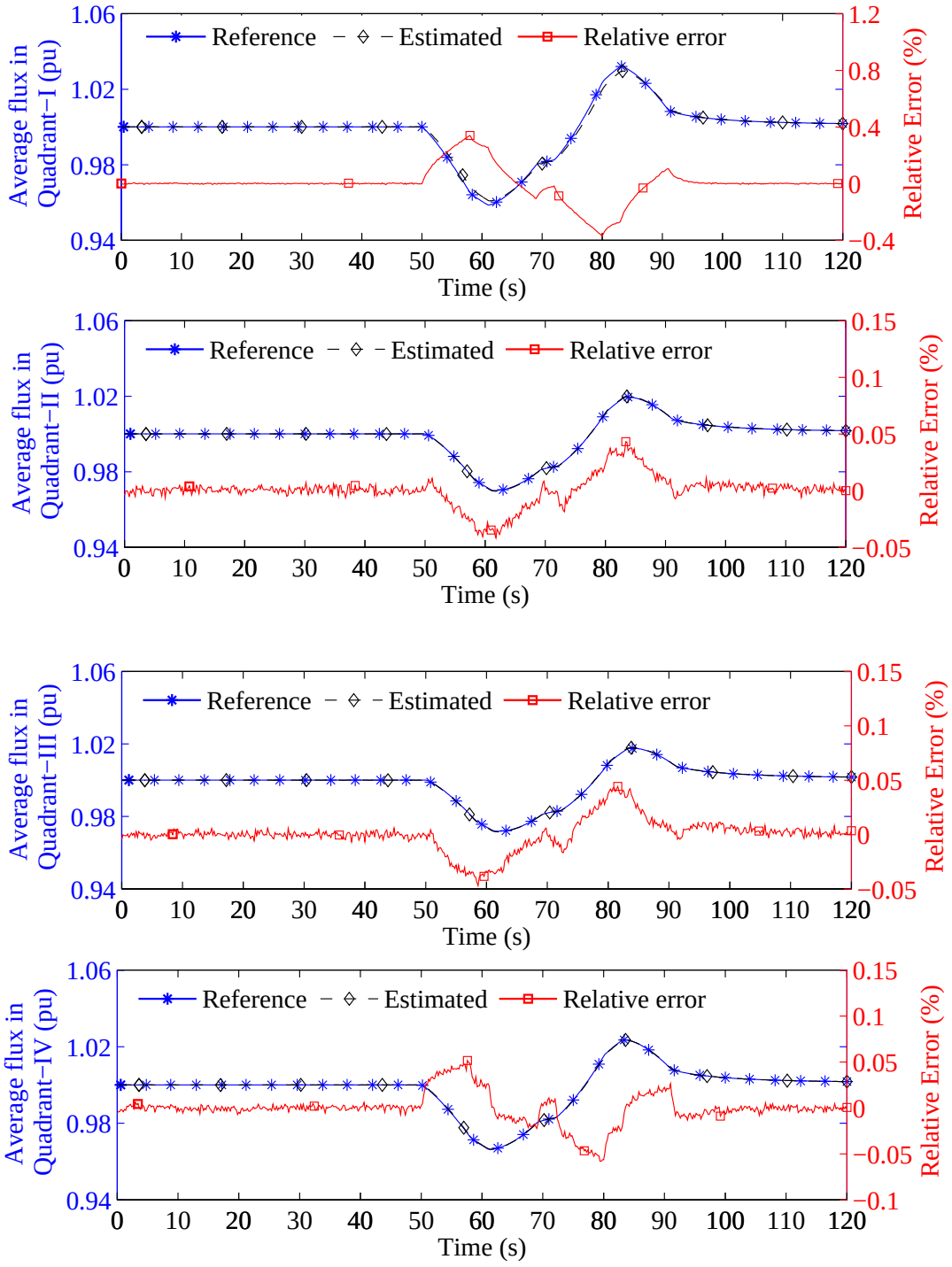

Figure 6.6: Average flux in Quadrants I, II, III and IV during the transient involving the movement of RR in quadrant-I.

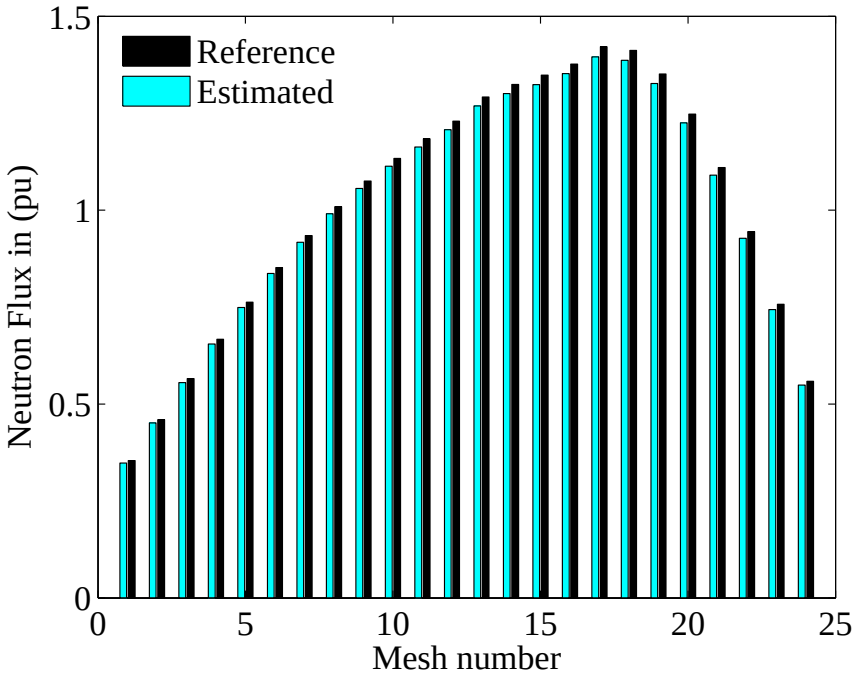

Figure 6.7: Axial flux distribution in the channel E16 (in the vicinity of RR), where maximum errors occur.

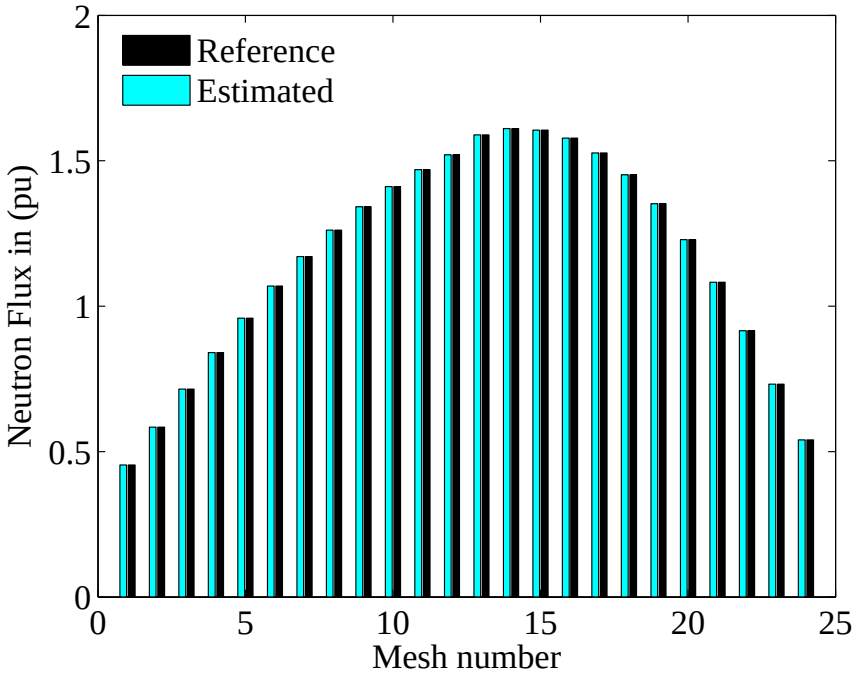

Figure 6.8: Axial flux distribution in the channel N20 (away from RR), where minimum errors occur.

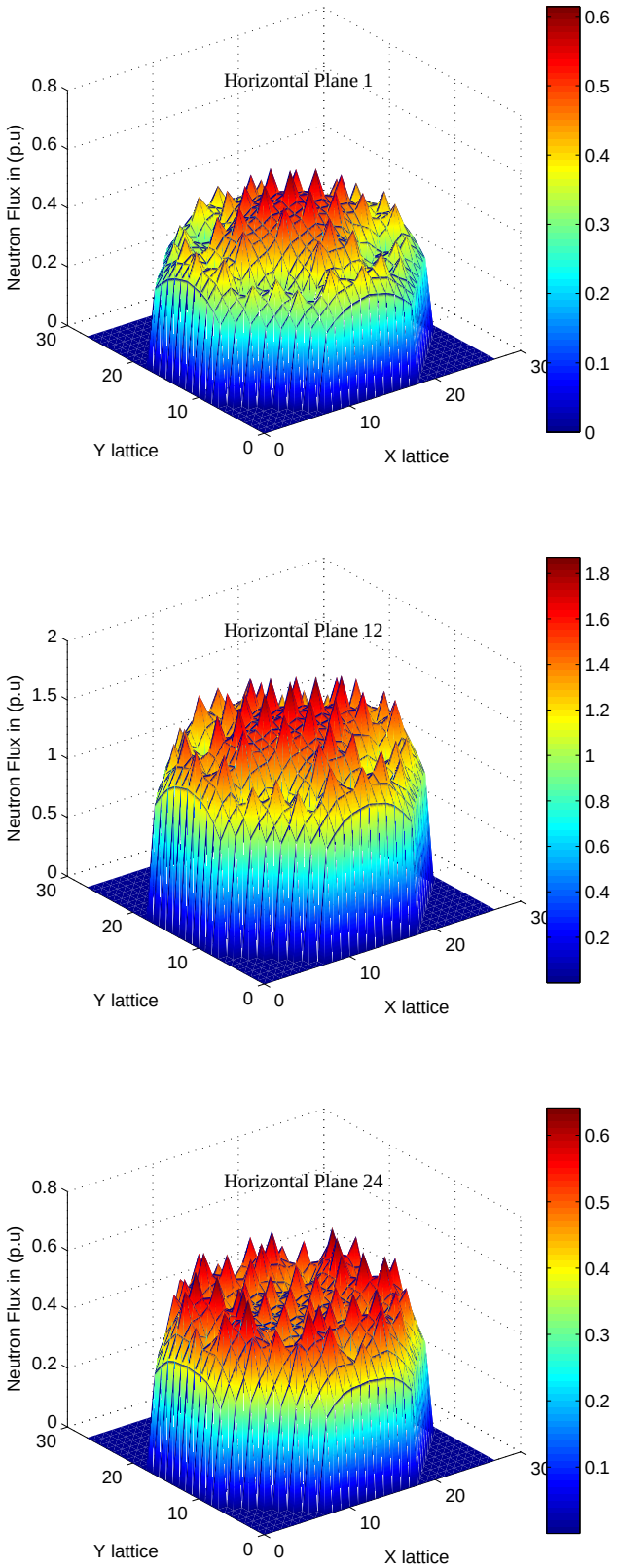

Figure 6.9: 3-D flux distribution in horizontal planes z=1, z=12 and z=24 at $t = 0$ s.

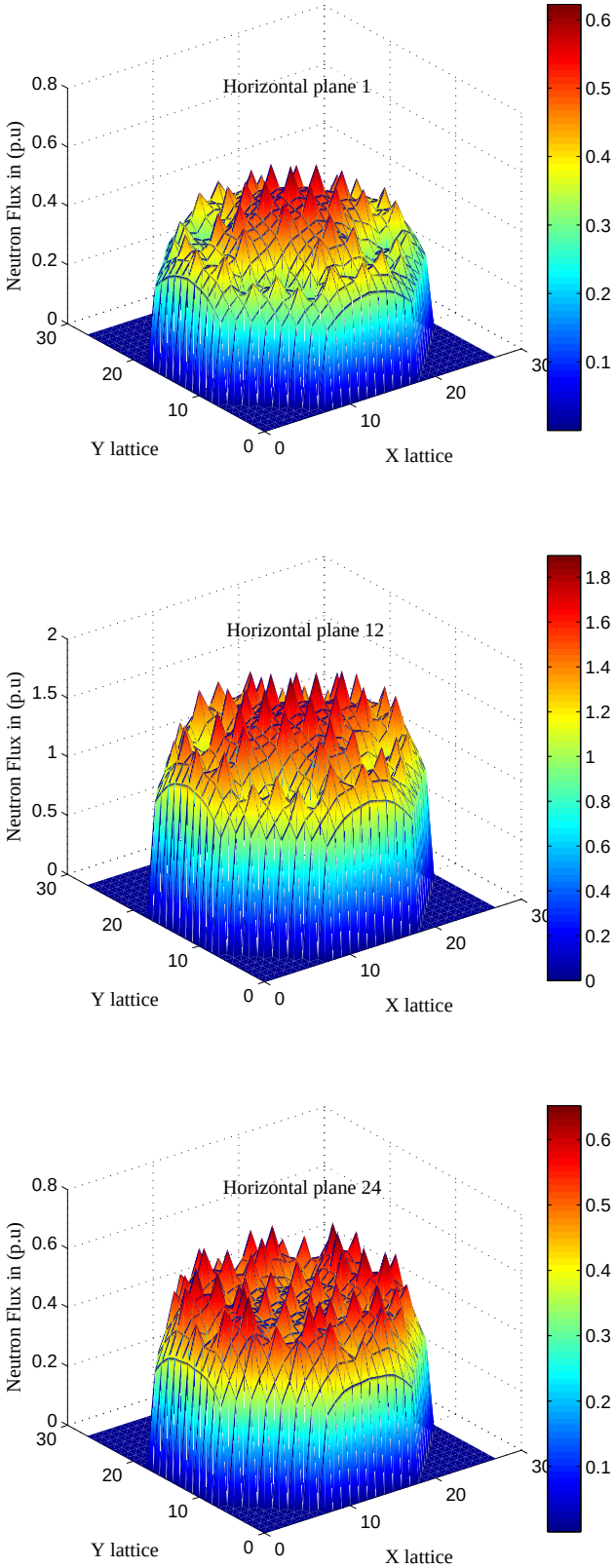

Figure 6.10: 3-D flux distribution in horizontal planes z=1, z=12 and z=24 at $t = 80$ s.

Table 6.5: Absolute relative average error (%) in fluxes

Test case	Quadrants (4)	Channels		Mesh boxes		
		Fuel locations (452)	All locations (513)	Core (10848)	Reflector (12102)	Total (22950)
1 RR	0.1196	0.1899	0.1895	0.1895	0.2396	0.2127
2 RR	0.1813	0.2557	0.2551	0.2551	0.3995	0.3220
4 RR	0.3171	0.3589	0.3617	0.3617	0.6883	0.5108
2 RR-D	0.2316	0.3705	0.3695	0.3695	0.4515	0.4075

Table 6.6: Maximum and minimum relative error (%) in channels

Test case	Negative				Positive			
	Maximum	Location	Minimum	Location	Maximum	Location	Minimum	Location
1 RR	1.7987	E16	0.0036	S24	0.4700	J14	0.0002	N20
2 RR	1.7324	B17	0.0025	S12	0.2885	J14	0.0025	J12
4 RR	2.4033	H5	0.0034	N11	0.2021	R14	0.0010	U16
2 RR-D	1.9025	V10	0.0050	A14	1.8715	E16	0.0043	R8

Table 6.7: Absolute relative error in quadrant and core average flux

Test case	Q-I	Q-II	Q-III	Q-IV	Core average
1 RR	0.3621	0.0194	0.0325	0.0194	0.0911
2 RR	0.3243	0.0383	0.3247	0.0378	0.1804
4 RR	0.3269	0.3076	0.3273	0.3065	0.3161
2 RR-D	0.3779	0.0794	0.3925	0.0470	0.0058

applied control voltage to RR drive and corresponding position of the RR in the core during the test case. Fig. 6.5 shows the core average flux and the relative error in the estimation of the core average flux. Fig. 6.6 shows the average values of flux in quadrant-I, II, III and IV of the reactor. Axial flux distribution for 24 volume elements in the channel E16, which is near to RR, is shown in Fig. 6.7. Flux distribution in channel N20, where minimum error occurs is shown in Fig. 6.8. During the transient, the maximum error between estimated and reference values alongwith the time of occurrence is computed for 22950 mesh boxes, 452 fuel channels and 4 quadrants. It occurs at t=80 s and corresponding values are shown in Table 6.3. As described in Section 3.3, the core region of AHWR is divided into 24 horizontal planes. The 3-D flux distribution in horizontal planes z=1, z=12 and z=24 of reactor core at steady–state (t=0 s) and at t=80 s are shown in Fig. 6.9 and Fig. 6.10 respectively.

To asses the performance of DKF algorithm further, similar analysis is carried out

for the remaining test cases listed in Table 6.2. RMS error between estimated and reference distribution were computed and are shown in Table 6.4. At the instant when the maximum RMS error occurred, absolute relative average errors (%) in fluxes are computed and shown in Table 6.5. Channelwise maximum and minimum relative errors (%) are shown in Table 6.6. Absolute relative error in quadrant fluxes and core average fluxes are also computed and shown in Table 6.7.

It is worthy to note from the numerical values presented in Table 6.4–6.7, that the average relative error and maximum RMS error in quadrant fluxes are 0.31% and 0.34% respectively; in case of channel fluxes they are 0.37% and 0.57% respectively; and in the case of mesh fluxes they are 0.37% and 0.51% respectively. These are of the same order as reported in [52, 71]. From the Table 6.6 it can be claimed that the maximum relative error in the estimation of channel flux from the DKF method is 2.4%. This is of the same order as reported in elsewhere, e.g., in [47], but the DKF has been evaluated for transient situations.

6.4.3 Xenon-Induced Oscillations

As already stated, due to large physical dimensions, operational perturbations might lead to slow xenon induced-oscillations in AHWR. If these oscillations are left uncontrolled, the power density and time rate of change of power at some locations in the reactor core may exceed the respective design limits, resulting into increased chance of fuel failure. Therefore, to maintain the total power and power distribution within the design limits, AHWR is provided with total power control and spatial power control schemes. If due to some hypothetical reason, the spatial control scheme is ineffective, xenon-induced oscillations might occur. These xenon-induced spatial oscillations and subsequent local overpowers pose a potential threat to the fuel integrity of the reactor. Therefore, the detailed knowledge of axial and radial flux distribution in the core during the operational condition is crucial.

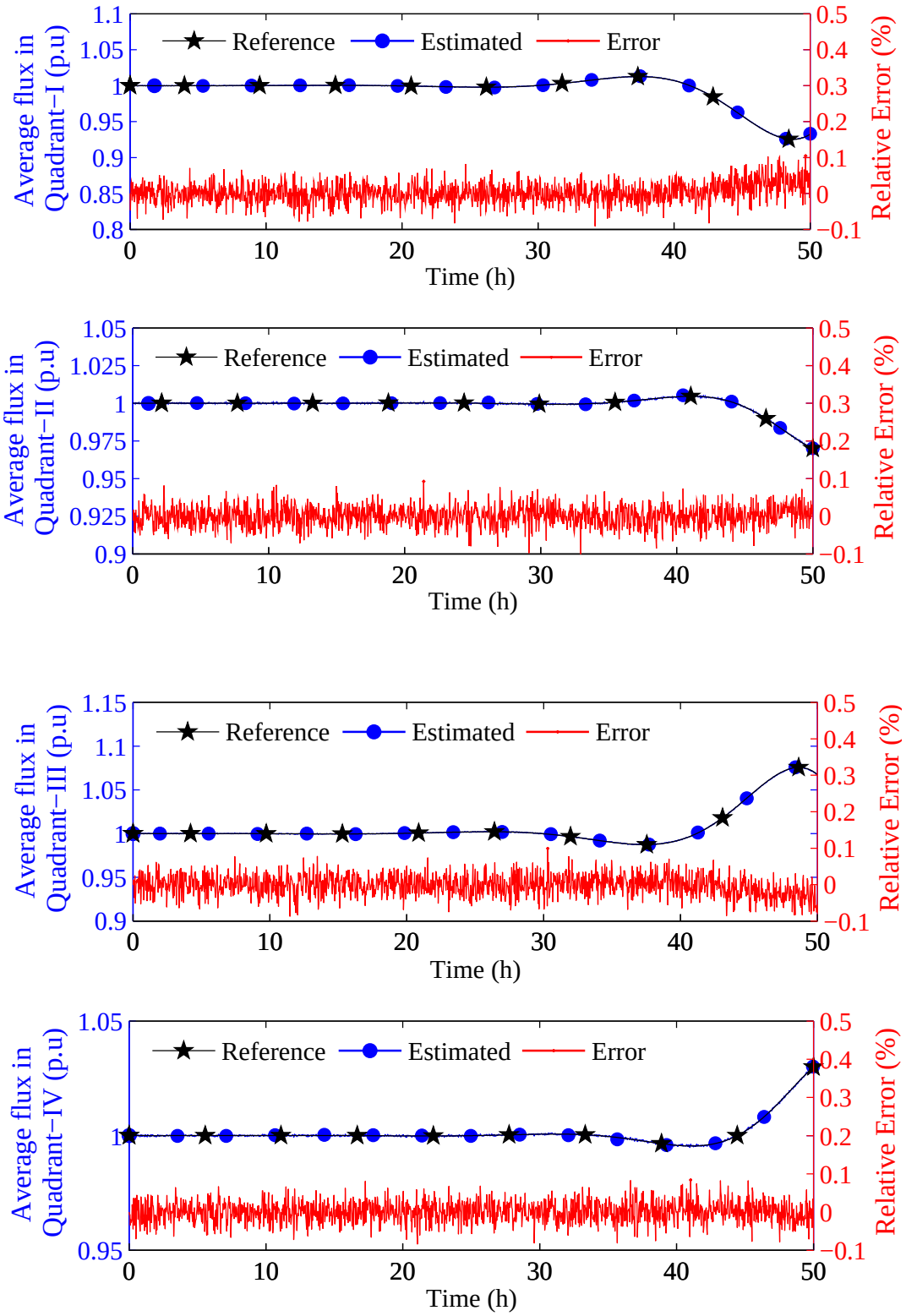

Figure 6.11: Average flux in Quadrants I, II, III and IV during the transient involving Xenon Oscillations.

Table 6.8: Error Statistics in case of Xenon-Induced Spatial Oscillations

(A) RMS Error and Relative Error in fluxes

	Quadrants (4)	**Fuel locations (452)**	**All locations (513)**	**All Mesh boxes (22950)**
Max. RMS Error (%)	0.1327	0.2278	0.2271	0.1746
Absolute Relative Error (%)	0.1155	0.1763	0.1741	0.1502

(B) Maximum and Minimum Relative Error in Channels

	Value of Error (%)	**Location**
Max. Negative Error	0.5385	K19
Min. Negative Error	0.0225	C15
Max. Positive Error	0.4061	U12
Min. Positive Error	0.0050	K2

(C) Absolute Relative Error in Quadrants

Quadrant	**Value of Error** (%)
I	0.0554
II	0.1838
III	0.1777
IV	0.0451

To ascertain this, simulation of transient involving spatial power variation was carried out using nonlinear model of AHWR described by (3.18)–(3.22), xenon and iodine dynamic equations described by (3.23) and (3.25) were also incorporated in the model. The reactor was initially assumed to be under steady–state operation at full power. A small disturbance was enforced for a short duration by the simultaneous counter movement of two diagonally opposite RRs. The RR in quadrant-I was driven 4% in, while the RR in quadrant-III was driven 4% out simultaneously in order to maintain the net reactivity nearly zero. The response of model subsequent to this disturbance, was simulated for about 50 hours. Reference values of mesh box fluxes were determined using (3.35) and SPND signals were generated using (3.36). Again, in these signals 2% noise was added. Now the DKF based flux mapping algorithm was processed for the estimation of flux distribution in AHWR. Fig. 6.11 shows the average values of flux in quadrant-I, II, III and IV of the reactor during the xenon-induced oscillations. Error analysis as described in Sec. 6.4 has been carried out to determine the RMS percentage error and relative error (%) in flux for volume elements, channels and quadrants. The various

types of errors in estimation are given in Table 6.8. In general, the errors are observed to be insignificant.

From the simulations, it can be concluded that, the proposed DKF algorithm can accurately estimate the time dependent neutron flux distribution during the typical reactor operating conditions. The degradation of DKF algorithm accuracy is also very less against the detector random errors.

6.5 Discussion

In this chapter, the task of flux mapping problem in the AHWR has been formulated as a problem of optimally estimating the time dependent neutron flux at a large number of mesh points in the core. The solution is obtained using the well known Kalman filtering technique which works alongwith a space–time kinetics model of the reactor. However, the attempt to solve the Kalman filtering problem in a straight forward manner is not successful due to severe numerical ill-conditioning caused by the simultaneous presence of slow and fast phenomena, typically present in a nuclear reactor. Hence, a grouping of state variables has been suggested whereby the original high order model of the reactor is decoupled into a slow subsystem and a fast subsystem. Now according to order of the slow and fast subsystems, the original time update and Kalman gain equations have also been decoupled into separate sets of equations for the slow and fast subsystems. The decoupled sets of equations could be solved easily. The proposed method has been validated in a number of typical transient situations. Overall accuracy in the estimation using the proposed methodology has been very good for mesh fluxes, channel fluxes, quadrant fluxes and the core average flux. Therefore, the proposed method can serve an effective alternate to the existing flux mapping techniques.

Chapter 7

Conclusions and Future Scope

The neutron flux distribution in a large nuclear reactor undergoes continuous variation due to routine perturbations, non-uniform burn up at different locations, *etc.* The operating procedure and core control philosophy generally ensure that the time dependent flux variations are maintained within prescribed limits. However, the flux profile is continuously monitored and displayed to operator. The knowledge of flux distribution in the reactor core during its operation is helpful to the operator in planning of refueling scheme as well as in zonal power correction. Therefore, for safe, reliable and economic operation these large nuclear reactor cores should be provided with online spatial flux/power distribution monitoring schemes during the course of operation. This has been the motivating factor for pursuing the type of research work presented in this thesis. More specifically, the flux mapping problem of the 920 MW (thermal) AHWR as a particular case of study has been accomplished in this thesis.

The time varying neutron flux distribution in nuclear reactor is computed by an online FMS, with the help of flux mapping algorithms. The measurement signals of several in-core SPND detectors are processed to generate the detailed three dimensional flux map, which helps for spatial control purpose. These measurement signals are corrupted by random noise, which is inevitable. Existing flux mapping algorithms for online computation of flux/power distribution suffer from a drawback that they might fail to

account for the time variation of neutron flux and the accuracy of mapping might be degraded in presence of uncertainty in the detector readings. Recent trends and developments in state estimation theory, modern control system theory (state-space analysis) provide us with systematic method for designing an efficient optimal flux mapping algorithm based on Kalman filtering technique for the AHWR, which has significant importance in practical online application. This has been the other important factor for the research work reported in this thesis.

For the AHWR, an estimation model has been derived for flux mapping computations. The nonlinear mathematical model (core neutronics and control rod dynamics equations) is linearized around the steady–state full power operation by considering a small perturbation in the system and then the equations are cast into standard state-space form. It is characterized by 80 states, 4 inputs and 200 outputs. From the spectrum of eigenvalues of the estimation model, it has been observed that model is associated with two-time scale property. The direct implementation of the DKF algorithm to this high-order stiff estimation model is not feasible as the designing procedure is accompanied by serious numerical ill-conditioning caused by the simultaneous presence of slow and fast phenomena typically present in a nuclear reactor. In particular, the set of recursive equations for computation of DKF gains, as a solution to weighted least squares problem, is ill-conditioned. Application of the model order reduction techniques alleviates the numerical ill-conditioning.

Simplified models alleviating the high dimensionality as well as numerical ill-conditioning can be obtained with the application of model order reduction techniques. Application of model order reduction techniques preserve the important dynamic characteristics of the estimation model, while certain less important characteristics are ignored. In particular, for the AHWR estimation model the application of Davison's and Marshall's dominant mode retention techniques; balanced truncation technique and model decomposition into slow and fast subsystems based on singular perturbation analysis have been explored. All of these four methods are found to be effective in obtaining simplified models of

AHWR. However, reduced order model based on the balanced truncation method is of much lower order in spite of negligible error between the response of the original system and that obtained from the reduced order model.

Application of methods based on retention of dominant modes requires diagonalization. For the estimation model, it is quite difficult task to get the model into diagonal form as there are multiple eigenvalues at the origin of the complex s-plane. This is due to the fact that the model contains slow control rod dynamics. In this thesis, a systematic method has been suggested to handle the numerical ill-conditioning occurring in the computations due to the presence of the slow control rod dynamics by decoupling the higher order model into slow and fast models. Model order reduction techniques based on Davison's and Marshall's dominant mode retention are then applied to retain the slow dynamics. Finally the reduced order model has been formulated by augmenting the control rod dynamics to the model corresponding to the slow dynamics. In this thesis, a novel approach for the application of balanced truncation technique to estimation model having nontrivial unstable part based on stable and unstable decomposition has also been suggested. This is accomplished easily while the direct application of balanced truncation for model order reduction is not feasible.

Due to the two-time-scale behavior, revealed by AHWR, direct implementation of DKF algorithm is not feasible as the design procedure is accompanied by serious numerical ill-conditioning issues. Therefore, the estimation model of AHWR has been decomposed into slow and fast subsystems based on singular perturbation analysis (block diagonalization) by suggesting a regrouping of state variables. Then, according to the order of the slow and fast subsystems, the original time update and Kalman gain equations have also been decoupled into separate sets of equations for the slow and fast subsystems. The decoupled sets of equations could be solved easily and efficiently.

The important aspect of the proposed DKF technique is that it attempts solving for smaller order state prediction equations, process covariance matrices and Kalman gain. Moreover, it yields excellent accuracy in flux estimation as evident from simulation

exercises. For validation of different techniques of flux mapping, computation results generated using a high fidelity model is a necessity. Hence, a model based on 128-nodes in the core resulting into 1168 th order has also been developed.

Feasibility of Kalman filtering technique to the estimation of time varying neutron flux distribution in AHWR has been successfully explored in this thesis. It also leads to some future directions for research. Advanced state of the art approaches of estimation such as EKF, UKF etc., also can be applied to the same problem. Optimality and the availability of the DKF based flux mapping algorithm can also be verified under the faults in some detectors. In addition to this, a reduced order DKF can be designed based on the simplified model obtained from the balanced truncation approach for the estimation of core flux distribution in AHWR in future.

Before deployment in the AHWR, the efficacy of the technique needs to be established further, and it should be demonstrated using plant data, such as from PHWRs that it yields improvement in accuracy compared to that resulting from existing techniques. It should also be assessed from the viewpoint of implementation that the computations could be performed in real-time using hardware and other resources, suitable for control and instrumentation systems in nuclear reactors.

References

[1] *DESIGN BASIS REPORT ON FLUX MAPPING SYSTEM.* AHWR/DBR/637/63715/0. Rev.0.

[2] A. C. Antoulas. *Approximation of Large-Scale Dynamical Systems.* Advances in Design and Control. SIAM, Philadelphia, 2005.

[3] M. Aoki. Control of large-scale dynamic systems by aggregation. *IEEE Trans. Autom. Control*, 13(3):246–253, 1968.

[4] P. Benner, V. Mehrmann, and D. C. Sorensen. *Dimension reduction of large-scale systems*, volume 45. Lecture Notes in Computational Science and Engineering. Springer, Berlin, 2005.

[5] P. Benner, E. S. Quintana-Ortı, and G. Quintana-Ortı. State-space truncation methods for parallel model reduction of large-scale systems. *Parallel Computing*, 29(11):1701–1722, 2003.

[6] T. U. Bhatt, S. R. Shimjith, A. P. Tiwari, K. P. Singh, S. K. Singh, K. Singh, and R. K. Patil. Estimation of sub-criticality using extended kalman filtering technique. *Ann. Nucl. Energy*, 60:98–105, 2013.

[7] R. Bonalumi and N. Kherani. Rational mapping (ram) of in-core data. *Nucl. Sci. and Eng.g*, 90:47, 1985.

[8] J. W. Bryson, J. C. Lee, and J. A. Hassberger. Optimal flux map genera-

tion through parameter estimation techniques. *Nuclear science and engineering*, 114(3):238–251, 1993.

[9] K. W. Chang. Singular perturbations of a general boundary value problem. *SIAM Journal on Mathematical Analysis*, 3(3):520–526, 1972.

[10] C. F. Chen and L. S. Shieh. A novel approach to linear model simplification. *International Journal of Control*, 8(6):561–570, 1968.

[11] T. C. Chen, C. Y. Chang, and K. W. Han. Reduction of transfer functions by the stability-equation method. *Journal of the Franklin Institute*, 308(4):389–404, 1979.

[12] J. H. Chow and P. V. Kokotovic. A decomposition of near-optimum regulators for systems with slow and fast modes. *IEEE Trans. on Autom. Contr.*, 21(5):701–705, 1976.

[13] F. E. Daum and R. J. Fitzgerald. Decoupled kalman filters for phased array radar tracking. *IEEE Trans. Autom. Control*, 28(3):269–283, 1983.

[14] E. J. Davison. A method for simplifying linear dynamic systems. *IEEE Trans. Autom. Control*, 11(1):93–101, 1966.

[15] E. J. Davison. Further comments on "a method for simplifying linear dynamic systems". *IEEE Trans. Autom. Control*, 12(6):799–800, 1967.

[16] E. J. Davison. Further remarks on simplifying linear dynamic systems. *IEEE Trans. Autom. Control*, 12(2):213–214, 1967.

[17] E. J. Davison. On "a method for simplifying linear dynamic systems". *IEEE Trans. Autom. Control*, 12(1):119–121, 1967.

[18] E. J. Davison. A new method for simplifying large linear dynamic systems. *IEEE Trans. Autom. Control*, 13(2):214–215, 1968.

[19] J. J. Duderstadt and L. J. Hamilton. *Nuclear reactor analysis*. John Wiley and Sons, New York, 1976.

[20] Z. Elrazaz and N. K. Sinha. On the selection of the dominant poles of a system to be retained in a low-order model. *IEEE Trans. Autom. Control*, 24(5):792–793, 1979.

[21] D. F. Enns. Model reduction with balanced realizations: An error bound and a frequency weighted generalization. In *Decision and Control, 1984. The 23rd IEEE Conference on*, pages 127–132. IEEE, 1984.

[22] W. H. Enright and M. S. Kamel. On selecting a low-order model using the dominant mode concept. *IEEE Trans. Autom. Control*, 25(5):976–978, 1980.

[23] H. EZURE. Estimation of most probable power distribution in BWRs by least squares method using in-core measurements. *J. of Nucl. Sci. and Tech.*, 25(9):731–740, 1988.

[24] R. J. Fitzgerald. Divergence of the Kalman filter. *IEEE Trans. Autom. Control*, 16(6):736–747, 1971.

[25] L. Fortuna, G. Nunnari, and A. Gallo. *Model Order Reduction Techniques with Applications in Electrical Engineering*. Springer Science & Business Media, 1992.

[26] A. Fossard. On a method for simplifying linear dynamic systems. *IEEE Trans. Autom. Control*, 15(2):261–262, 1970.

[27] L. Fu, L. Zhengpei, and H. Yongming. Harmonics synthesis method for core flux distribution reconstruction. *Prog. in Nucl. Energy*, 31(4):369–372, 1997.

[28] Z. Gajic. Numerical fixed-point solution for near-optimum regulators of linear quadratic gaussian control problems for singularly perturbed systems. *International Journal of Control*, 43(2):373–387, 1986.

[29] Z. Gajic. *Optimal control of singularly perturbed linear systems and applications*. CRC Press, 2001.

[30] Z. Gajic, M. T. Lim, and X. Shen. The study of discrete singularly perturbed linear-quadratic control systems. *Control and Dynamic Systems*, 70(C):199–242, 1995.

[31] Z. Gajic and X. Shen. Parallel reduced-order controllers for stochastic linear singularly perturbed discrete systems. *Automatic Control, IEEE Transactions on*, 36(1):87–90, 1991.

[32] Z. Gajic and X. S. Shen. *Parallel algorithms for optimal control of large scale linear systems*. Springer-Verlag London, 1993.

[33] C. F. Gauss. *Theory of the motion of the heavenly bodies moving about the sun in conic sections: a translation of Carl Frdr. Gauss" Theoria motus corporum coelestium": With an appendix. By Ch. H. Davis*. Little, Brown and Comp., 1857.

[34] A. Gelb. *Applied Optimal Estimation*. MIT Press, 1974.

[35] R. Genesio and M. Milanese. A note on the derivation and use of reduced-order models. *IEEE Trans. Autom. Control*, 21(1):118–122, 1976.

[36] A. Ghafoor and V. Sreeram. A survey/review of frequency-weighted balanced model reduction techniques. *Journal of Dynamic Systems, Measurement, and Control*, 130(6):061004, 2008.

[37] S. Glasstone and A. Sesonske. *Nuclear reactor engineering: reactor systems engineering*. Springer Science & Business Media, 2012.

[38] K. Glover. All optimal Hankel-norm approximations of linear multivariable systems and their L^∞-error bounds. *International journal of control*, 39(6):1115–1193, 1984.

[39] M. Gopal and S. Mehta. On the selection of the eigenvalues to be retained in the reduced order models. *Automatic Control, IEEE Transactions on*, 27(3):688–690, 1982.

[40] K. M. Grigoriadis. Optimal H^∞ model reduction via linear matrix inequalities: continuous and discrete-time cases. In *proceedings of the 34th IEEE Conference on Decision and Control, 1995*, volume 3, pages 3074–3079. IEEE, 1995.

[41] L. M. Grossman and J. P. Hennart. Nodal diffusion methods for space-time neutron kinetics. *Progress in Nuclear Energy*, 49(3):181–216, 2007.

[42] S. Gugercin and A. C. Antoulas. A survey of model reduction by balanced truncation and some new results. *International Journal of Control*, 77(8):748–766, 2004.

[43] A. Haddad. Linear filtering of singularly perturbed systems. *Automatic Control, IEEE Transactions on*, 21(4):515–519, 1976.

[44] A. Haddad and P. Kokotovic. Stochastic control of linear sigularly perturbed systems. *Automatic Control, IEEE Transactions on*, 22(5):815–821, 1977.

[45] H. Hamidi-Hashemi and C. Leondes. Reduction of high-order discrete-time systems. *International journal of systems science*, 19(9):1883–1890, 1988.

[46] E. Hinchley and G. Kugler. On-line control of the CANDU PHW power distribution. In *IAEA Specialists Meet. on Spatial Control Problems, Studsvik, Sweden*, oct., 1974.

[47] I. S. Hong, C. H. Kim, and H. C. Suk. Advanced Online Flux Mapping of CANDU PHWR by Least-Squares Method. *Nucl. Sci and Engg.*, 150(3):299–309, 2005.

[48] M. F. Hutton. Routh approximation method and singular perturbations. In *Annual Allerton Conference on Circuit and System Theory, 13 th, Monticello, Ill*, pages 29–38, 1976.

[49] M. F. Hutton and B. Friedland. Routh approximations for reducing order of linear, time-invariant systems. *IEEE Trans. Autom. Control*, 20(3):329–337, 1975.

[50] H. Ikeda and T. Takeda. Development and verification of an efficient spatial neutron kinetics method for reactivity-initiated event analyses. *Journal of nuclear science and technology*, 38(7):492–502, 2001.

[51] Z. IWAI and Y. KUBO. Determination of eigenvalues in marshall's model reduction. *International Journal of Control*, 30(5):823–836, 1979.

[52] C. J. Jeong and N. Z. Cho. Power Mapping in a Canada Deuterium Uranium Reactor Using Kalman Filtering Technique. *J. of Nucl. Sci. and Tech.*, 37(9):758–768, 2000.

[53] R. E. Kalman. A new approach to linear filtering and prediction problems. *Journal of Fluids Engineering*, 82(1):35–45, 1960.

[54] R. E. Kalman. Toward a theory of difficulty of computation in optimal control. In *proc. IBM Scientific Comput. Symp. on Contr. Theory and Appl.*, 1966.

[55] H. Kando. State estimation of stochastic singularly perturbed discrete-time systems. *Optimal Control Applications and Methods*, 18(1):15–28, 1997.

[56] S. Kaplan, O. Marlowe, and J. Bewick. Application of synthesis techniques to problems involving time dependence. *Nuclear Science and Engineering*, 18(2):163–176, 1964.

[57] C. Kenney and G. Hewer. Necessary and sufficient conditions for balancing unstable systems. *IEEE Trans. Autom. Control*, 32(2):157–160, 1987.

[58] H. Khalil and Z. Gajic. Near-optimum regulators for stochastic linear singularly perturbed systems. *Automatic Control, IEEE Transactions on*, 29(6):531–541, 1984.

[59] H. KOKAME and Y. HATTORI. Kalman Filter Applied to Estimation of Neutron Flux Distribution and Optimum Allocation of In-Core Detectors. *J. of Nucl. Sci. and Tech.*, 14(10):695–704, 1977.

[60] P. Kokotovic, H. K. Khali, and J. O'reilly. *Singular perturbation methods in control: analysis and design*, volume 25. Siam, 1999.

[61] P. V. Kokotovic. A Riccati equation for block-diagonalization of ill-conditioned systems. *IEEE Trans. on Autom. Contr.*, 20(6):812–814, 1975.

[62] P. V. Kokotovic. Applications of Singular Perturbation Techniques to Control Problems. *SIAM review*, 26(4):501–550, 1984.

[63] P. V. Kokotovic, J. J. Allemong, J. R. Winkelman, and J. H. Chow. Singular perturbation and iterative separation of time scales. *Automatica*, 16(1):23–33, 1980.

[64] P. V. Kokotovic and H. K. Khalil. *Singular perturbations in systems and control*. IEEE press, 1986.

[65] P. V. Kokotovic, R. E. O'malley, and P. Sannuti. Singular perturbations and order reduction in control theory an overview. *Automatica*, 12(2):123–132, 1976.

[66] P. V. Kokotovic and P. Sannuti. Singular perturbation method for reducing the model order in optimal control design. *Automatic Control, IEEE Transactions on*, 13(4):377–384, 1968.

[67] S. Kyu-Hong and M. E. Sawan. Kalman Filter Design for Singularly Perturbed Systems by Unified Approach Using Delta Operators. In *Proceedings of the American Contr. Conference*, volume 6, pages 3873–3877. IEEE, 1999.

[68] G. S. Ladde and S. G. Rajalakshmi. Diagonalization and stability of multi-time-scale singularly perturbed linear systems. *Applied mathematics and computation*, 16(2):115–140, 1985.

[69] G. S. Ladde and D. D. Siljak. Multiparameter singular perturbations of linear systems with multiple time scales. *Automatica*, 19(4):385–394, 1983.

[70] A. J. Laub, M. T. Heath, C. C. Paige, and R. C. Ward. Computation of system balancing transformations and other applications of simultaneous diagonalization algorithms. *IEEE Trans. Autom. Control*, 32(2):115–122, 1987.

[71] K. Lee and C. H. Kim. The Least-Squares Method for Three-Dimensional Core Power Distribution Monitoring in Pressurized Water Reactors. *Nucl. Sci and Engg.*, 143(3):268–280, 2003.

[72] Y. C. Lee, C. Hwang, and L. S. Shieh. Order reduction of z-transfer functions via multipoint jordan continued-fraction expansion. *Journal of the Franklin Institute*, 329(3):583–590, 1992.

[73] L. Litz. Order reduction of linear state-space models via optimal approximation of the non-dominant modes. *Large Scale Syst*, 2(3):171–184, 1981.

[74] G. B. Mahapatra. A note on selecting a low-order system by davison's model simplification technique. *IEEE Trans. Autom. Control*, 22(4):677–678, 1977.

[75] G. B. Mahapatra. A further note on selecting a low-order system using the dominant eigenvalue concept. *IEEE Trans. Autom. Control*, 24(1):135–136, 1979.

[76] M. S. Mahmoud, Y. Chen, and M. G. Singh. Discrete two-time-scale systems. *International journal of systems science*, 17(8):1187–1207, 1986.

[77] S. A. Marshall. An approximate method for reducing the order of a linear system. *Contr. Eng*, 10:642–648, 1966.

[78] P. S. Maybeck. *Stochastic models Estimation and Control*, volume 1. Academic Press, Newyork, 1982.

[79] A. K. Mishra, S. R. Shimjith, , T. U. Bhatt, and A. P. Tiwari. Kalman Filter-Based Dynamic Compensator for Vanadium Self Powered Neutron Detectors. *IEEE Trans. on Nucl. Sci.*, 61(3):1360–1368, 2014.

[80] S. Mishra, R. S. Modak, and S. Ganesan. Computational Schemes for Online flux mapping system in a Large-Sized Pressurized Heavy Water Reactor. *Nucl. Sci and Engg.*, 170(3):280–289, 2012.

[81] B. Moore. Principal component analysis in linear systems: Controllability, observability, and model reduction. *IEEE Trans. Autom. Control*, 26(1):17–32, 1981.

[82] C. T. Mullis and R. A. Roberts. Synthesis of minimum roundoff noise fixed point digital filters. *Circuits and Systems, IEEE Transactions on*, 23(9):551–562, 1976.

[83] R. K. Munje, P. S. Londhe, J. G. Parkhe, B. M. Patre, and A. P. Tiwari. Spatial control of advanced heavy water reactor by fast output sampling technique. In *proceedings of International Conference on Industrial Instrumentation and Control (ICIC) 2015*, pages 1212–1217. IEEE, 2015.

[84] R. K. Munje, J. G. Parkhe, and A. P. Tiwari. Control of xenon oscillations in advanced heavy water reactor via two-stage decomposition. *Ann. Nucl. Energy*, 77:326–334, 2015.

[85] R. K. Munje, B. M. Patre, S. R. Shimjith, and A. P. Tiwari. Sliding Mode Control for Spatial Stabilization of Advanced Heavy Water Reactor. *IEEE Trans. on Nucl. Sci.*, 60(4):3040–3050, 2013.

[86] S. K. Nagar and S. K. Singh. An algorithmic approach for system decomposition and balanced realized model reduction. *Journal of the Franklin Institute*, 341(7):615–630, 2004.

[87] D. Naidu. Singular perturbations and time scales in control theory and appli-

cations: an overview. *Dynamics of Continuous Discrete and Impulsive Systems Series B*, 9:233–278, 2002.

[88] M. Naskar, A. P. Tiwari, S. V. G. Menon, and V. Kumar. Finite difference approximation for computation of neutron flux distribution in large phwr. *Proceedings of International Conference on Quality, Reliability and Control (ICQRC), Le Royal Meridien, Mumbai, India*, 2001.

[89] G. Obinata and B. D. Anderson. *Model reduction for control system design*. Springer Science & Business Media, 2012.

[90] H. M. Oloomi and C. Pomalaza-Raez. Two time scale discrete Kalman filter design for an F-8 aircraft. In *Proceedings of the Tactical Communications Conference*, pages 517–522. IEEE, 1996.

[91] K. Ott and D. Meneley. Accuracy of the quasistatic treatment of spatial reactor kinetics. *Nuclear Science and Engineering*, 36(3):402–411, 1969.

[92] X. Peng, K. Wang, and Q. Li. A new power mapping method based on ordinary kriging and determination of optimal detector location strategy. *Annals of Nuclear Energy*, 68:118–123, 2014.

[93] T. Penzl. Algorithms for model reduction of large dynamical systems. *Linear Algebra and its Applications*, 415(2):322–343, 2006.

[94] L. Pernebo and L. M. Silverman. Model reduction via balanced state space representations. *IEEE Trans. Autom. Control*, 27(2):382–387, 1982.

[95] M. E. Pomerantz, C. R. Calabrese, and C. Grant. Nuclear reactor power and flux distribution fitting from a diffusion theory model and experimental data. *Annals of Nucl. Energy*, 29(9):1073–1083, 2002.

[96] A. K. Rao and D. S. Naidu. Singular perturbation method for Kalman filter in discrete systems. In *IEEE Proceedings(Control Theory and Applications)*, volume 131, pages 39–46. IET, 1984.

[97] H. Rosenbrock. Distinctive problems of process control. *Chemical Engineering Progress*, 58(9):43–50, 1962.

[98] M. Safonov and R. Chiang. A schur method for balanced-truncation model reduction. *IEEE Trans. Autom. Control*, 34(7):729–733, 1989.

[99] M. Safonov, E. Jonckheere, M. Vermaj, and D. Limebeer. Synthesis of positive real multivariable feedback systems. *International Journal of Control*, 45(3):817–842, 1987.

[100] Y. V. Sagar, A. K. Mishra, A. P. Tiwari, and S. B. Degweker. Online Fault Detection and Diagnosis of In-core Neutron Detectors Using Generalized Likelihood Ratio Method. *IEEE Trans. on Nucl. Sci.*, 62(6):3311–3323, 2015.

[101] Y. V. Sagar, A. P. Tiwari, S. R. Shimjith, M. Naskar, and S. B. Degweker. Space-time kinetics modeling for the determination of neutron detector signals in advanced heavy water reactor. In *Proceedings of International Conference on Contr. Applications (CCA)*, pages 1224–1229. IEEE, 2013.

[102] V. R. Saksena, J. O'Reilly, and P. V. Kokotovic. Singular perturbations and time-scale methods in control theory: Survey 1976–1983. *Automatica*, 20(3):273–293, 1984.

[103] S. F. Schmidt, J. D. Weinberg, and J. S. Lukesh. Application of Kalman filtering to the c-5 guidance and control system. *ch. 13 in Theory and Application of Kalman Filtering*, (139):312–312, 1970.

[104] S. Shahruz and S. Behtash. Balanced realizations of singularly perturbed systems. *International Journal of Control*, 49(1):207–217, 1989.

[105] Y. Shamash. Continued fraction methods for the reduction of discrete-time dynamic systems. *International Journal of Control*, 20(2):267–275, 1974.

[106] Y. Shamash. Stable reduced-order models using padé-type approximations. *IEEE Trans. Autom. Control*, 19(5):615–616, 1974.

[107] Y. Shamash. Linear system reduction using padé approximation to allow retention of dominant modes. *International Journal of Control*, 21(2):257–272, 1975.

[108] Y. Shamash. Model reduction using the routh stability criterion and the padé approximation technique. *International Journal of Control*, 21(3):475–484, 1975.

[109] Y. Shamash and D. Feinmesser. Reduction of discrete time systems using a modified routh array. *International Journal of Sysyem Science*, 9(1):53–64, 1978.

[110] X. Shen, M. Rao, and Y. Ying. Decomposition method for solving kalman filter gains in singularly perturbed systems. *Optimal Control Applications and Methods*, 14(1):67–73, 1993.

[111] S. R. Shimjith, A. P. Tiwari, and B. Bandyopadhyay. Design of Fast Output Sampling Controller for Three-Time-Scale Systems: Application to Spatial Control of Advanced Heavy Water Reactor. *IEEE Trans. on Nucl. Sci.*, 58(6):3305–3316, 2011.

[112] S. R. Shimjith, A. P. Tiwari, and B. Bandyopadhyay. A Three-Time-Scale Approach for Design of Linear State Regulator for Spatial Control of Advanced Heavy Water Reactor. *IEEE Trans. on Nucl. Sci.*, 58(3):1264–1276, 2011.

[113] S. R. Shimjith, A. P. Tiwari, and B. Bandyopadhyay. *Modeling and control of a large nuclear reactor: a three-time-scale approach*, volume 431. Springer, 2012.

[114] S. R. Shimjith, A. P. Tiwari, and B. Bandyopadhyay. *Modeling and Control of a Large Nuclear Reactor: A three-Time-Scale Approach.* Lecture Notes in Control and Information Sciences. Springer, 2012.

[115] S. R. Shimjith, A. P. Tiwari, B. Bandyopadhyay, and R. K. Patil. Spatial stabilization of Advanced Heavy Hater Reactor. *Ann. Nucl. Energy*, 38(7):1545–1558, 2011.

[116] S. R. Shimjith, A. P. Tiwari, M. Naskar, and B. Bandyopadhyay. Space-time kinetics modeling of Advanced Heavy Water Reactor for control studies. *Ann. Nucl. Energy*, 37(3):310–324, 2010.

[117] D. Simon. *Optimal state estimation: Kalman, H_∞, and nonlinear approaches*. John Wiley & Sons, 2006.

[118] D. Simon. Kalman filtering with state constraints: a survey of linear and nonlinear algorithms. *Control Theory & Applications, IET*, 4(8):1303–1318, 2010.

[119] R. K. Sinha and A. Kakodkar. Design and development of the AHWR– the Indian thorium fuelled innovative nuclear reactor. *Nucl. Engg. and Design*, 236(7):683–700, 2006.

[120] J. M. Siret, G. f. Michailesco, and P. Bertrand. Representation of linear dynamical systems by aggregated models. *International Journal of Control*, 26(1):121–128, 1977.

[121] S. Skogestad. *Multivariable feedback control: analysis and design*, volume 2. 2007.

[122] H. W. Sorenson. *Kalman filtering: theory and application*. IEEE, 1985.

[123] W. M. Stacey. *Space-time nuclear reactor kinetics*, volume 5. Academic Press, 1969.

[124] T. Sutton and B. Aviles. Diffusion theory methods for spatial kinetics calculations. *Progress in nuclear energy*, 30(2):119–182, 1996.

[125] G. Syrcos and P. Sannuti. Singular perturbation modelling of continuous and discrete physical systems. *International Journal of Control*, 37(5):1007–1022, 1983.

[126] D. B. Talange, B. Bandyopadhyay, and A. P. Tiwari. Spatial control of a large phwr by decentralized periodic output feedback and model reduction techniques. *IEEE Trans. Nucl. Sci.*, 53(4):2308–2317, 2006.

[127] A. N. Tikhonov and V. Y. Arsenin. *Solutions of ill-posed problems*. Wasington, DC: Winston, 1977.

[128] A. P. Tiwari. *Modeling and Control of a Large Pressurized Heavy Water Reactor*. PhD thesis, IIT BOMBAY, 1999.

[129] A. P. Tiwari, B. Bandyopadhyay, and G. Govindarajan. Spatial Control of a Large Pressurized Heavy Water Reactor. *IEEE Trans. on Nucl. Sci.*, 43(4):2440–2453, 1996.

[130] A. P. Tiwari, B. Bandyopadhyay, and H. Werner. Spatial Control of a Large PHWR by Piecewise Constant Periodic Output Feedback. *IEEE Trans. Nucl. Sci.*, 47(2):389–402, 2000.

[131] M. S. Tombs and I. Postlethwaite. Truncated balanced realization of a stable non-minimal state-space system. *International Journal of Control*, 46(4):1319–1330, 1987.

[132] A. Varga. Efficient minimal realization procedure based on balancing. In *Prepr. of the IMACS Symp. on Modelling and Control of Technological Systems*, volume 2, pages 42–47, 1991.

[133] C. Wang, H. Wu, L. Cao, and P. Yang. On-line reconstruction of in-core power distribution by harmonics expansion method. *Nucl. Engg. and Design*, 241(8):3042–3050, 2011.

[134] N. Wiener. *The Extrapolation, Interpolation and Smoothing of Stationary Time Series*. New York: Wiley, 1949.

[135] Y. Zhang, D. S. Naidu, C. Cai, and Y. Zou. Singular perturbation and time scales in control theories and applications: An overview 2002–2012. *Int. J. Inf. Syst. Sci*, 9(1):1–36, 2014.

[136] B. Zhong, K. Wang, and G. Yu. A new method on flux mapping by function expansion. In *18th International Conference on Nuclear Engineering*, pages 63–68. American Society of Mechanical Engineers, 2010.

[137] K. Zhou, G. Salomon, and E. Wu. Balanced realization and model reduction for unstable systems. *International Journal of Robust and Nonlinear Control*, 9(3):183–198, 1999.